UNIVERSITEIT VAN PRETORIA
UNIVERSITY OF PRETORIA
YUNIBESITHI YA PRETORIA

In silico docking and ADMET studies on clinical targets for type 2 diabetes correlated to *in vitro* inhibition of pancreatic alpha-amylase and alpha-glucosidase by rutin, caffeic acid, *p*-coumaric acid, and vanillin

Final report

By: Jamie McMillan (16016760)

Supervisor: Prof Zeno Apostolides

Co-supervisor: Prof Megan Bester

December 2021

Submitted in fulfilment of the degree: MSc Biochemistry

Department of Biochemistry, Genetics and Microbiology

Declaration of originality

The Department of Biochemistry, Genetics and Microbiology places great emphasis upon integrity and ethical conduct in the preparation of all written work submitted for academic evaluation. While academic staff teach you about referencing techniques and how to avoid plagiarism, you too have a responsibility in this regard. If you are at any stage uncertain as to what is required, you should speak to your lecturer before any written work is submitted. You are guilty of plagiarism if you copy something from another author's work (eg. a book, an article, or a website) without acknowledging the source and pass it off as your own. In effect you are stealing something that belongs to someone else. This is not only the case when you copy work word-for-word (verbatim), but also when you submit someone else's work in a slightly altered form (paraphrase) or use a line of argument without acknowledging it. You are not allowed to use work previously produced by another student. You are also not allowed to let anybody copy your work with the intention of passing if off as his/her work. Students who commit plagiarism will not be given any credit for plagiarised work. The matter may also be referred to the Disciplinary Committee (Students) for a ruling. Plagiarism is regarded as a serious contravention of the University's rules and can lead to expulsion from the University. The declaration which follows must accompany all written work submitted while you are a student of the Department of Biochemistry, Genetics and Microbiology No written work will be accepted unless the declaration has been completed and attached.

Full names of student: Jamie McMillan

Student number: 16016760

Topic of work: Final report

Declaration 1. I understand what plagiarism is and am aware of the University's policy in this regard. 2. I declare that this report is my own original work. Where other people's work has been used (either from a printed source, internet, or any other source), this has been properly acknowledged and referenced in accordance with departmental requirements. 3. I have not used work previously produced by another student or any other person to hand in as my own. 4. I have not allowed, and will not allow, anyone to copy my work with the intention of passing it off as his or her own work.

SIGNATURE 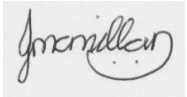

Abstract

Diabetes mellitus affects millions of people worldwide and if left untreated leads to many serious complications such as hypertension, stroke, coma, or even death. Although drugs are commercially available, often these are unaffordable and have undesirable side effects. Therefore, discovering new and more effective treatments is of importance. Several edible plants have been found to have antidiabetic properties and the compounds contributing to activity may be an alternative source of compounds for the treatment of type 2 diabetes (T2D). The study aimed to analyse the *in silico* properties, the digestive enzyme inhibition and cellular glucose-uptake inducing ability of the selected compounds present in herbs, spices, and medicinal plants.

The docking scores of 1070 compounds in 30 herbs, spices, and medicinal plants were obtained using the virtual docking simulations known as Glide and AutoDock Vina. Twenty compounds were selected that had a range of docking scores for pancreatic alpha-amylase and alpha-glucosidase. The ADMET properties of these compounds were predicted using Canvas and pkCSM, and the potential cross reactions of six selected compounds were predicted using SwissTargetPrediction. The pancreatic alpha-amylase and the alpha-glucosidase inhibitory activity of these compounds were determined with the 3,5-dinitrosalicylic acid (DNSA) and *p*-nitrophenyl α-D-glucopyranoside (*p*NPG) assays, respectively, and the inhibition constant (K_i) values were compared with acarbose. The enzyme kinetics were determined using Lineweaver-Burk and secondary plots. Caffeic acid, vanillin, ethyl gallate, and *p*-coumaric acid had K_i values that were similar ($p > 0.05$) to the K_i of acarbose (Student's t-test) for pancreatic alpha-amylase. Rutin, caffeic acid, vanillin, and *p*-coumaric acid had K_i values that were similar ($p > 0.05$) to the K_i of acarbose for alpha-glucosidase. A positive correlation between the Glide docking score and the K_i value was obtained.

The IC_{50} of the compounds and acarbose in the Caco2, HepG2, and C2C12 cell lines was determined with the sulforhodamine B (SRB) assay. Caffeic acid, *p*-coumaric acid, rutin, and vanillin in the Caco2 cell line had IC_{50} values that were similar ($p > 0.05$) to acarbose (IC_{50} = 715±89.1 μM); whereas for the negative controls, ethyl gallate and oxalic acid, the IC_{50} values were significantly ($p < 0.05$) smaller than acarbose. Cytotoxicity in the HepG2 and C2C12 cell lines was less than that observed for the Caco2 cell line. These compounds were then analysed for their glucose uptake activity in C2C12 and HepG2 cell lines with the 2-NBDG assay. None of the compounds, including metformin, significantly increased the glucose uptake in the HepG2 or insulin resistant HepG2 cells when compared with the control. Some of the compounds, including metformin, significantly ($p < 0.05$) increased the glucose uptake ability in the C2C12 cell line when compared with the control.

Sources of these compounds were then determined, and common verbena, sweet basil, tarragon, pepper, parsley, sorrel, and vanilla were found to be rich sources of caffeic acid, *p*-coumaric acid, rutin, and vanillin. These compounds in addition to epigallocatechin and epigallocatechin gallate with known antidiabetic properties were present in green tea indicating that green tea was an excellent source of compounds with antidiabetic properties. As green tea is widely consumed and easily accessible, in the second part of this study untargeted metabolomic analysis on five commercial green tea brands (Dilmah, Eve's, Livewell, Tetley, and Five Roses) using ultra-performance liquid chromatography/ mass spectrometry (UPLC/MS) analysis was undertaken. The data was analysed using MassLynx, MSDIAL, and MSFINDER. MSFINDER used several metabolomic databases to annotate the peaks detected by the Waters UPLC/MS. Targeted metabolomic analysis was performed to determine the content of selected standards in each green tea sample. The most abundant standards were epigallocatechin (5 - 8.5% dry weight), and epigallocatechin gallate (7 - 9% dry weight). The content of caffeic acid and *p*-coumaric acid was less than 0.01% and the content of rutin ranged from 0.4% to 2.9%. The pancreatic alpha-amylase and alpha-glucosidase inhibitory activity of the five green tea brands was determined with the *in vitro* enzyme inhibition assays. Tetley was the only brand that had a pancreatic alpha-amylase IC_{50} value that was similar ($p > 0.05$) to acarbose, whereas the other four brands had significantly ($p < 0.05$) higher pancreatic alpha-amylase IC_{50} values when compared with acarbose. All five green tea brands had significantly ($p < 0.05$) lower alpha-glucosidase IC_{50} values when compared to acarbose. MetaboAnalyst identified two annotated compounds that were significantly ($p < 0.05$) more abundant in the green tea brands that had a low IC_{50} values which suggests that these two compounds could be responsible for the enhanced enzyme inhibition ability of those green tea brands. The presence of several inhibitory compounds in a single plant (*Camellia sinensis*) is most advantageous when it comes to complementary and alternative medicines because each compound could have a different mode of action and can act synergistically. In addition, when used in combination with antidiabetic drugs may have a beneficial effect.

Table of Contents

List of Abbreviations

2-NBDG	2-[N-(7nitrobenz-2-oxa-1,3-diazol-4-yl) amino]-2-deoxy-d-glucose
ABC	ATP binding cassette
ABF	Analysis base file
AMPK	Adenosine monophosphate-activated protein kinase
BBB	Blood-brain barrier
BPI	Base peak intensity
CNS	Central nervous system
CYP	Cytochrome P_{450}
DFFITS	Difference in fits
DMEM	Dulbecco′s Modified Eagle′s Medium
DMSO	Dimethyl sulfoxide
DNSA	3,5-Dinitrosalicylic acid
EC	Epicatechin
ECG	Epicatechin gallate
EGC	Epigallocatechin
EGCG	Epigallocatechin gallate
F26BP	Fructose-2,6-bisphospate
FCS	Foetal calf serum
GDM	Gestational diabetes
GIT	Gastrointestinal tract
GK	Glucokinase
GP	Glycogen phosphorylase
GS	Glycogen synthase
GSK-3	Glycogen synthase kinase 3
HTVS	Hight-throughput virtual screening
IC_{50}	Inhibition concentration
IGC_{50}	Inhibits the growth of 50%
IR	Insulin receptor
IRS	Insulin receptor substrates
K_i	Inhibition constant
LC	Liquid chromatography
LC_{50}	Lethal concentration that kills 50% of a population
LOAEL	Lowest observed adverse effect
MRTD	Maximum recommended tolerated dosage
MS	Mass spectrometry
MS^e	Mass spectrometry everything
NMUR2	Neuromedin-U receptor 2
PBS	Phosphate buffered saline
PC1	First principal component
PC2	Second principal component
PCA	Principal component analysis
PDA	Photodiode array
PDK1	Phosphoinositide-dependent kinase 1

PFK-1	Phosphofructokinase-1
PFK-2	Phosphofructokinase-2
PI3K	Phosphoinositide-3-kinase
PIP2	Phosphotidylinositol-3,4-bisphosphate
PIP3	Phosphatidylinositol-3,4,5-trisphosphate
PKB	Protein kinase B
PLS-DA	Partial least squares-discriminant analysis
*p*NP	*p*-Nitrophenyl
*p*NPG	*p*-Nitrophenyl α-D-glucopyranoside
PP-1	Protein phosphatase-1
PTP1B	Protein tyrosine phosphatase 1B
QSAR	Quantitative structure-activity relationship
QTOF	Quadrupole time-of-flight
ROS	Reactive oxygen species
SEM	Standard error of the mean
SMILES	Simplified molecular-input line-entry system
SRB	Sulforhodamine B
T1D	Type 1 diabetes
T2D	Type 2 diabetes
TCA	Trichloroacetic acid
TIC	Total ion current
TOF	Time-of-flight
UPLC	Ultra-performance liquid chromatography
VDss	Volume of distribution

List of Figures

List of Tables

CHAPTER 1: Literature review

1.1.Diabetes

Diabetes mellitus is a metabolic disease that affects the body's ability to metabolise carbohydrates, proteins, and lipids. This disorder results from a deficiency in insulin production or the resistance of target cells to the effects of insulin. Decreased insulin action causes hyperglycemia which leads to diabetic symptoms such as polyphagia, polydipsia, polyuria, and ketoacidosis. The hyperglycemic consequences of diabetes can also cause several complications such as nerve damage, kidney failure, vision loss, heart attack, stroke, and leg amputation. If left untreated, these symptoms and complications can have fatal consequences (Sharma, 2018).

1.1.1. Types of diabetes

There are several types of diabetes, such as type 1 diabetes (T1D) which is also known as insulin-dependent diabetes or juvenile-onset diabetes, as it usually manifests at a fairly young age. T1D is caused by the autoimmune destruction of pancreatic beta-cells which leads to the absolute deficiency of insulin production. T1D treatment consists of daily insulin injections to regulate the blood glucose concentration and to avoid a diabetic coma caused by ketoacidosis (Roglic, 2016).

The most common type of diabetes is type 2 diabetes (T2D) which is also known as non-insulin-dependent diabetes or adult-onset diabetes. T2D results from the resistance of target cells to the effects of insulin and the inability of the pancreas to produce enough insulin to compensate for this resistance. The metabolic syndrome increases your risk for T2D and is a cluster of metabolic abnormalities that include hypertension, obesity, insulin resistance, and hyperlipidemia (Rochlani *et al.*, 2017). There are several risk factors associated with the manifestation of T2D, such as genetic predispositions, ethnicity, and family history of diabetes as well as environmental factors, such as age, body weight, unhealthy diet, physical inactivity, and smoking (Luo *et al.*, 2013). A range of treatments is available for the management of T2D, such as changes in diet and regular exercise, as well as several types of antidiabetic agents and insulin injections (Roglic, 2016).

Another type of diabetes is gestational diabetes (GDM) which is a temporary condition that occurs during pregnancy when the blood glucose concentration is above normal. Both the mother and child are at risk of developing T2D because of a GDM pregnancy. GDM can be managed by going for regular medical check-ups, eating healthy, and regular exercise (WHO, 2013).

1.1.2. Global prevalence

According to the World Health Organization (WHO), diabetes is the seventh leading cause of death in the world. In 2019, 463 million adults were suffering from diabetes and this number is expected to increase to 578 million in 2030 and 700 million in 2045. More people die from diabetes than from tuberculosis, HIV and malaria combined. The global prevalence of diabetes is shown in **Figure 1**. In 2019, adults who were 65 years and older had the highest prevalence of diabetes (20%) compared to younger individuals (<20%). Men also had a slightly higher diabetes prevalence (9.6%) than women (9.0%). Individuals living in high-income urban areas had a greater diabetes prevalence than individuals living in low-income rural areas. Of concern, only half of the individuals with diabetes are aware of their condition (Saeedi *et al.*, 2019).

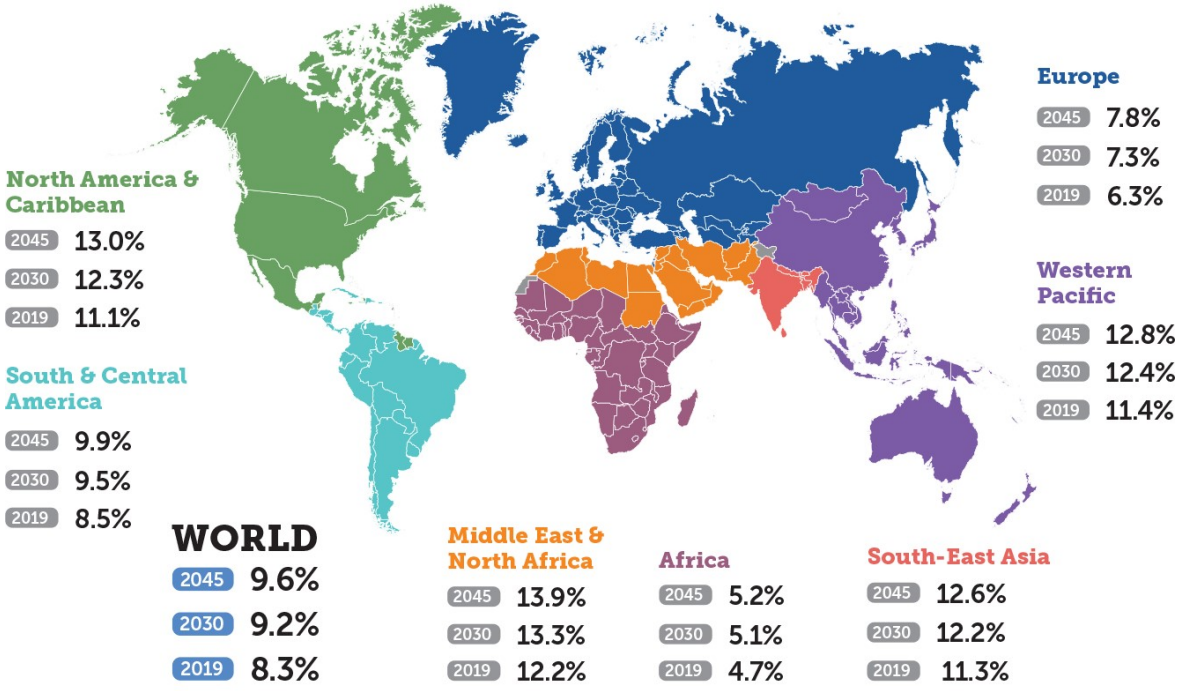

Figure 1: The global prevalence of diabetes
The present and predicted global prevalence of diabetes in adults (20-79 years) in 2019, 2030, and 2045 (Federation, 2019).

1.1.3. Cost of diabetes treatment

Proper management of diabetes has become increasingly problematic due to the rise in individuals with diabetes, especially in low-income countries, which lack basic medical care facilities, and the associated availability and cost of oral antidiabetic drugs either as brand name or generic forms. Diabetes-related health expenditure has greatly increased from $232 billion (US dollars) in 2007 to $760 billion in 2019,

worldwide. This number is expected to increase to $825 billion by 2030 and $845 billion by 2045 (Atlas, 2019).

For patients with T1D, the price of insulin has increased over the past few years, and patients especially in rural areas, lack access to sufficient amounts of insulin as insulin is difficult to transport and needs to remain refrigerated (Atlas, 2003). Especially in third world countries, there is a need for new treatments that are both affordable and easily accessible.

1.2. Biochemistry of diabetes

Diabetes is caused by the deficiency of insulin production or the resistance of target cells to the effects of insulin. Insulin is a peptide hormone that is produced in the pancreas and is responsible for regulating the metabolism of carbohydrates, proteins, and lipids. Insulin secretion increases proportionally to the increase of glucose levels, such as after a meal, and promotes glucose uptake into adipose and skeletal muscle cells. In addition, insulin also inhibits the endogenous production of glucose in the liver.

1.2.1. Carbohydrate digestion

Pancreatic alpha-amylase is an enzyme produced in the pancreas and secreted into the small intestine. Pancreatic alpha-amylase is responsible for the hydrolysis of consumed starch. Several food sources that contain starch include potatoes, rice, wheat, maize, and sorghum. Starch is a polysaccharide that consists of amylose and amylopectin residues, **Figure 2**. Pancreatic alpha-amylase hydrolyses the α-(1-4) linkage of starch to produce maltose, maltotriose and α-limit dextrins. These oligosaccharides are further hydrolysed by brush border enzymes in the small intestine (Singh *et al.*, 2010).

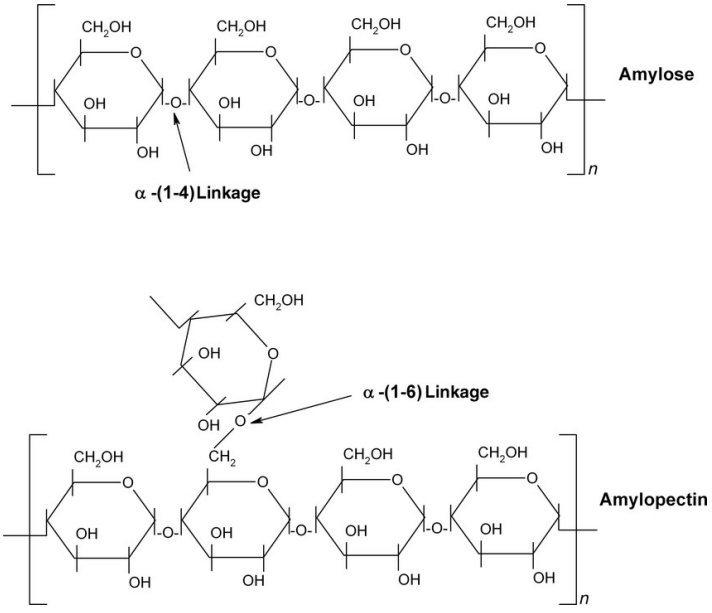

Figure 2: Starch
The amylose and amylopectin residues of starch (Visakh, 2014).

Alpha-glucosidase, specifically maltase, is a brush border enzyme in the small intestine that is responsible for the hydrolysis of the α-(1-4) linkages of maltose and maltotriose to produce glucose residues, **Figure 3**. The other types of alpha-glucosidases include: sucrase which hydrolyses sucrose to glucose and fructose; lactase which hydrolyses lactose to glucose and galactose; and isomaltase which hydrolyses the α-(1-6) linkage of α-limit dextrins. Maltase is perhaps the most important alpha-glucosidase because most complex carbohydrates consumed are in the form of starch. The resulting monosaccharides are actively transported across intestinal epithelial cells and into the bloodstream. Glucose, for example, is transported into the bloodstream via a sodium-glucose symporter, on the brush border membrane of intestinal epithelial cells and then the GLUT2 transporter on the basolateral membrane (Holmes, 1971, Koepsell, 2020).

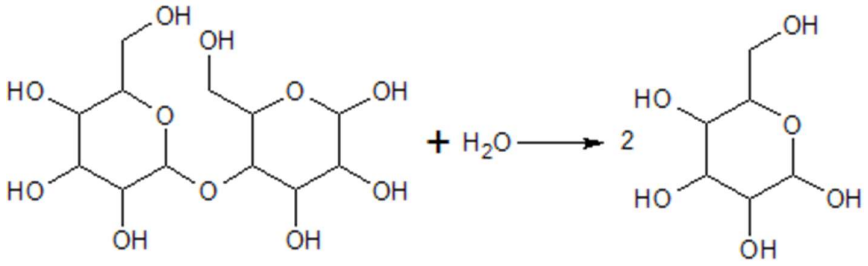

Figure 3: Maltase hydrolysis
The hydrolysis of maltose into glucose (Pantazis, 2013).

The inhibition of both pancreatic alpha-amylase and alpha-glucosidase is a critical first step in lowering the blood glucose concentration and thereby reducing the hyperglycemic status of diabetic patients.

1.2.2. Insulin secretion

Glucose reaches pancreatic beta-cells and enters the cell via a GLUT2 membrane transport protein, **Figure 4**. Glucose is then broken down by the glycolytic pathway into pyruvate which is metabolised by the citric acid cycle to produce ATP. Increased levels of ATP lead to the closure of ATP-sensitive potassium channels which reduces the efflux of potassium ions. The build-up of potassium ions in the cell causes the cell membrane to depolarize which stimulates voltage-dependent calcium channels to take up more calcium ions. The increased influx of calcium ions stimulates the calcium-dependent secretion of insulin granules from pancreatic beta-cells.

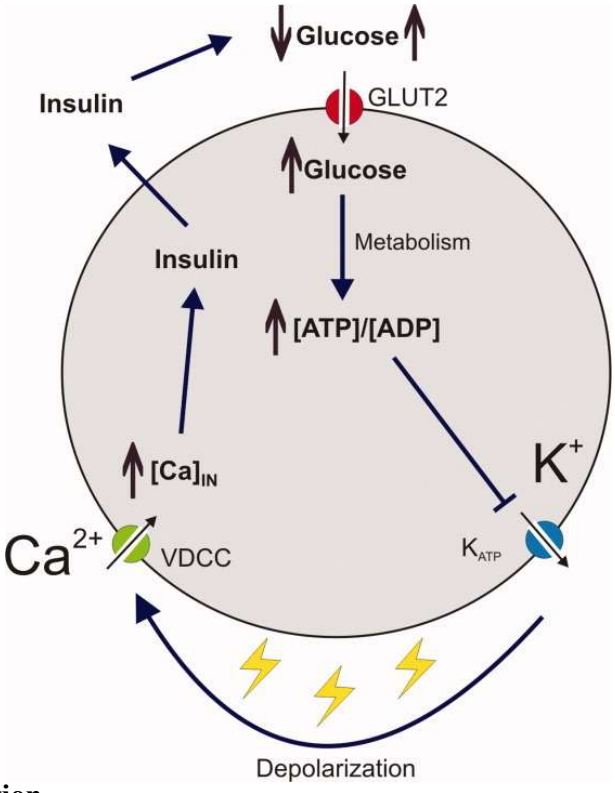

Figure 4: Insulin secretion
The glucose stimulated secreation of insulin from pancreatic beta-cells (Alejandro *et al.*, 2009).

Insulin enters the bloodstream and stimulates target cells to increase glucose uptake thereby decreasing the blood glucose concentration. Insulin also inhibits the secretion of glucagon from pancreatic alpha-cells. Glucagon is a peptide hormone that increases the blood glucose concentration by promoting the release of glucose from skeletal muscle cells and hepatocytes (Wang *et al.*, 2013).

Several factors can affect the functionality of pancreatic beta-cells which could ultimately lead to T2D. The autoimmune destruction of pancreatic beta-cells that is normally associated with T1D is usually caused by monogenetic factors. On the other hand, T2D can be caused by a wide range of gene expression defects as well as several environmental factors, such as an unhealthy diet of saturated fatty acids and simple sugars. Increased consumption of glucose can lead to glucotoxicity and oxidative stress in pancreatic beta-cells. Furthermore, increased consumption of saturated fats can cause lipotoxicity in pancreatic beta-cells. The increased need for insulin can also cause beta-cell exhaustion, endoplasmic reticulum stress, and islet amyloidosis. Pancreatic beta-cells become exhausted when insulin granules are depleted and insulin availability decreases. Exposure to high levels of glucose and fatty acids also causes endoplasmic reticulum stress when beta-cells become overwhelmed by the production of the proteins required for insulin production and secretion. Islet amyloid fibrils are formed from amylin which is deposited around the capillaries and eventually within the islets. These mechanisms of beta-cell dysfunction all contribute to the manifestation of T2D (Girgis and Gunton, 2012).

1.2.3. The effects of insulin

Insulin binds to the transmembrane insulin receptor (IR) of skeletal muscle cells, adipocytes, and hepatocytes. This binding initiates a signalling cascade that ultimately leads to a decrease in blood glucose concentration. The binding of insulin to the extracellular domain of the IR stimulates the autophosphorylation of the intracellular domain. Insulin receptor substrate (IRS) is then able to bind to intracellular receptor sites and become phosphorylated by the activated IR. Phosphorylated IRS activates phosphoinositide-3-kinase (PI3K) by recruiting it to the plasma membrane and by phosphorylation. Activated PI3K phosphorylates phosphotidylinositol-3,4-bisphosphate (PIP2) to produce phosphatidylinositol-3,4,5-trisphosphate (PIP3). PIP3 activates phosphoinositide-dependent kinase 1 (PDK1) which is then able to activate protein kinase B (PKB), also known as Akt. Activated PKB stimulates the translocation of GLUT4-containing vesicles to deliver GLUT4 to the plasma membranes of skeletal muscle cells and adipocytes, **Figure 5**. Additional GLUT4 allows for increased uptake of glucose from the bloodstream and subsequently there is a reduction in the blood glucose concentration. This insulin-stimulated cascade is terminated when protein tyrosine phosphatase 1B (PTP1B) dephosphorylates the IR (Schinner *et al.*, 2005).

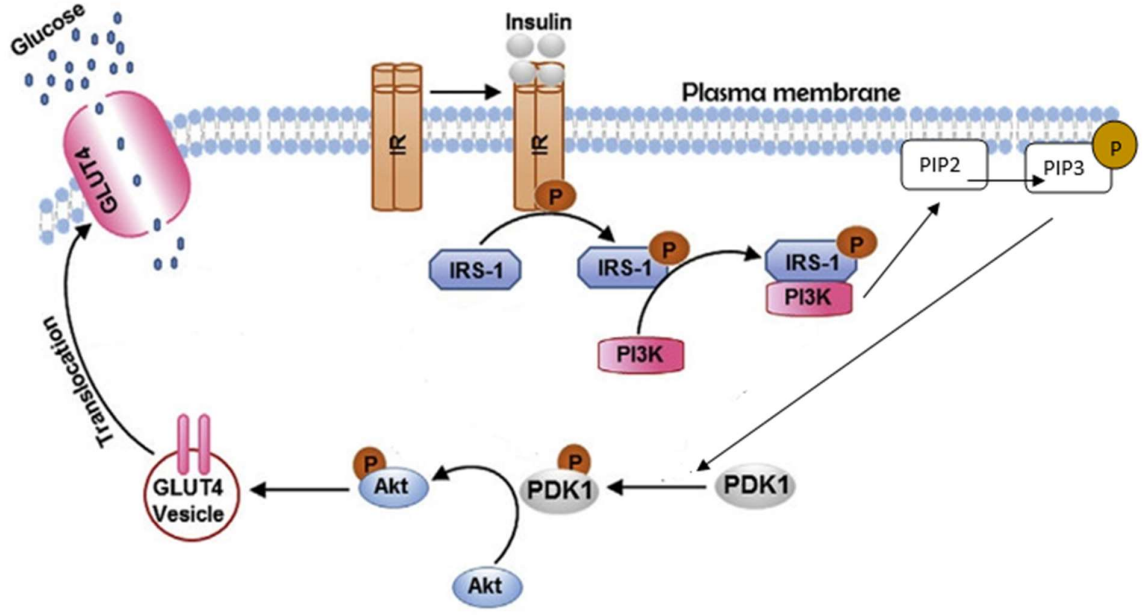

Figure 5: Glucose uptake
The insulin-dependent uptake of glucose in skeletal muscle cells and adipocytes (Alam *et al.*, 2019b).

Insulin activates the rate-limiting enzymes of glycolysis which is the process that breaks down incoming glucose. Glycolysis provides ATP as well as substrates that enter energy storage pathways such as glycogenesis and lipogenesis. Glucokinase (GK) is the enzyme that catalyses the first step of glycolysis

and phosphorylates glucose to produce glucose-6-phosphate in hepatocytes (Hodgkin, 1971). Activated PKB activates GK gene expression and thereby stimulates the phosphorylation of incoming glucose. Another rate-limiting enzyme of glycolysis is phosphofructokinase-1 (PFK-1) which is allosterically activated by fructose-2,6-bisphosphate (F26BP). Activated PKB activates a protein phosphatase that dephosphorylates and thereby activates phosphofructokinase-2 (PFK-2) which is the enzyme responsible for the phosphorylation of fructose-6-phosphate to produce F26BP, **Figure 6** (Wu *et al.*, 2005).

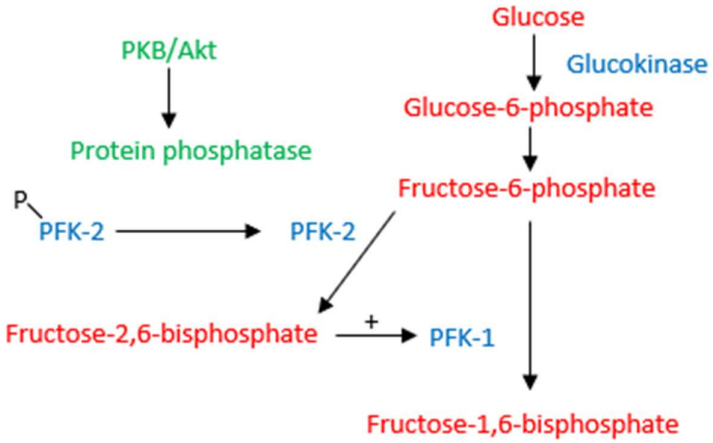

Figure 6: PFK-1 regulation

Insulin stimulates the storage of glucose as glycogen in a process known as glycogenesis. Activated PKB is also responsible for the phosphorylation and inactivation of glycogen synthase kinase 3 (GSK-3). Inactivated GSK-3 is unable to catalyse the conversion of inactive phosphorylated glycogen synthase (GS) to active dephosphorylated GS, is responsible for the incorporation of glucose into glycogen, **Figure 7**. GS is also allosterically activated by glucose-6-phosphate which increases when glucose enters hepatocytes via GLUT2. Activated PKB can activate protein phosphatase-1 (PP-1) which is also responsible for the dephosphorylation of GS as well as the inactivation of glycogen phosphorylase (Nagpal *et al.*, 2012). Inactivation of GP decreases the release of glucose from glycogen stores and thereby prevents glucose secretion by the liver (Jensen and Lai, 2009).

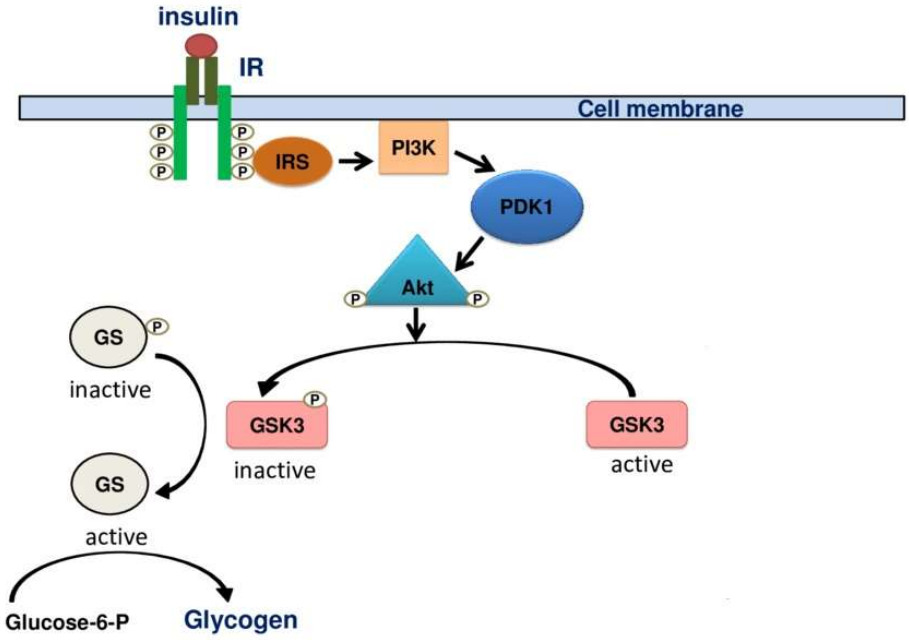

Figure 7: Glycogenesis activation
The activation of glycogenesis by insulin-signalling pathway in hepatocytes (Ahmed *et al.*, 2013).

Insulin also inhibits glucose production and release from hepatocytes. Activated PKB can regulate the expression of the rate determining enzymes of gluconeogenesis at the transcriptional level. These enzymes are phosphoenolpyruvate carboxykinase and glucose-6-phosphatase. Gluconeogenesis is the process of glucose production from lactate, glycerol, and alanine during the fasting state when the glycogen stores are depleted. This process must be inhibited during the fed state by insulin to prevent the release of glucose into the bloodstream (Hatting *et al.*, 2018).

Insulin affects the metabolism of lipids in adipose tissue by decreasing the concentration of non-esterified fatty acids available to muscle cells for energy production. This allows incoming glucose to be used as an energy source instead of fatty acids. Insulin reduces the release of non-esterified fatty acids by inhibiting hormone-sensitive lipase activity which decreases the rate of lipolysis. Insulin also affects the metabolism of proteins in muscle cells by decreasing the release of amino acids and increasing their incorporation into proteins. Reducing the amino acid concentration in the bloodstream prevents the liver from producing glucose via gluconeogenesis (Dimitriadis *et al.*, 2011).

1.3. Antidiabetics

1.3.1. Current treatments

Several antidiabetics are available to manage T2D; however, most of these commercially available antidiabetics have some undesirable side effects. Insulin is mostly used to treat T1D and some severe cases of T2D (Roglic, 2016). Diabetes is a complex disease and existing drugs target specific aspects of diabetes such as inhibiting the systemic uptake of glucose or promoting glucose uptake in insulin sensitive tissues or inhibiting gluconeogenesis.

Inhibition of digestive enzymes such as pancreatic alpha-amylase and alpha-glucosidase, which are involved in the hydrolysis of consumed carbohydrates, results in delayed glucose absorption and thereby prevents a rapid increase in blood glucose concentration after a meal. The drug acarbose is an inhibitor of this process. However, acarbose has some undesirable side effects such as abdominal pain, flatulence, and diarrhea (Ross *et al.*, 2004).

In contrast, the drug metformin, a common antidiabetic drug, lowers blood glucose levels by inhibiting gluconeogenesis. One of the advantages of metformin is that it does not cause hypoglycemia or stimulate insulin secretion. Metformin also stimulates glucose-uptake in insulin-resistant skeletal muscle cells by stimulating adenosine monophosphate-activated protein kinase (AMPK) which activates AKT to initiate GLUT4 translocation to the cell membrane (Elmadhun *et al.*, 2013). Metformin does however have some gastrointestinal side effects, such as, abdominal discomfort, bloating, and metallic taste (Ross *et al.*, 2004). The focus of this research is to address these limitations by identifying which natural plants contain compounds that could possibly have similar antidiabetic effects as current drugs but with fewer side effects.

1.3.2. Natural compounds

One of the unfortunate consequences of hyperglycemia is the generation of reactive oxygen species (ROS) which cause lipid peroxidation and membrane damage. ROS are also responsible for the development of complications associated with T2D such as neuropathy, nephropathy, and cataracts. Natural compounds contain antioxidants, such as polyphenols which scavenge free radicals and inhibit hydrolytic and oxidative enzymes (Patel *et al.*, 2012).

Several edible plants have already been determined to inhibit pancreatic alpha-amylase as well as alpha-glucosidase (Seetaloo *et al.*, 2019). They have also been shown to exhibit insulin-mimicking properties that lead to the stimulation of glucose-uptake in skeletal muscle cells and adipocytes, as well as increased glucose utilization and storage (Bi *et al.*, 2017).

Serval advantages to using natural compounds as an alternative to synthetic hypoglycemic drugs is that they have fewer side effects, are easily available, and contain numerous bioactive compounds. Another advantage of using natural compounds as a treatment for T2D is that one compound could have multiple protein targets to lower blood glucose concentration (Pereira *et al.*, 2019).

1.4. Aim

To analyse the *in silico* properties, the digestive enzyme inhibition and cellular glucose-uptake inducing ability of the selected compounds present in herbs, spices, and medicinal plants.

1.4.1. Null hypothesis

$H_0$1: There will be no statistically significant difference in the K_i values between acarbose and the compounds at a 95% level of confidence.

$H_0$2: The compounds will not significantly increase the glucose-uptake ability of selected cell lines at a 95% level of confidence.

1.4.2. Objectives

1. *In silico* analysis of the compounds in herbs and spices
2. Pancreatic alpha-amylase enzyme assay on selected compounds
3. Alpha-glucosidase enzyme assay on selected compounds
4. SRB cytotoxicity assay of selected compounds in Caco2, HepG2, and C2C12 cell lines
5. Glucose-uptake assay of selected compounds in HepG2 and C2C12 cell lines
6. Extraction and analysis of the content of selected compounds in green tea (*Camellia sinensis*)
7. Targeted and untargeted tea metabolomics with *in vitro* inhibition of digestive enzymes

1.5. Experimental design

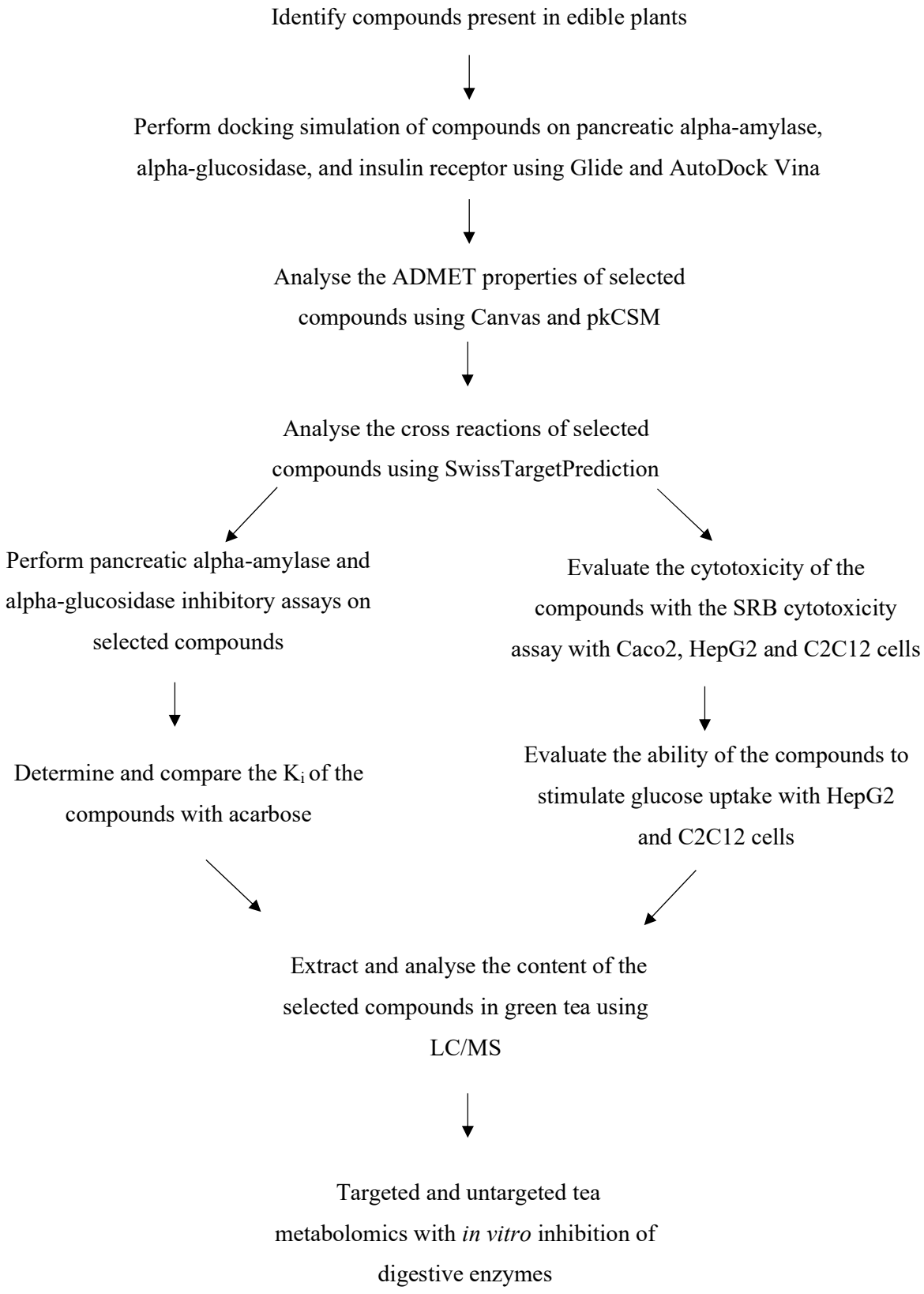

CHAPTER 2: *In silico* analysis

2.1. Introduction

In silico docking is a powerful tool, to initially determine if compounds can bind enzymes or receptors of interest. Likewise, the absorption, distribution, metabolism, excretion, and toxicity (ADMET) of the compounds can also be estimated. As this study focuses on the identification of compounds that can be used for the treatment of diabetes the focus is on the ability of the selected compounds to bind and inhibit pancreatic alpha-amylase and alpha-glucosidase, as well as the ability to stimulate cellular uptake of glucose by stimulation of the insulin receptor and inhibition of tyrosine-protein phosphatase.

2.1.1. Virtual docking simulation

The *in silico* analysis of the compounds in herbs and spices is a quick and inexpensive way to narrow down which compounds should be analysed using *in vitro* methods.

Before the ligands can be virtually docked, they need to be prepared using LigPrep (Schrödinger, 2015a). LigPrep has a smiles_to_mae conversion tool that converts simplified molecular-input line-entry system (SMILES) into a Maestro-formatted file (mae) and is further prepared by LigPrep. LigPrep uses Epik, a template-based tautomerization software program that generates different ionization states for each ligand (Shelley *et al.*, 2007). LigPrep also uses a tautomerize and stereoizer tool to generate different tautomers and stereoisomers for each ligand.

Glide (Schrödinger, 2021) is the virtual docking program that determines the free energy required by each compound to bind to the active site of pancreatic alpha-amylase, alpha-glucosidase, and the insulin receptor. A negative docking score represents a spontaneous reaction and, therefore, a greater binding affinity of the compound to the enzyme. The docking score of each compound can be compared to the docking score of acarbose and metformin. Each compound will produce several docking scores, each score representing a different pose and possible ligand-protein binding combinations. The most negative docking score for each compound will be compared to each other as well as acarbose and metformin.

Glide uses an empirical scoring function known as GlideScore that estimates the free energy for a protein-ligand complex. Each ligand has several contacts with the ligand-binding site which is in the Glide grid of the enzyme. Each interaction between the ligand and the protein either releases or requires free energy which can be predicted by the Glide algorithm (Eldridge *et al.*, 1997). Glide is a software package that uses a series of hierarchical filters that eliminates unlikely docking conformations and orientations and only calculates the docking score for the most likely orientations. The GlideScore function, **Figure 8**, can then predict the binding affinity and rank these compounds.

$$\Delta G_{bind} = C_{lipo\text{-}lipo}\Sigma f(r_{lr})^1 + C_{hbond\text{-}neut\text{-}neut}\Sigma g(\Delta r)h(\Delta\alpha)^2 + C_{hbond\text{-}neut\text{-}charged}\Sigma g(\Delta r)h(\Delta\alpha)^3 + C_{hbond\text{-}charged\text{-}charged}\Sigma g(\Delta r)h(\Delta\alpha)^4 + C_{max\text{-}metal\text{-}ion}\sum f(r_{lm})^5 + C_{polar\text{-}phob}V_{polar\text{-}phob}{}^6 + C_{rotb}H_{rotb}{}^7 + C_{coul}E_{coul}{}^8 + C_{vdW}E_{vdW}{}^9 + \text{solvation terms}^{10}$$

Figure 8: GlideScore function

The free energy of each type of interaction between the protein and ligand. The lipophilic-lipophilic term[1] considers the interaction energies between lipophilic atoms. The hydrogen-bonding term is separated into three components depending on whether the donor and acceptor are both neutral[2], both charged[4], or one is charged and one is neutral[3]. The metal-ligand interaction term[5] considers any interactions of metal atoms with donor or acceptor ions. The sixth term[6] considers when a polar atom is found in a hydrophobic region. The next terms consider the contributions of rotatable bonds[7], Coulomb[8], and Van der Waals[9] interaction energies between the ligand and the protein. The solvation terms[10] consider the restrictions on the ligand that arise from the requirement of charged and polar groups to be adequately solvated (Friesner *et al.*, 2004).

DIA-DB is a database and web server for the prediction of diabetes drugs that uses AutoDock Vina to perform docking-based calculations. AutoDock Vina uses a structure-based docking approach that determines whether a compound interacts with the active site of the protein. These protein targets are the enzymes that are involved in insulin secretion and sensitivity (**Figures 4, 5, 6, and 7**) as well as the enzymes involved in glucose and lipid metabolism (Perez-Sanchez *et al.*, 2020). The AutoDock Vina scoring function works similar to the GlideScore function because it also determines the bound conformation preference and the free energy of binding (Trott and Olson, 2010).

2.1.2. ADMET screening

The ADMET properties of a drug can also be predicted using a computer program known as Canvas version 3.8 by Schrodinger and an online tool known as pkCSM. pKCSM uses predictive quantitative structure-activity relationship (QSAR) modelling of ADMET properties (Obrezanova *et al.*, 2007). The ideal drug should obey Lipinski's rule of five' which predicts the drug-likeness of a compound intended for an oral route of administration. The rule of five pertains to the molecular weight of the compound which should be less than 500 g/mol, and the logP value which should be less than 5. The number of hydrogen donors should be less than or equal to 5, and the number of hydrogen acceptors should be less than or equal to 10 (Chagas *et al.*, 2018). The number of stars refers to the number of QikProp descriptors whose values fall outside the 95% range of similar values for known drugs (Ntie-Kang *et al.*, 2014). A large number of stars suggests that the compound is less drug-like than compounds with fewer stars (Schrödinger, 2015b, Jorgensen and Duffy, 2000).

The absorption of a drug is described by the percentage of human intestinal absorption also known as bioavailability and relates to the compound's molecular weight, lipophilicity, and polar surface area. The bioavailability represents the percentage of the consumed compound that is absorbed into the bloodstream from the small intestine (Kelder *et al.*, 1999). Another predictor of oral absorption potential

is Caco2 permeability which represents Caco2 cell permeability in the small intestine (Yazdanian *et al.*, 1998). Orally active drugs are primarily absorbed in the small intestine because it has the largest surface area for drug absorption when compared to the rest of the gastrointestinal tract, it has a higher pH than the stomach, and the drug is in contact with the small intestine for a longer period of time (Vertzoni *et al.*, 2019). Caco-2 permeability can be predicted as the logarithm of the apparent permeability coefficient (logPapp) in log cm/s. The Caco-2 cell line is composed of human epithelial colorectal adenocarcinoma cells which are usually used to determine the *in vitro* absorption of orally administered drugs. P-glycoprotein is an ATP binding cassette (ABC) transporter that exports xenobiotic compounds from diverse cells and interferes with therapeutic drug delivery. pkCSM can predict whether a compound is a P-glycoprotein substrate or inhibitor (Alam *et al.*, 2019a).

The distribution of a drug can be described by the steady state volume of distribution (VDss) which measures the extent to which the compound distributes itself throughout the body. VDss is defined as the volume of blood that contains the same concentration of compound as the vascular tissues (Yates and Arundel, 2008). The fraction unbound refers to the fraction of compound that is not bound to plasma proteins which enhances drug efficiency (Berezhkovskiy, 2010). The penetration of the drug across the blood-brain barrier (BBB) would be undesirable in this case because the compounds that are being analysed are not intended to be active in the central nervous system. pkCSM is able to predict BBB permeability and central nervous system (CNS) permeability.

The metabolism of a drug can be described by its ability to activate or inhibit cytochrome P_{450} isoenzymes. Unwanted inhibition of CYP_{450} isoenzymes can result in drug toxicities and adverse drug reactions (Ogu and Maxa, 2000). The elimination of a drug can be described by the total drug clearance which encompasses the hepatic and renal clearance of the drug. Total drug clearance was defined as the volume of plasma completely cleared of the drug per unit time (Chiou, 1982).

Several toxicity properties can be predicted by pkCSM such as rat LD_{50} which is the dosage of a compound that would kill 50% of a group of test rats. AMES toxicity predicts the compound's mutagenic potential. *Tetrahymena pyriformis* toxicity predicts the dosage of the compound that inhibits the growth of 50% (IGC_{50}) *T. pyriformis.* Minnow toxicity predicts the lethal concentration (LC_{50}) of the compound that kills 50% of fathead minnows. The maximum tolerated dose of the compound can help estimate the recommended starting dose of the compound. Oral rat chronic toxicity predicts the highest dose of the compound where no adverse effects are observed. Hepatotoxicity predicts whether the compound is likely to disrupt normal liver function (Pires *et al.*, 2015). Another measure of toxicity is whether the compound is a hERG inhibitor. The hERG channels are K^+ channels in the heart and drug-induced

blockage of K^+ channels leads to QT prolongation and the occurrence of torsades de points (Cavalli *et al.*, 2002).

2.1.3. SwissTargetPrediction

SwissTargetPrediction is an online tool that predicts the most likely protein targets of small molecules out of 3068 macromolecular targets. These predictions are based on the similarity principle through reverse screening (Daina *et al.*, 2019). Compounds that interact with unintended proteins in the body could lead to unforeseen side effects (Gfeller *et al.*, 2013).

The aim of the research undertaken in this chapter is to narrow down the number of possible antidiabetics present in herbs, spices, and medicinal plants from 1070 to 6. *In silico* studies allows for the rapid sorting of hundreds of compounds based on their chemical structure. Virtual docking was performed on the 1070 compounds and 20 compounds with a range of docking scores was selected. The ADMET properties of these 20 compounds was predicted and compared to acarbose and metformin. Six compounds, that were less toxic than acarbose, were selected for *in vitro* testing.

2.2. Methods

Virtual docking simulations were performed using a computer program known as Maestro version 11.8 which uses the Glide algorithm. The SMILES of 1070 compounds in herbs and spices was provided by Pereira *et al.* (2019) as well as acarbose and metformin, and docked into the active site of pancreatic alpha-amylase, alpha-glucosidase, and insulin receptor (Jhong *et al.*, 2015). The protein database code for pancreatic alpha-amylase is 4GQR, alpha-glucosidase is 3L4Y, the insulin receptor is 3EKN and tyrosine-protein phosphatase non-receptor type 9 is 4GE6.

The three-dimensional structure of each protein was imported from the Protein Data Bank. The protein was prepared by preprocessing it using default settings. After preprocessing, all the proteins, chains, and waters were deleted except for the ligand. The preprocessed protein was optimized and minimized using the default settings. The receptor Glide grid was generated from the minimized protein using the default settings, similar to the preparation steps described by Tendulkar and Mahajan (2014).

The 1070 compounds were imported into Glide and prepared using the ligand preparation default settings. The prepared ligands and Glide grid were imported into the virtual screening workflow. The ligands were docked with Glide HTVS, and 100% of the results were kept after docking.

The selected compounds were submitted to the DIA-DB web server (http://bio-hpc.ucam.edu/dia-db/) and the AutoDock Vina scoring function was obtained. The Glide and AutoDock Vina docking scores was compared using the Pearson's and Spearman's correlation coefficinents. The Pearson's coeffiecent was calculated using the Pearson formula in excel and the Spearman's coefficient was calculated by using the Correl formula in excel based on the rank of each value.

The docking score of each compound in herbs and spices was obtained by this high-throughput screening process. A more negative docking score represents a high binding affinity because a negative free energy change is associated with a more spontaneous reaction. Six compounds with a range of docking scores were selected and analysed further using Canvas, pkCSM, and SwissTargetPrediction.

The selected compounds were imported into Canvas 3.8. These structures were minimized and incorporated automatically using default settings. The physiochemical descriptors were calculated and incorporated automatically using default settings. pkCSM (http://biosig.unimelb.edu.au/pkCSM/) was used to predict ADMET properties for the selected compounds (Pires *et al.*, 2015). The selected compounds were imported into pkCSM as smi files, and the results were exported as an Excel file. SwissTargetPrediction (http://www.swisstargetprediction.ch/) was used to predict the potential protein targets of the selected compounds in *Homo sapiens*. Each compound's SMILES was imported into the SwissTargetPrediction website, and the results were exported as an Excel file (Daina *et al.*, 2019).

2.3. Results

2.3.1. Docking scores

Glide is a virtual docking program by Schrodinger that predicts the Glide docking score of the compounds in the proteins of interest. DIA-DB is a web server that predicts the AutoDock Vina score of the compounds using inverse docking procedures.

The Glide docking scores of rutin, caffeic acid, *p*-coumaric acid, vanillin, ethyl gallate, and oxalic acid were compared to acarbose for pancreatic alpha-amylase (4GQR) and alpha-glucosidase (3L4Y). Rutin has a more negative docking score than acarbose for 4GQR, which suggests that rutin could potentially be a better inhibitor than acarbose. Caffeic acid, *p*-coumaric acid, and ethyl gallate had similar docking scores to that of acarbose for 4GQR. Vanillin and oxalic acid had more positive docking scores than acarbose. The docking score of rutin was similar to that of acarbose for 3L4Y, and the other five compounds had more positive docking scores than acarbose. The AutoDock Vina scores of rutin and acarbose were similar for 4GQR and 3L4Y. Caffeic acid, *p*-coumaric acid, ethyl gallate, and vanillin had more positive AutoDock Vina scores than acarbose and rutin for 4GQR and 3L4Y, and oxalic acid had the most positive AutoDock Vina score. **Supplementary Table 1** shows the docking scores of acarbose, rutin, caffeic acid, *p*-coumaric acid, vanillin, ethyl gallate, and oxalic acid docked in the active site of pancreatic alpha-amylase (4GQR), and alpha-glucosidase (3L4Y) as well as the number interactions that each ligand has with the amino acids in the protein's binding pocket. **Supplementary Figure 1** shows the selected compounds docked into the active site of pancreatic alpha-amylase (4GQR) and alpha-glucosidase (3L4Y) as well as the binding pocket for these two proteins. This experiment does not have known inhibitors for 3EKN or 4GE6; therefore, the selected compounds cannot be compared to a positive control. The correlation between the Glide and AutoDock Vina docking scores for each compound is represented in **Figure 9**.

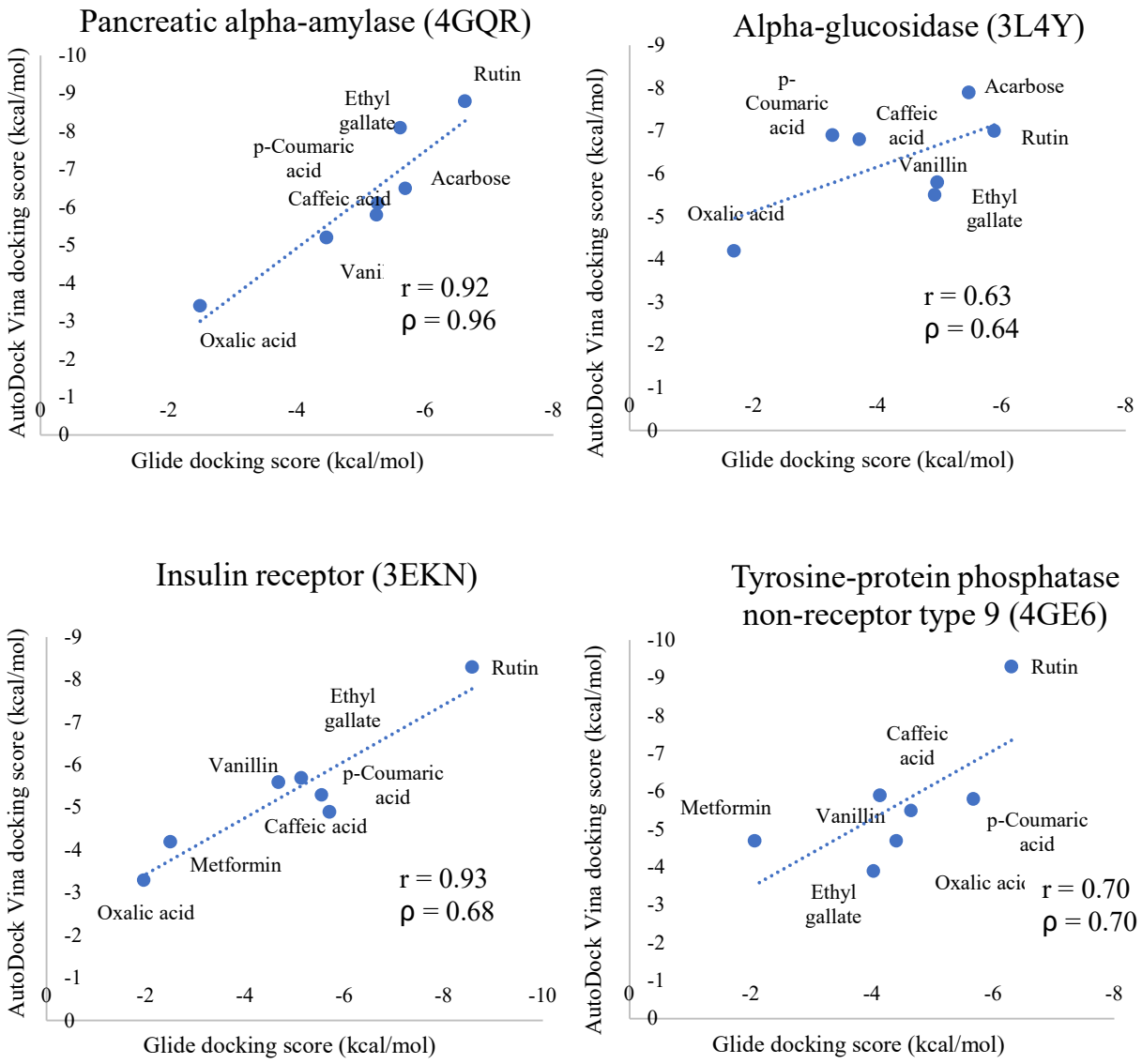

Figure 9: The correlation of Glide and AutoDock Vina docking scores

There was a strong positive Pearson correlation coefficient (r) between the Glide and AutoDock Vina docking scores for 4GQR, and 3EKN ($r \approx 0.9$), and a moderate correlation for 3L4Y, and 4GE6 ($r \approx 0.6$). The Spearman correlation coefficient (ρ) is similar to the Pearson correlation coefficient for 4GQR, 3L4Y, and 4GE6. However, the Pearson and Spearman correlation coefficients for 3EKN were different which suggests that the rankings of compounds for AutoDock Vina and Glide docking scores were different (Schober *et al.*, 2018).

2.3.2. ADMET results

Canvas is a software program by Schrodinger that can determine the molecular weight, logP value, and number of hydrogen donors and acceptors. **Table 1** lists these properties of selected compounds as well as the number of stars associated with each compound. The number of stars represents the number of

QikProp descriptor values that fall outside the 95% range of similar values for known drugs; a large number of stars suggests that a compound is less drug-like than a compound with fewer stars (Schrödinger, 2015b).

Table 1: Lipinski's rule of five for acarbose (control) and the selected compounds

Compound	MW (g/mol)	logP	HBA	HBD	#rule of 5 violations	#stars
Acarbose	645.60	-6.84	18	13	3	13
Caffeic acid	180.16	1.26	2	2	0	0
Ethyl gallate	198.17	1.23	5	3	0	0
Insulin	5777.65	-18.73	82	77	3	-
Metformin	129.16	-0.74	2	1	0	2
Oxalic acid	90.03	-0.48	0	0	0	7
***p*-Coumaric acid**	164.16	1.53	1	1	0	0
Rutin	610.52	-0.23	16	10	3	9
Vanillin	152.15	1.31	3	1	0	0

MW – molecular weight, logP – logarithm of the partition coefficient, HBA- number of hydrogen bond acceptors, HBD – number of hydrogen bond donors

According to Lipinski's rule of 5, an orally active drug should have a molecular weight less than 500 g/mol. Acarbose and rutin have molecular weights greater than 500 g/mol and so does insulin. Insulin is a peptide hormone, and due to the proteolytic enzymes in the gastrointestinal tract (GIT) will lose activity, therefore is administered intravenously (Kelly, 2014, Wilcox, 2005). The logP value for all the selected compounds is less than 5. The number of hydrogen bond acceptors should be less than or equal to 10 and the number of hydrogen bond donors should be less than or equal to 5, which is not the case for acarbose, insulin, and rutin. Metformin, *p*-coumaric acid, caffeic acid, vanillin, ethyl gallate, and oxalic acid do not violate Lipinski's rule of 5. Acarbose has the greatest number of stars when compared to the selected compounds.

pkCSM is an online tool that can predict the ADMET properties of a potential orally active drug. **Table 2** lists the absorption properties of the selected compounds which include Caco2 permeability, intestinal absorption, and whether the compound is a P-glycoprotein substrate or inhibitor.

Table 2: pkCSM absorption analysis of acarbose and the selected compounds

Compound	Caco2 permeability (log cm/s)	Intestinal absorption (%)	P-glycoprotein substrate	P-glycoprotein I inhibitor	P-glycoprotein II inhibitor
Acarbose	-0.64	0	Yes	No	No
Caffeic acid	0.50	52.97	No	No	No
Ethyl gallate	0	76.70	Yes	No	No
Insulin	-2.55	0	No	No	No
Metformin	-0.34	59.40	Yes	No	No
Oxalic acid	0.41	79.42	No	No	No
***p*-Coumaric acid**	1.21	93.49	No	No	No
Rutin	-0.95	23.45	Yes	No	No
Vanillin	1.19	84.71	No	No	No

Caco2 cells are human epithelial colorectal adenocarcinoma cells, and Caco2 permeability is predicted as the logarithm of the apparent permeability coefficient. A high Caco2 permeability would be more than 0.90 log cm/s (7.94 cm/s). *p*-Coumaric acid, caffeic acid, vanillin, ethyl gallate, and oxalic acid have a greater Caco2 permeability than acarbose and metformin. In general, *p*-coumaric acid and vanillin have high Caco2 permeability. The intestine is the primary site for the absorption of an orally active drug. A compound with a percentage intestinal absorption less than 30% is considered to be poorly absorbed. Metformin, *p*-coumaric acid, caffeic acid, vanillin, ethyl gallate, and oxalic acid are well absorbed by the small intestine. In contrast, acarbose and rutin are poorly absorbed or not at all. P-glycoprotein is an ABC transporter that exports toxins and xenobiotics out of cells. Acarbose, metformin, rutin, and ethyl gallate were predicted to be P-glycoprotein substrates. All the selected compounds were predicted not to inhibit P-glycoprotein I or II.

The distribution properties of the selected compounds are listed in **Table 3**. Distribution properties include the VDss, the fraction of compounds unbound to serum proteins, and whether the compounds can cross the BBB and be active in the CNS.

Table 3: pkCSM distribution analysis of acarbose and the selected compounds

Compound	VDss (log L/kg)	Fraction unbound (human)	BBB permeability (logBB)	CNS permeability (logPS)
Acarbose	-0.74	0.42	-2.62	-8.18
Caffeic acid	-0.92	0.51	-0.71	-2.93
Ethyl gallate	0.41	0.61	-1.10	-3.38
Insulin	0.01	0.38	-11.43	-17.27
Metformin	-0.23	0.81	-0.95	-4.24
Oxalic acid	-0.62	0.74	0.02	-3.42
***p*-Coumaric acid**	-1.15	0.43	-0.23	-2.42
Rutin	1.66	0.19	-1.90	-5.18
Vanillin	-0.08	0.48	-0.21	-2.12

Human VDss is considered low if it is less than -0.15 log L/kg (0.71 L/kg) and high if it is above 0.45 log L/kg (2.81 L/kg). Rutin, vanillin, ethyl gallate, and oxalic acid have larger VDss values than acarbose. Rutin, vanillin, and ethyl gallate have larger VDss values than metformin. The efficacy of the compound can be affected by the degree to which it binds to serum proteins; a large fraction of unbound compound means that it can diffuse more effectively across cellular membranes. *p*-Coumaric acid, caffeic acid, vanillin, ethyl gallate, and oxalic acid all have larger or similar fractions than acarbose, but none have fractions larger than metformin. A compound with a logBB greater than 0.3 is considered to readily cross the BBB. The logBB value is the logarithmic ratio of brain to plasma drug concentration. All the selected compounds have logBB values less than 0.3. CNS permeability is predicted as the blood-brain permeability-surface area product (logPS), and compounds with logPS values greater than -2 can potentially penetrate the CNS. None of these compounds have logPS values less than -2.

The metabolic properties of the selected compounds were determined by predicting their interaction with the five main cytochrome P_{450} isoenzymes. **Table 4** indicates whether the selected compound is a CYP2D6 or CYP3A4 substrate or inhibitors of CYP1A2, CYP2C19, CYP2C9, CYP2D6, or CYP3A4.

Table 4: pkCSM metabolism analysis of acarbose and the selected compounds

Compound	CYP2D6 substrate	CYP3A4 substrate	CYP1A2 inhibitor	CYP2C19 inhibitor	CYP2C9 inhibitor	CYP2D6 inhibitor	CYP3A4 inhibitor
Acarbose	No	No	No	No	No	No	No
Caffeic acid	No	No	No	No	No	No	No
Ethyl gallate	No	No	No	No	No	No	No
Insulin	No	Yes	No	No	No	No	No
Metformin	No	No	No	No	No	No	No
Oxalic acid	No	No	No	No	No	No	No
***p*-Coumaric acid**	No	No	No	No	No	No	No
Rutin	No	No	No	No	No	No	No
Vanillin	No	No	Yes	No	No	No	No

All the selected compounds were not CYP2D6 substrates and only insulin is a CYP3A4 substrate. All the selected compounds were not CYP inhibitors except for vanillin which was predicted to be a CYP1A2 inhibitor.

The excretion properties of the selected compounds were predicted by pkCSM. **Table 5** lists the total drug clearance which represents the excretion of the compounds by the liver and kidneys.

Table 5: pkCSM excretion analysis of acarbose and the selected compounds

Compound	Total Clearance (log mL/min/kg)
Acarbose	0.48
Caffeic acid	0.54
Ethyl gallate	0.67
Insulin	-13.58
Metformin	0.10
Oxalic acid	0.77
***p*-Coumaric acid**	0.66
Rutin	-0.37
Vanillin	0.67

p-Coumaric acid, caffeic acid, vanillin, ethyl gallate, and oxalic acid have greater total clearance than acarbose and metformin.

The toxicity properties predicted by pkCSM are listed in **Table 6** and include AMES toxicity, the maximum recommended tolerated dosage (MRTD), hERG inhibition ability, oral rat chronic (LOAEL) and acute toxicity, hepatotoxicity, *T. pyriformis* and minnow toxicity.

Table 6: pkCSM toxicity analysis of acarbose and the selected compounds

Compound	AMES toxicity	Max. tolerated dose (log mg/kg/day)	hERG I inhib	hERG II inhib	Rat Acute Toxicity (mol/kg)	LOAEL (log mg/kg/ day)	Hepato - toxicity	*T.pyriformis* toxicity (µg/L)	Minnow toxicity (log mM)
Acarbose	No	0.47	No	Yes	2.39	7.49	No	0.29	13.31
Caffeic acid	No	0.96	No	No	2.09	3.16	No	0.34	2.18
Ethyl gallate	Yes	-0.32	No	No	1.94	2.39	No	0.20	2.71
Insulin	No	0.44	No	No	2.48	35.00	Yes	0.29	88.42
Metformin	Yes	0.90	No	No	2.45	2.16	No	0.25	3.97
Oxalic acid	No	1.40	No	No	1.68	2.96	No	0.28	2.40
***p*-Coumaric acid**	No	1.11	No	No	2.16	2.53	No	0.32	1.61
Rutin	No	0.45	No	Yes	2.49	3.67	No	0.29	7.68
Vanillin	No	1.40	No	No	1.87	2.96	No	0.08	1.60

Metformin and ethyl gallate are AMES positive and may have mutagenic properties. An MRTD greater than 0.48 log mg/kg/day (3.0 mg/kg/day) was considered high. Metformin, *p*-coumaric acid, caffeic acid, vanillin, and oxalic acid have MRTDs greater than 0.48 log mg/kg/day. None of the selected compounds were hERG I inhibitors, and only acarbose and rutin were hERG II inhibitors. The selected compounds have a rat LD_{50} between 1.6 and 2.5 mol/kg. The LOAEL of the selected compounds were less than that of acarbose but more than that of metformin. Only insulin is considered hepatotoxic, and the other compounds were not considered to cause drug-induced liver injury. A *T. pyriformis* IGC_{50} greater than 0.32 µg/L is considered toxic. All compounds, except caffeic acid, had an IGC_{50} less than or equal to 0.32 µg/L. A minnow LC_{50} less than -0.3 log mM is regarded as highly toxic. All the selected compounds had a minnow LC_{50} more than -0.3 log mM.

2.3.3. SwissTargetPrediction

SwissTargetPrediction predicts the probability with which the selected compounds interact with proteins in humans. **Supplementary Table 2** lists the probability that the selected compounds are predicted to interact with protein targets. Acarbose has a near 100% probability of interacting with salivary amylase (AMY1C), and lysosomal alpha-glucosidase. Acarbose has a 77% probability of interacting with pancreatic alpha-amylase and a 42% probability of interacting with maltase-glucoamylase (alpha-glucosidase). Metformin is not predicted to strongly interact with any proteins in the

SwissTargetPrediction database. Rutin is predicted to interact with acetylcholinesterase, adrenergic receptor alpha-2, alpha-2a adrenergic receptor, and neuromedin-U receptor 2 with 100% probability. *p*-Coumaric acid has a 100% probability of interacting with aldose reductase, estrogen receptor beta and several carbonic anhydrase isoenzymes. Caffeic acid also has a 100% probability of interacting with carbonic anhydrase isoenzymes as well as matrix metalloproteinase isoenzymes, arachidonate 5-lipoxygenase, and protein tyrosine phosphatase 1B. Both vanillin and oxalic acid are predicted to not interact strongly with any of the proteins in the SwissTargetPrediction database. Ethyl gallate is predicted to interact with squalene monooxygenase with 100% probability.

2.4. Discussion

In silico drug discovery is a great way of testing the drug-likeness of thousands of compounds in a quick and effective manner. Virtual docking was used to predict the Gibbs free energy change associated with the protein-ligand interaction also known as a docking score. A more negative docking score represents a more spontaneous interaction and better binding affinity. Glide uses a Glide scoring function, and DIA-DB uses an AutoDock Vina scoring function. Even though Glide and AutoDock Vina use slightly different formulas to predict the docking score, the relative docking scores should be similar, and the ranking should correspond.

Compounds that had docking scores similar to acarbose were selected. These compounds should be less toxic or at least as toxic as the currently available commercial antidiabetics. Compounds with a weaker binding affinity than acarbose were also selected to act as negative controls. The three compounds that were selected were rutin, *p*-coumaric acid, and caffeic acid, and the three negative controls selected were ethyl gallate, vanillin, and oxalic acid. As presented in **Figure 10,** acarbose is a pseudotetrasaccharide that is a known alpha-glucosidase and pancreatic alpha-amylase inhibitor. Rutin, also known as quercetin 3-rutinoside, is a flavonoid. Caffeic acid and *p*-coumaric acid are hydroxycinnamic acid derivatives. Ethyl gallate is the ethyl ester of gallic acid which is a type of phenolic acid. Vanillin is the reduced form of vanillic acid; and oxalic acid is a dicarboxylic acid (NCBI, 2020).

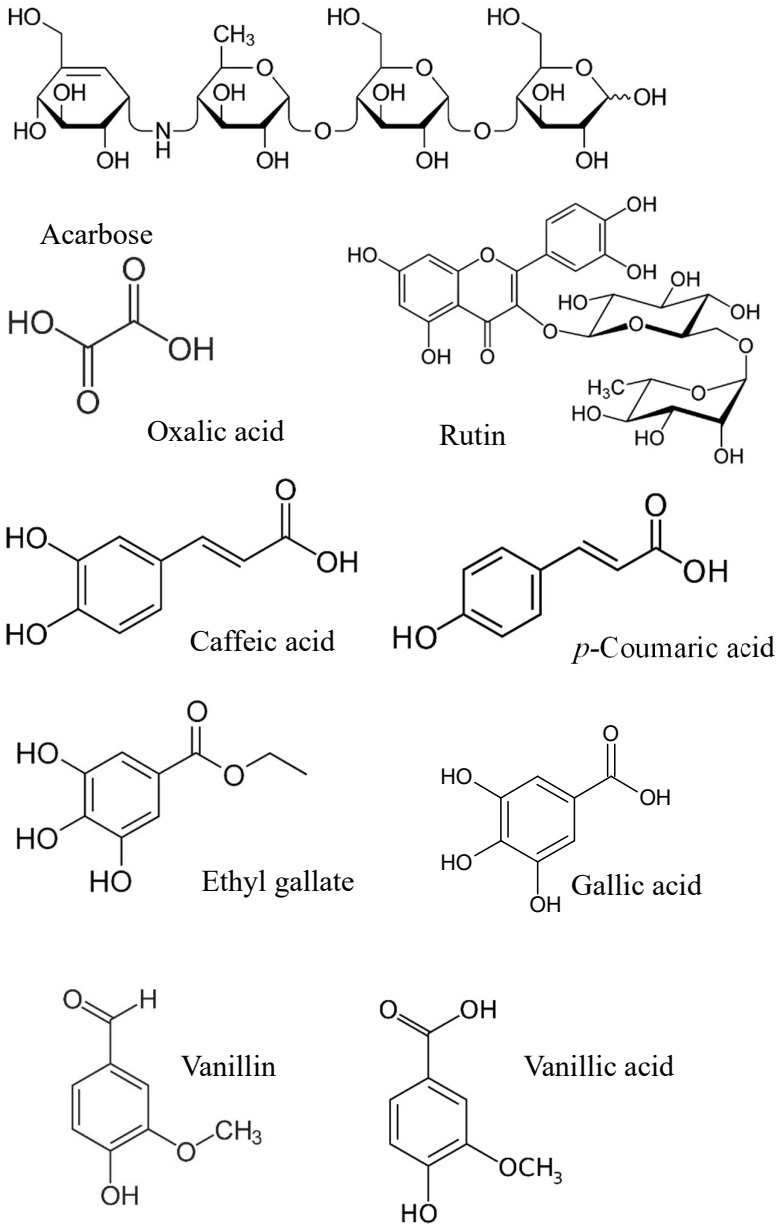

Figure 10: Chemical structures of acarbose and the selected compounds

DIA-DB docks the selected compounds into eighteen protein targets associated with diabetes. Four of these protein targets are pancreatic alpha-amylase (4GQR), intestinal maltase-glucoamylase (3L4Y), insulin receptor (3EKN), and tyrosine-protein phosphatase non-receptor type 9 (4GE6). These same PDB codes were used to dock the compounds in Maestro. Pancreatic alpha-amylase and intestinal maltase-glucoamylase are digestive enzymes in the small intestine that hydrolyse starch into maltose and maltose into glucose, respectively. The inhibition of these enzymes would slow down the release of glucose from starch and, therefore, the rise in blood glucose concentration. The insulin receptor is present on hepatocytes, adipocytes, and skeletal muscle cells. In diabetes these cells are insensitive to the effects of insulin. Stimulation of the insulin receptor initiates the signal cascade that leads to an increase in intracellular glucose associated with a decrease in blood glucose levels. Tyrosine-protein phosphatase non-receptor type 9 is an enzyme in insulin-target cells that dephosphorylates and, therefore, inactivates the insulin receptor which terminates the signal cascade. The inhibition of this enzyme would allow the signal cascade to continue and the blood glucose level to decrease.

Supplementary Table 1 shows the docking scores of acarbose and the selected compounds for pancreatic alpha-amylase and alpha-glucosidase in the order of most to least negative. Maestro predicts several docking scores for each compound that represent the different poses and conformations of the compound. The most negative docking score for each compound is represented in **Figure 9 and Supplementary Table 1**. The compounds with the most negative docking scores also have the most number of interaction points between the ligand and the binding pocket. The docking score of acarbose can be compared to the selected compounds for pancreatic alpha-amylase and alpha-glucosidase. The docking score of metformin cannot be compared to the selected compounds because metformin does not interact with the insulin receptor or tyrosine-protein phosphatase non-receptor type 9 (Jingchun *et al.*, 2015). In **Figure 9,** the positive correlation between the Glide and AutoDock Vina docking scores for all four protein targets is presented. This positive correlation demonstrates that the docking scores between Glide and AutoDock Vina are quantitatively different but relatively the same. The difference in docking score values between these two programs is due to the difference in algorithms used to calculate the docking score. There was a strong Spearman correlation coefficient which suggests that the compounds are ranked in a similar manner according to the Glide and AutoDock Vina docking scores. It can be concluded that either program can be used to rank the docking scores of compounds as diabetes protein targets.

Rutin, had a better Glide docking score than acarbose. Caffeic acid, *p*-coumaric acid, and ethyl gallate had similar Glide docking scores to acarbose for pancreatic-alpha amylase. Rutin, ethyl gallate, and vanillin had similar Glide docking scores to acarbose for alpha-glucosidase. Rutin had a similar

AutoDock Vina docking score to acarbose for pancreatic-alpha amylase. Rutin, caffeic acid, and *p*-coumaric acid had AutoDock Vina docking scores similar to acarbose for alpha-glucosidase. Oxalic acid had the largest Glide and AutoDock Vina docking score for both enzymes when compared with the other selected compounds. Ethyl gallate and vanillin had AutoDock vina docking scores larger than acarbose for both enzymes, **Supplementary Table 1**. Oxalic acid, ethyl gallate, and vanillin were selected as negative controls.

The next step in predicting the drug-likeness of a compound is to determine whether the compound follows Lipinski's rule of five and predict its ADMET properties. Canvas is a computer program that predicts the molecular weight, logP value, the number of hydrogen bond acceptors and donors. According to Lipinski *et al.* (2012), poor absorption is more likely when the compound has a molecular weight greater than 500 g/mol, a logP value greater than 5, more than 10 hydrogen bond acceptors, and more than 5 hydrogen bond donors. **Table 1** shows that acarbose, insulin, and rutin violate three of the rule of five, because these compounds are too large to be absorbed from the small intestine into the bloodstream. When analysing a compound as a potential digestive enzyme inhibitor, it is not required to enter the bloodstream but remain in the small intestine. In contrast, a potential glucose-uptake stimulator is required to be absorbed into the bloodstream to reach the target cells. **Table 1** also lists the number of stars associated with each compound. Acarbose has 13 stars which is more than the selected compounds indicating more drug-like properties than acarbose.

pkCSM is a web-based server that can predict several ADMET properties of selected compounds. Absorbance, in this case, refers to the drug's ability to be transported across the small intestine's membrane into the bloodstream. The compounds that have greater Caco-2 permeability than acarbose and metformin are *p*-coumaric acid, caffeic acid, vanillin, ethyl gallate, and oxalic acid. Human intestinal absorption was predicted as the percentage of compound absorbed through the small intestine. Acarbose and insulin are not absorbed through the small intestine and rutin is poorly absorbed. Metformin, *p*-coumaric acid, caffeic acid, vanillin, ethyl gallate, and oxalic acid are well absorbed through the small intestine. Acarbose, rutin, and insulin do not follow three of the rules of five explaining why these compounds are not well absorbed through the small intestine. When assessing these compounds as digestive enzyme inhibitors, absorption is not a requirement as these enzymes are active in the lumen of the small intestine. In contrast, as glucose uptake stimulators, the compounds must be absorbed into the bloodstream to be able to reach insulin target cells.

pkCSM also predicts whether these compounds interfere with the functions of P-glycoprotein. P-glycoprotein belongs to the ABC superfamily and functions to limit cellular uptake, distribution, excretion, and toxicity of drugs by acting as a unidirectional efflux pump in several organs. The

inhibition or activation of these P-glycoproteins by potential antidiabetic agents could have unforeseen side effects (Prachayasittikul and Prachayasittikul, 2016). None of the compounds were P-glycoprotein I or II inhibitors and only acarbose, metformin, rutin, and ethyl gallate were predicted to be P-glycoprotein substrates. Acarbose and rutin are not well absorbed into the body and therefore would not interfere with P-glycoprotein function. Metformin was predicted to be a P-glycoprotein substrate which suggests that metformin can be pumped out of a cell. Compounds that are not P-glycoprotein substrates are preferable as they will not be pumped out of the insulin target cells. However, compounds that are pumped out of insulin target cells can still stimulate glucose uptake by extracellular activation of the insulin receptor from outside the cell.

Distribution was predicted as the volume of distribution, the fraction of unbound serum proteins, BBB and CNS permeability. The distribution, metabolism, excretion, and toxicity of acarbose is irrelevant because it is not absorbed into the bloodstream. The ADMET properties of insulin were not compared to the compounds as insulin is not an orally active drug. The VDss is the volume that the total dose of a drug would need to be uniformly distributed to give the same concentration as in the blood. VD_{ss} is therefore the theoretical volume that would be necessary to obtain the total amount of drug at the same concentration as in the blood plasma. A high VDss indicates that more of the drug is distributed in the tissue rather than the plasma. VDss is considered high when the log VDss is greater than 0.45 log L/kg (2.8 L/kg) which is the case for rutin. The other compounds do not have such a high VDss but some of them have higher log VDss than metformin, such as, vanillin and ethyl gallate. The efficacy of a drug can be affected by the degree to which it binds to proteins within the blood. Efficacy increases as the fraction of unbound serum proteins increases. Metformin has the largest fraction of unbound serum proteins; this suggests that the selected compounds are not as effectively distributed to target tissues when compared to metformin. Some of the compounds do, however, have a fraction of unbound serum proteins greater than 50%. The BBB permeability is predicted as a logBB value and the CNS permeability is predicted as logPS which is a more direct measurement of the BBB permeability. Metformin and the selected compounds are not intended to be active in the CNS and crossing the BBB could lead to unforeseen side effects. A compound is predicted to readily cross the BBB when the logBB is more than 0.3. Metformin and all the selected compounds have a logBB value less than 0.3 which suggests that these compounds are unable to cross the BBB. A compound is considered to penetrate the CNS when the logPS value is more than -2. Metformin and all the selected compounds have a logPS value less than -2 which suggests that these compounds do not enter the CNS.

Cytochrome P_{450} are detoxification enzymes in the body that oxidises xenobiotics to facilitate their excretion. Inhibition of these isoenzymes could affect drug metabolism. pkCSM also predicts whether the compounds are CYP2D6 or CYP3A4 substrates which indicates whether the compounds are

metabolised by these enzymes. None of the selected compounds are inhibitors of CYP1A2, CYP2C19, CYP2C9, CYP2D6, or CYP3A4; except for vanillin which was predicted to be a CYP1A2 inhibitor, possibly interfering with the metabolism of other drugs. None of the compounds are CYP2D6 or CYP3A4 substrates, suggesting that these compounds are excreted without being oxidised or metabolised by other enzymes.

Total drug clearance occurs as a combination of hepatic and renal clearance, and is measured by the proportionality constant (logCLtot) as log mL/min/kg. All the selected compounds, except for rutin, have a greater total clearance than metformin. It is important for a drug to be cleared from the body to avoid toxic accumulation; however, rapid clearance could interfere with the ability to reach steady state concentrations.

The AMES toxicity test is a method used to assess the mutagenic potential of a compound. Metformin and ethyl gallate were predicted to be AMES positive which suggests that these compounds could be carcinogenic. The MRTD estimates the dosage of the compound that is toxic to humans. MRTD is predicted as log mg/kg/day and an MRTD greater than 0.477 log mg/kg/day (3.0 mg/kg/day) is high. Only rutin and ethyl gallate have an MRTD less than 0.477 log mg/kg/day. Rutin is not well absorbed which means that the amount of rutin consumed is not necessarily the amount that ends up in the body. Ethyl gallate was selected as a negative control with a poor docking score which means that its small MRTD and AMES positive test might be irrelevant. The LOAEL is the highest dose at which no adverse effects are observed and is measured as log mg/kg/day. All the selected compounds have a log LOAEL greater than metformin which suggests that the selected compounds are slightly less toxic than metformin. The rat LD_{50} was used to predict the relative toxicity of different compounds in mol/kg. Most of the selected compounds have smaller rat LD_{50} values than metformin which suggests that these compounds are slightly more toxic. *T. pyriformis* toxicity was measured as the negative logarithm of the concentration required to inhibit 50% growth of *T. pyriformis* ($pIGC_{50}$) in log µg/L. A $pIGC_{50}$ value greater than -0.5 log µg/L (0.32 µg/L) indicates possible toxicity. All the selected compounds, except caffeic acid, had an IGC_{50} less than or equal to 0.32 µg/L which indicates that these compounds may be *T. Pyriformis* toxic. *T. pyriformis* toxicity does not necessarily predict adverse effects as metformin, which is a well-established drug, is also *T. pyriformis* toxic. Minnow toxicity is measured as log LD_{50} in log mM and a log LD_{50} less than -0.3 log mM is considered to be toxic. All the compounds have a minnow log LD_{50} greater than -0.3 which suggests that none of these compounds are toxic to minnows. The inhibition of hERG I and II could lead to the development of long QT syndrome. All the selected compounds were predicted not to inhibit hERG I or II except for rutin and acarbose which inhibits hERG II. Rutin and acarbose are poorly absorbed into the bloodstream and these predictions may not be relevant. None of the compounds were predicted to cause hepatic toxicity.

SwissTargetPrediction analyses the probability that the selected compounds interact with the 3068 human macromolecular targets in their database. Acarbose primarily interacts with the carbohydrate digesting enzymes: salivary amylase, lysosomal alpha-glucosidase, pancreatic alpha-amylase, and maltase-glucoamylase. This is to be expected because acarbose is a known alpha-glucosidase and amylase inhibitor and will be used as a positive control for digestive enzyme inhibition assays. Metformin was not predicted to interact strongly with any of the proteins in the SwissTargetPrediction database. Metformin was predicted to interact with AMPK in insulin target cells. AMPK activates protein kinase B which leads to increased glucose uptake and glycogen synthesis (Elmadhun *et al.*, 2013). Rutin was predicted to interact with acetylcholinesterase which is an enzyme in the CNS that terminates impulse transmissions at cholinergic synapses (Milkani *et al.*, 2011). Rutin was predicted to interact with adrenergic receptor alpha-2 and its subtype alpha-2a adrenergic receptor which are generally responsible for the inhibition of adenylyl cyclase, activation of receptor-operated K^+ channels, and inhibition of voltage-gated Ca^{2+} channels. These receptors are mostly found in the CNS, but can also be found in several peripheral tissues (Saunders and Limbird, 1999). Neuromedin-U receptor 2 (NMUR2) was predicted to interact with rutin. NMUR2 is predominantly expressed in the CNS and is associated with the regulation of food intake and energy balance (Liu *et al.*, 2009). pkCSM predicted that rutin is not well absorbed into the body, nor does it cross the BBB and enter the CNS; therefore, rutin will not necessarily interact with these CNS enzymes.

p-Coumaric acid was predicted to interact with aldose reductase which catalyses the conversion of glucose into sorbitol in the polyol pathway. Aldose reductase is associated with diabetes complications in the eye and peripheral nervous system (Petrash, 2004). *p*-Coumaric acid is almost completely absorbed in the small intestine, and possibly can act as an aldose reductase inhibitor to alleviate some diabetes complications. *p*-Coumaric acid also interacts with estrogen receptor beta which plays a role in the female cardiovascular system (Muka *et al.*, 2016). Both *p*-coumaric acid and caffeic acid were predicted to interact with carbonic anhydrase isoenzymes. These isoenzymes have different tissue distributions and intracellular locations where they catalyse the reversible hydration of carbon dioxide. Carbonic anhydrase inhibitors have been researched for their ability to help treat glaucoma (Lindskog, 1997). Caffeic acid was predicted to interact with matrix metalloproteinase isoenzymes and arachidonate 5-lipoxygenase. Matrix metalloproteinase isoenzymes are zinc-containing endopeptidases that cleave most of the extracellular matrix constituents. The inhibition of these isoenzymes has been studied for the treatment of periodontal diseases (Birkedal-Hansen *et al.*, 1993). Arachidonate 5-lipoxygenase is an enzyme that catalyses the synthesis of leukotrienes which are mediators of inflammation derived from arachidonic acid. Leukotrienes have been identified as mediators of a variety of inflammatory and allergic reactions and the inhibition of arachidonate 5-lipoxygenase helps alleviate these symptoms

(Werz and Steinhilber, 2006). Caffeic acid was most notably predicted to inhibit protein tyrosine phosphatase 1B (PTP1B). PTP1B is an intracellular enzyme responsible for the termination of the insulin-induced signalling pathway. PTP1B has been analysed as a therapeutic target for the treatment of T2D (Wang *et al.*, 2004). Both vanillin and oxalic acid are predicted to not interact strongly with any of the proteins in the SwissTargetPrediction database. Ethyl gallate is predicted to interact with squalene monooxygenase, which is involved in the steroid biosynthesis pathway and its inhibition could lead to possible side effects (Pollier *et al.*, 2019).

Supplementary Table 3 shows the proteins identified by SwissTargetPrediction that had a high probability (100%) of interacting with the selected compounds as well as the protein's natural substrate found in the body, as well as the percentage probability of the natural substrate interacting with the corresponding protein. Some of the natural substrates have a zero percent probability of interacting with the corresponding protein. This suggests that this predictive program requires further *in vitro* studies.

2.5. Chapter summary

Compounds were selected with a range of docking scores for the following proteins: pancreatic alpha-amylase, intestinal maltase-glucoamylase, insulin receptor, and tyrosine-protein phosphatase non-receptor type 9. Their ADMET properties were determined and compared with acarbose and metformin. The selected compounds were predicted to have similar or better drug-likeness than acarbose and metformin. These compounds were also predicted to have similar toxicity or be less toxic than acarbose and metformin. Most of the predicted cross reactions could result in beneficial side effects. The next step was to analyse the *in vitro* inhibition of the selected compounds against pancreatic alpha-amylase and alpha-glucosidase.

2.5.1. Limitations and future work

The docking studies was performed by docking the ligand into the active site of the protein; however, ligands can dock to other sites on the protein and possible have an allosteric effect on the enzyme. The limitations of SwissTargetPrediction would be the database of proteins which does not encompass all of the proteins within the human body and its predictive algorithm only recognises compounds that are similar to known inhibitors. Future work could include comparing natural compounds to other commercial antidiabetic drugs, such as miglitol, or voglibose, alpha-glucosidase inhibitors (Van De Laar *et al.*, 2005).

CHAPTER 3: Digestive enzyme inhibition

3.1. Introduction

The research in the previous chapter has identified, via *in silico* studies, several compounds with the ability to inhibit pancreatic alpha-amylase and alpha-glucosidase. However, it is necessary to confirm these results *in vitro*. The inhibition kinetics is also an important parameter to measure as the inhibition constant (K_i) which represents the binding affinity of a compound. The relationship between the docking score and K_i value can provide insight into the ability of virtual docking simulations to identify potential pancreatic alpha-amylase and alpha-glucosidase inhibitors.

3.1.1. Pancreatic alpha-amylase assay

Pancreatic alpha-amylase is an enzyme in the small intestine that hydrolyses starch into maltose. Alpha-amylase from porcine pancreas was used in this study. Alpha-amylase has a molecular mass of 51 – 54 kDa. It has a single polypeptide chain of ~475 residues, containing a tightly bound calcium ion for stability. Chloride ions are necessary for activity and stability at pH 6.9 at 20˚C (Gates, 2010). *In vitro* activity of this enzyme is determined using starch as a substrate and measures the amount of maltose released in the presence and absence of the selected compounds. Maltose concentration will be determined using the DNSA method. Maltose reduces 3,5-dinitrosalicylic acid (DNSA) to produce 3-amino-5-nitrosalicylic acid which has an absorbance that can be measured at 540 nm, **Figure 11**. Acarbose, a known antidiabetic drug, is used as a positive control and has mixed-type inhibition (Kim *et al.*, 1999).

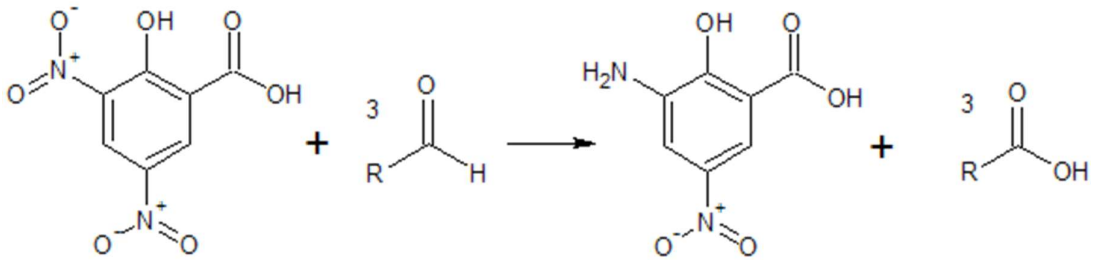

Figure 11: DNSA reduction
The reduction of 3, 5-dinitrosalicylic acid to 3-amino-5-nitrosalicylic acid (a coloured product with an absorbance at 540 nm) by a reducing sugar (Garriga *et al.*, 2017).

3.1.2. Alpha-glucosidase assay

Alpha-glucosidase is an enzyme in the small intestine that hydrolyses maltose into glucose. Alpha-glucosidase from *Saccharomyces cerevisiae* was used in this study. Alpha-glucosidase will liberate

glucose from maltose at pH 6.8 at 37 ˚C (Gates, 2010). To quantify the enzymatic activity, *p*-nitrophenyl α-D-glucopyranoside (*p*NPG) is used as a substrate which is hydrolysed by alpha-glucosidase into *p*-nitrophenyl (*p*NP) and α-D-glucopyranoside, **Figure 12**. The absorbance of *p*NP can be measured at 405 nm. Acarbose is used as a positive control and is a competitive inhibitor of alpha-glucosidase (Kim *et al.*, 1999).

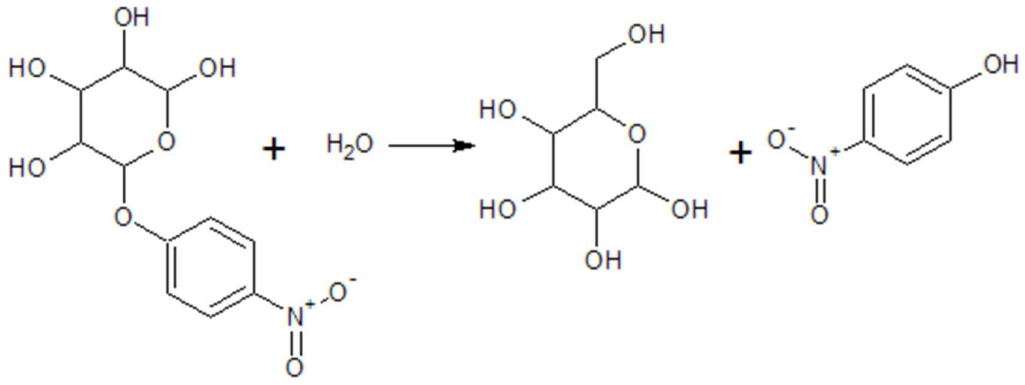

Figure 12: *p*NPG hydrolysis
The hydrolysis of *p*NPG by alpha-glucosidase into α-D-glucopyranoside and *p*NP (a coloured product with an absorbance at 405 nm) (Mohiuddin *et al.*, 2016).

3.1.3. Enzyme kinetics

The rate of an enzyme reaction is the concentration of the product produced by the enzyme in the presence or absence of an inhibitor divided by the time the reaction was allowed to occur. This is the initial velocity (v_0) of the reaction and can be plotted against varying concentrations of the substrate (S) to generate the Michaelis-Menten graph, **Figure 13**. The maximum velocity (V_{max}) of an enzyme represents the velocity when the enzyme is saturated with substrate. The Michaelis constant (K_M) is the substrate concentration where the enzyme has reached half its maximum velocity.

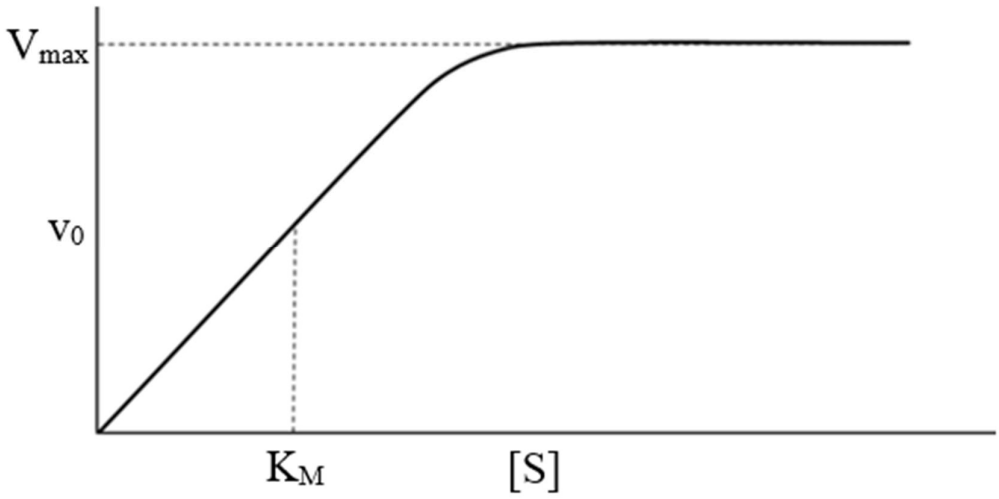

Figure 13: Michaelis-Menten graph

The Michaelis-Menten equation is $v_0 = \frac{V_{max}[S]}{[S] + K_M}$, where v_0 is in mol/min and [S] is in g/mL or mol/mL.

The Michaelis-Menten graph is a hyperbolic curve, and it is difficult to determine the V_{max} and K_M of the enzyme using this plot; the Lineweaver-Burk graph was then derived by transforming the hyperbolic Michaelis-Menten equation into a linear form, **Figure 14**, with the equation $\frac{1}{v_0} = \frac{K_M}{V_{max}}\frac{1}{[S]} + \frac{1}{V_{max}}$.

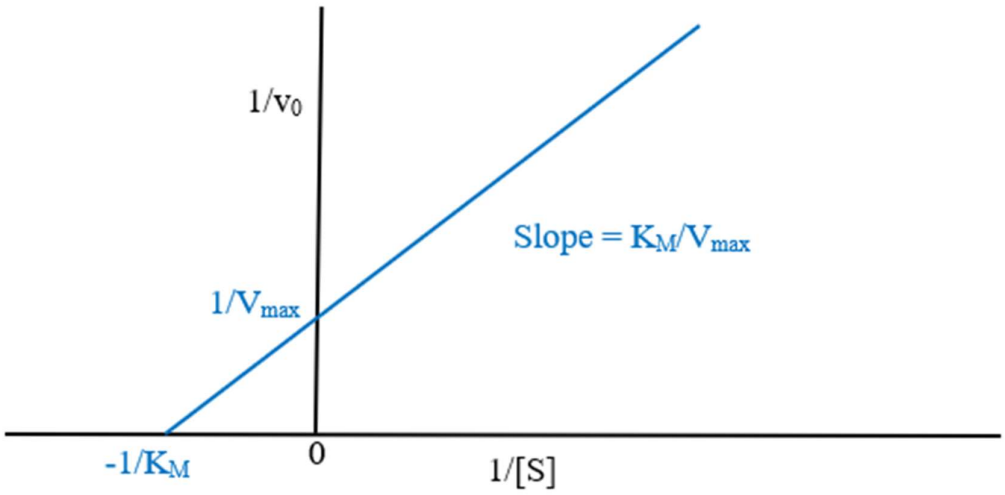

Figure 14: Lineweaver-Burk graph

The graph of $1/v_0$ against 1/[S] where the y-intercept is $1/V_{max}$, the x-intercept is $-1/K_M$, and the gradient is K_M/V_{max}.

The K_M and V_{max} of an enzyme can be affected by the presence of an inhibitor (I). An inhibitor can bind reversibly or irreversibly to the enzyme's active site or another site. There are several types of reversible inhibitors that affect the V_{max} and K_M differently. Competitive inhibitors resemble the substrate, and competes with the substrate for the active site, **Figure 15**. Uncompetitive inhibitors can only bind to the

enzyme-substrate complex [ES], **Figure 16**. Non-competitive inhibitors can bind to the free enzyme [E] or [ES], **Figure 17**. Inhibitors can also exhibit mixed inhibition, such as competitive-non-competitive inhibition, **Figure 18**, or non-competitive-uncompetitive inhibition, **Figure 19**. The extent to which the inhibitor decreases the reaction rate is represented by the inhibition constant (K_i or K_I), where $K_i = [E][I]/[EI]$ and $K_I = [ES][I]/[ESI]$.

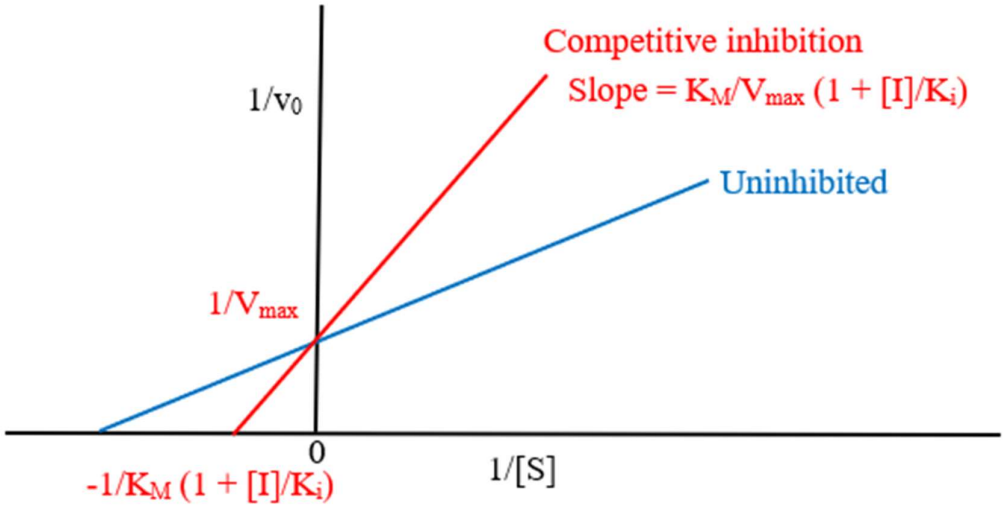

Figure 15: Competitive inhibition

The equation for the competitive inhibitor is $\frac{1}{v_0} = \frac{K_M}{V_{max}}\left(1 + \frac{[I]}{K_i}\right)\frac{1}{[S]} + \frac{1}{V_{max}}$. The competitive inhibitor increases the K_M and the V_{max} is unaffected.

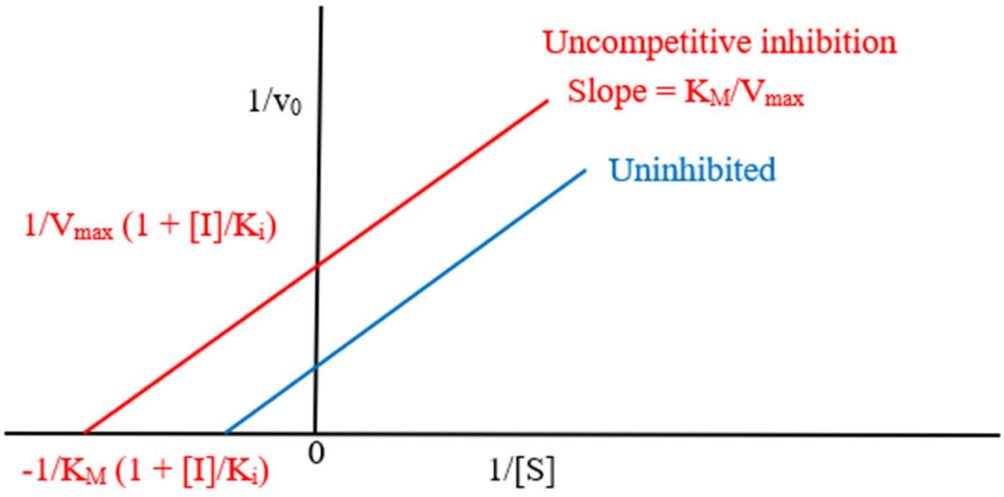

Figure 16: Uncompetitive inhibition

The equation for the uncompetitive inhibitor is $\frac{1}{v_0} = \frac{K_M}{V_{max}}\frac{1}{[S]} + \frac{1}{V_{max}}\left(1 + \frac{[I]}{K_i}\right)$. The uncompetitive inhibitor decreases the K_M and the V_{max}.

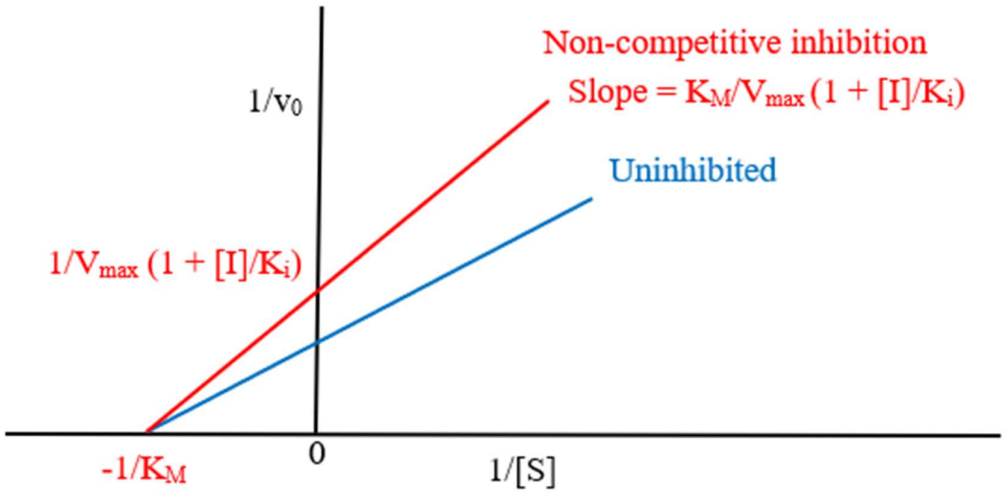

Figure 17: Non-competitive inhibition

The equation for the non-competitive inhibitor is $\frac{1}{v_0} = \frac{K_M}{V_{max}}\frac{1}{[S]}\left(1+\frac{[I]}{K_i}\right) + \frac{1}{V_{max}}\left(1+\frac{[I]}{K_i}\right)$. The non-competitive inhibitor decreases the V_{max} and the K_M is unaffected.

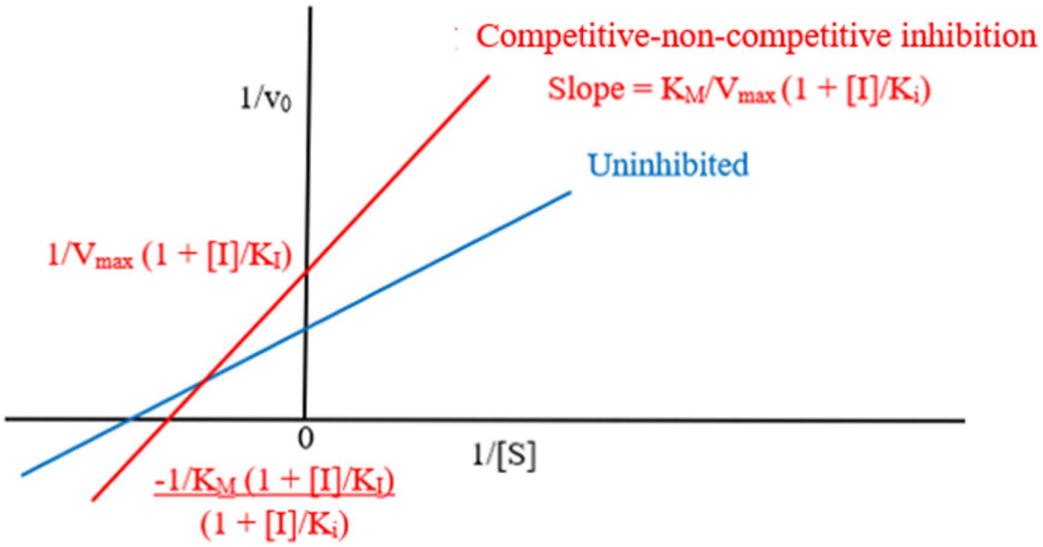

Figure 18: Competitive-non-competitive inhibition

The equation for the competitive-non-competitive inhibitor is $\frac{1}{v_0} = \frac{K_M}{V_{max}}\frac{1}{[S]}\left(1+\frac{[I]}{K_i}\right) + \frac{1}{V_{max}}\left(1+\frac{[I]}{K_I}\right)$. The competitive-non-competitive inhibitor decreases the V_{max} and increases the K_M.

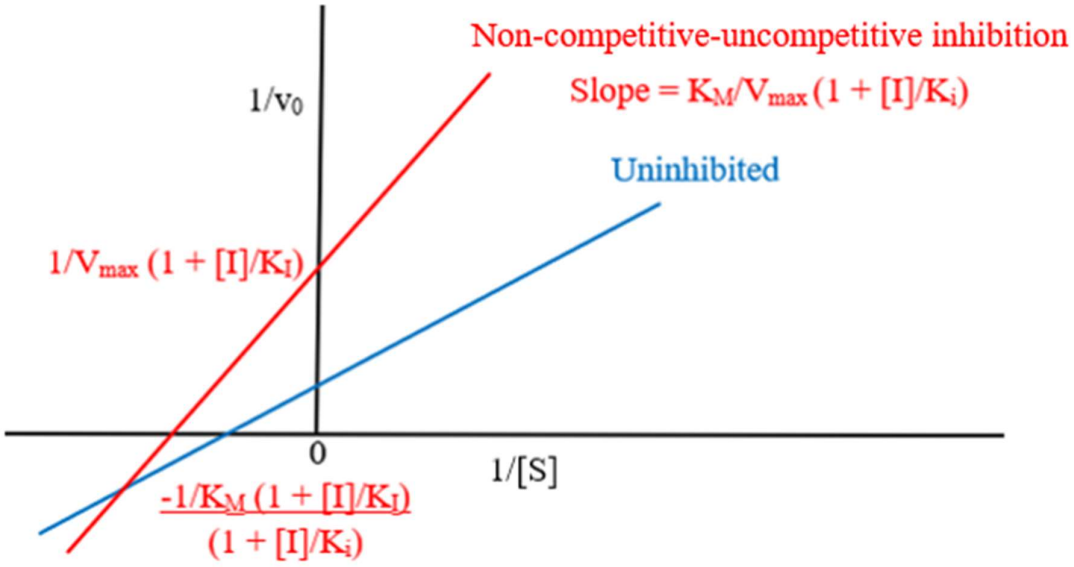

Figure 19: Non-competitive-uncompetitive inhibition

The equation for the non-competitive-uncompetitive inhibitor is $\frac{1}{v_0} = \frac{K_M}{V_{max}}\frac{1}{[S]}\left(1 + \frac{[I]}{K_i}\right) + \frac{1}{V_{max}}\left(1 + \frac{[I]}{K_I}\right)$. The non-competitive-uncompetitive inhibitor decreases the V_{max} and the K_M.

A secondary plot, **Figure 20** can also be produced by plotting the slope of the Lineweaver-Burk graph against different inhibitor concentrations. This plot can be used to determine the K_i as the x-intercept of the secondary plot is $-K_i$. An inhibitor with a small K_i has a greater binding affinity to the enzyme than an inhibitor with a large K_i.

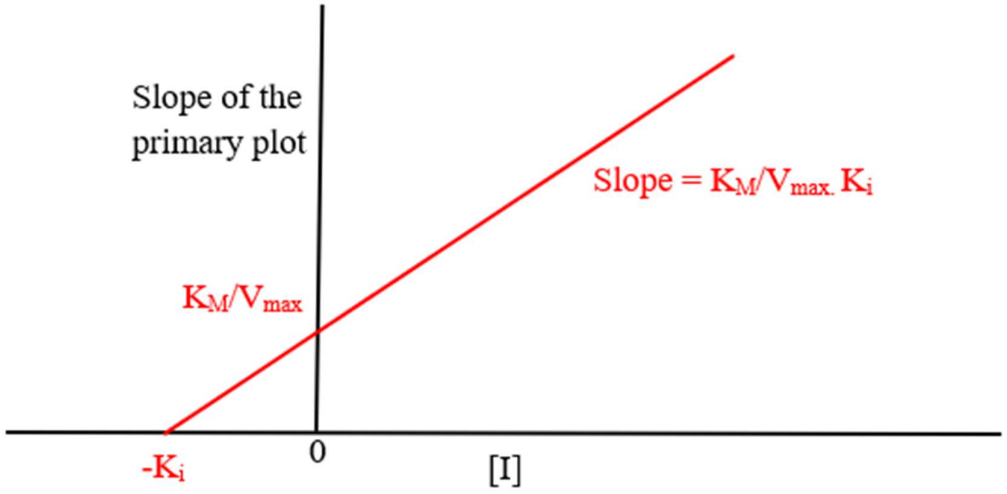

Figure 20: Secondary plot

The graph of the primary slope against the inhibitor concentration with a y-intercept of K_M/V_{max}, a x-intercept of $-K_i$, and a slope of $K_M/V_{max}.K_i$.

The Lineweaver-Burk plot can be used to determine the K_M and V_{max} of an enzyme in the presence and absence of an inhibitor. The type of inhibition can be determined using the statistical comparison of the K_M and V_{max} of the uninhibited and inhibited enzyme. The secondary plot can be used to determine the K_i which represents the binding affinity of the inhibitor to the enzyme (Palmer and Bonner, 2008).

The aim of the research presented in this chapter was to determine the K_i and type of inhibition of the previously selected compounds for pancreatic alpha-amylase and alpha-glucosidase. The K_i was compared with acarbose, a known antidiabetic drug, using the Student's t-test where $p < 0.05$ is considered to be significantly different. The relationship between the K_i value and the docking score was also examined.

3.2. Methods

3.2.1. Chemicals

Alpha-amylase from porcine pancreas type VI-B (EC 3.2.1.1), alpha-glucosidase type I from *Saccharomyce cerevisiae* (EC 3.2.1.20), starch from potatoes, D-(+)-maltose monohydrate, 3,5-dinitrosalicylic acid, potassium sodium tartrate tetrahydrate, *p*-nitrophenyl-alpha-D-glucopyranoside, *p*-nitrophenyl, acarbose, and rutin trihydrate were all purchased from Sigma-Aldrich (St. Louis, Missouri, USA). Ethyl gallate and *p*-coumaric acid were obtained from the Fluka (St. Louis, Missouri, USA) product line; and vanillin was obtained from the UniLab (St. Louis, Missouri, USA) product line. Oxalic acid was purchased from Merck (Darmstadt, Germany). The selected compounds were dissolved in dimethyl sulfoxide (DMSO). More details about the reagents are in **Annexure A**.

3.2.2. Pancreatic alpha-amylase assay

The DNSA colour reagent was prepared by dissolving 12.0 g of sodium potassium tartrate tetrahydrate in 8.0 ml of 2 M NaOH and 20 mL of a 96 mM 3,5-dinitrosalicylic acid solution. The standard curve was generated using a range of maltose concentrations (0.555 – 2.775 mM). Amylase was dissolved in sodium phosphate buffer (20 mM sodium phosphate dibasic/monobasic and 6.7 mM sodium chloride, pH 6.9) to prepare a 4 U/mL enzyme solution. The IC_{50} of each compound was determined by measuring the absorbance in the presence of a range of compound concentrations (0 – 5 mM). A volume of 50 µL compound solution was incubated with 50 µL amylase solution for 10 min at room temperature. Then a volume of 100 µL of 2% (w/v) starch solution was added to the reaction and incubated for 10 min at room temperature. The reaction was terminated by adding 100 µL DNSA solution and incubating for 10 min at 85°C in a heating block (Labnet, Edison, NJ, USA). The solution was then diluted by adding 1200 µL dH_2O, and 200 uL aliquots were transferred into a 96 well plate, in triplicate. The absorbance was measured at 540 nm (SpectraMax Paradigm, Molecular Devices, San Jose, California, USA).

To determine enzyme kinetics, various concentrations of compounds was plotted on a Lineweaver-Burk graph. For acarbose, caffeic acid, ethyl gallate, and vanillin the concentration range was 0 – 40 µM; for oxalic acid, and rutin, 0 – 400 µM; and lastly for *p*-coumaric acid, 0 – 1000 µM. The compounds were incubated with 50 µL of a 4 U/mL amylase solution for 10 min at room temperature. The reaction was then incubated with a range of starch concentrations (1.4 – 10 mg/mL) for 10 min at room temperature. The reaction was terminated by adding 100 µL DNSA solution and incubating in an oven (Labotec, Midrand, South Africa) set to 80°C for 25 min. A volume of 50 µL was transferred to another 96 well plate and diluted with 200 µL dH_2O in triplicate. The absorbance was measured at 540 nm. For details of the method see **Annexure B**.

3.2.3. Alpha-glucosidase assay

The standard curve was generated by converting 200 µL pNP (0.1 – 0.5 mM) to the conjugate base with 50 µL of a 0.8 M NaOH solution. Glucosidase was dissolved in sodium phosphate buffer (100 mM sodium phosphate dibasic/monobasic, pH 6.8) to prepare a 0.2 U/mL enzyme solution. The IC_{50} of each compound was determined by measuring the absorbance in the presence of a range of compound concentrations (0 – 12.5 mM). A volume of 50 µM compound solution was incubated with 50 µL glucosidase solution for 10 min at room temperature. A 100 µL volume of 2 mM *p*NPG solution was added to the reaction and incubated for 30 min at 37°C in an incubator (SepSci, Roodepoort, South Africa). The reaction was terminated by adding 50 µL of a 0.8 mM NaOH solution and the absorbance was then measured at 405 nm.

For the enzyme kinetics, various concentrations of each compound (0 – 1000 µM) were plotted on a Lineweaver-Burk graph. Each compound was incubated with 50 µL of a 0.2 U/mL glucosidase solution for 10 min at room temperature. The reaction was then incubated with a range of *p*NPG concentrations (0.14 – 1 mM) for 30 min at 37°C. The reaction was terminated by adding 50 µL of a 0.8 M NaOH. The absorbance was measured at 405 nm. Each reaction was performed in a 96 well plate in triplicate. For details of the method see **Annexure C**.

3.2.4. Statistical analysis

Four independent repeats were performed for each experiment, and three repeats (n = 3) were chosen that produced the smallest coefficient of variation. The data were expressed as the mean ± standard error of the mean (SEM). The two-tailed Student's t-test was used to determine significant differences between two values where a p-value less than 0.05 was considered statistically significant. The IC_{50} was determined using the NumPy package in Python. The difference in fits (DFFITS) method was used according to Belsley *et al.* (1980) on the Lineweaver-Burk and secondary graphs. The Lineweaver-Burk graphs were plotted using the ggplot2 library in RStudio and the Glide- K_i correlation graphs were plotted in Excel.

3.3. Results

3.3.1. Pancreatic alpha-amylase inhibition

The pancreatic alpha-amylase enzyme kinetics of acarbose, rutin, caffeic acid, *p*-coumaric acid, vanillin, ethyl gallate, and oxalic acid was determined by plotting Lineweaver-Burk graphs (**Figure 21**). The type of inhibition was determined by analysing the changes in V_{max} and K_M for pancreatic alpha-amylase in the presence and absence of the compound (**Supplementary Table 4**). Acarbose exhibited mixed-type (non-competitive-uncompetitive) inhibition at 40 and 20 µM as both lines intersect with the 0 µM line in quadrant III of the Lineweaver-Burk plot. Only the V_{max} of the 20 µM line was significantly less than that of the 0 µM line. Caffeic acid exhibited competitive inhibition as the V_{max} is the same for all concentrations while the K_M increases for some of the concentrations. Ethyl gallate exhibited uncompetitive inhibition as the V_{max} decreases, and the K_M significantly decreases in the presence of 5 µM ethyl gallate. Oxalic acid also exhibited competitive inhibition as the V_{max} is unchanged and the K_M increases, significantly for 400 µM oxalic acid. *p*-Coumaric acid and rutin exhibited uncompetitive inhibition as both the V_{max} and K_M decreased. Vanillin exhibited mixed-type (competitive-non-competitive) inhibition as the 5 µM line and 20 µM line intersect with the 0 µM line in quadrant IV of the Lineweaver-Burk plot. The V_{max} of 10 µM vanillin decreased significantly.

The K_i was determined by plotting secondary graphs. Smaller K_i values represent better binding affinities (**Table 7**). The order of K_i values from smallest to largest was as follows: acarbose < caffeic acid < vanillin < ethyl gallate < rutin < *p*-coumaric acid < oxalic acid. The K_i values of oxalic acid and rutin were significantly larger than that of acarbose, whereas the other compounds were not significantly different than acarbose. The IC_{50} was determined using the NumPy package in Python. Larger IC_{50} values indicates that a higher concentration of a compound is required to inhibit the enzyme by 50%. The order of IC_{50} values from smallest to largest was as follows: acarbose < *p*-coumaric acid < ethyl gallate < vanillin < rutin < caffeic acid < oxalic acid. All the selected compounds had IC_{50} values significantly greater than acarbose.

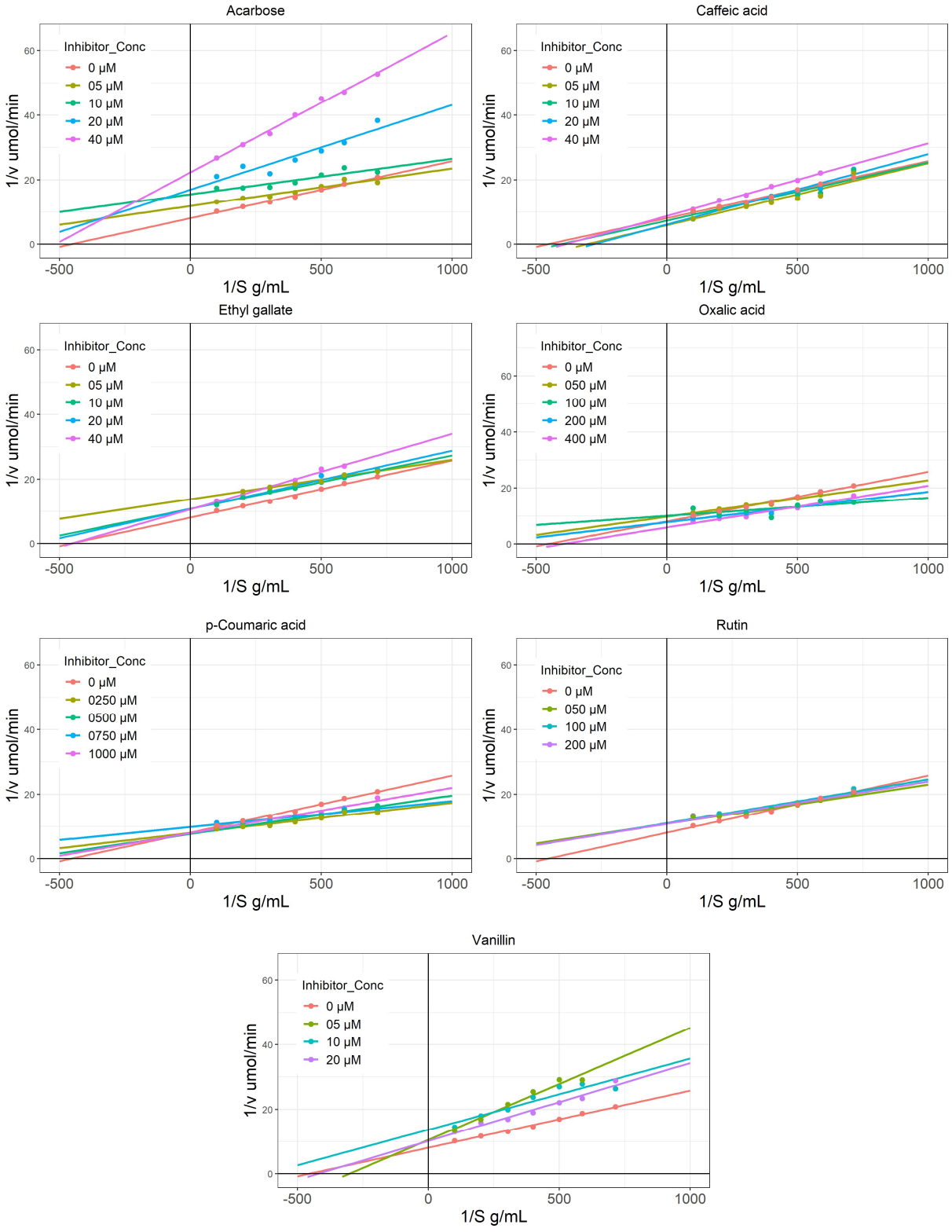

Figure 21: Lineweaver-Burk plots of acarbose (control) and the selected compounds for pancreatic alpha-amylase assay

The graph of 1/v (µmol/min) and 1/S (g/mL) where S is the starch concentration. Each compound has several plots representing different compound concentrations (µM).

Table 7: The pancreatic alpha-amylase inhibition ability of acarbose and the selected compounds

The type of inhibition, K_i (µM), and IC_{50} (mM) of selected compounds for pancreatic alpha-amylase.

Compound	Type of inhibition	K_i (µM)	IC_{50} (mM)
Acarbose	Mixed	14±1[a]	0.03±0.003[a]
Vanillin	Mixed	39±15[a]	3.83±0.642[b]
Caffeic acid	Competitive	28±6[a]	4.50±0.037[b]
Oxalic acid	Competitive	10800±177[b]	4.71±0.782[b]
***p*-Coumaric acid**	Uncompetitive	2460±627[a]	2.44±0.395[b]
Ethyl gallate	Uncompetitive	136±42[a]	3.65±0.355[b]
Rutin	Uncompetitive	1160±240[b]	4.39±0.243[b]

[a] Value is significantly similar ($p > 0.05$, n=3, two-tailed) to acarbose

[b] Value is significantly different ($p < 0.05$, n=3, two-tailed) to acarbose

3.3.2. Alpha-glucosidase inhibition

The alpha-glucosidase enzyme kinetics of acarbose, rutin, caffeic acid, *p*-coumaric acid, vanillin, ethyl gallate, and oxalic acid was determined by plotting Lineweaver-Burk graphs (**Figure 22**). The type of inhibition was determined by analysing the changes in V_{max} and K_M for alpha-glucosidase in the presence and absence of each compound (**Supplementary Table 5**). Acarbose, caffeic acid, ethyl gallate, and *p*-coumaric acid exhibit competitive inhibition as the V_{max} did not change, except for 1000 µM acarbose where the V_{max} was significantly different than 0 µM, and the K_M increases. Oxalic acid, rutin, and vanillin did not exhibit any type of inhibition at the concentrations that were analysed.

The K_i value was determined by plotting secondary graphs. Smaller K_i values represent better binding affinities (**Table 8**). The order of K_i values from smallest to largest was as follows: rutin < acarbose < caffeic acid < vanillin < ethyl gallate < oxalic acid < *p*-coumaric acid. The K_i of ethyl gallate and oxalic acid were significantly larger than that of acarbose, whereas for the other compounds the K_i values were not significantly different than acarbose. The IC_{50} was determined and the order of IC_{50} values from smallest to largest was as follows: acarbose < ethyl gallate < rutin < caffeic acid < vanillin < *p*-coumaric acid < oxalic acid. Rutin, caffeic acid, vanillin, *p*-coumaric acid, and oxalic acid had IC_{50} values significantly greater than acarbose, whereas ethyl gallate was not significantly different from acarbose.

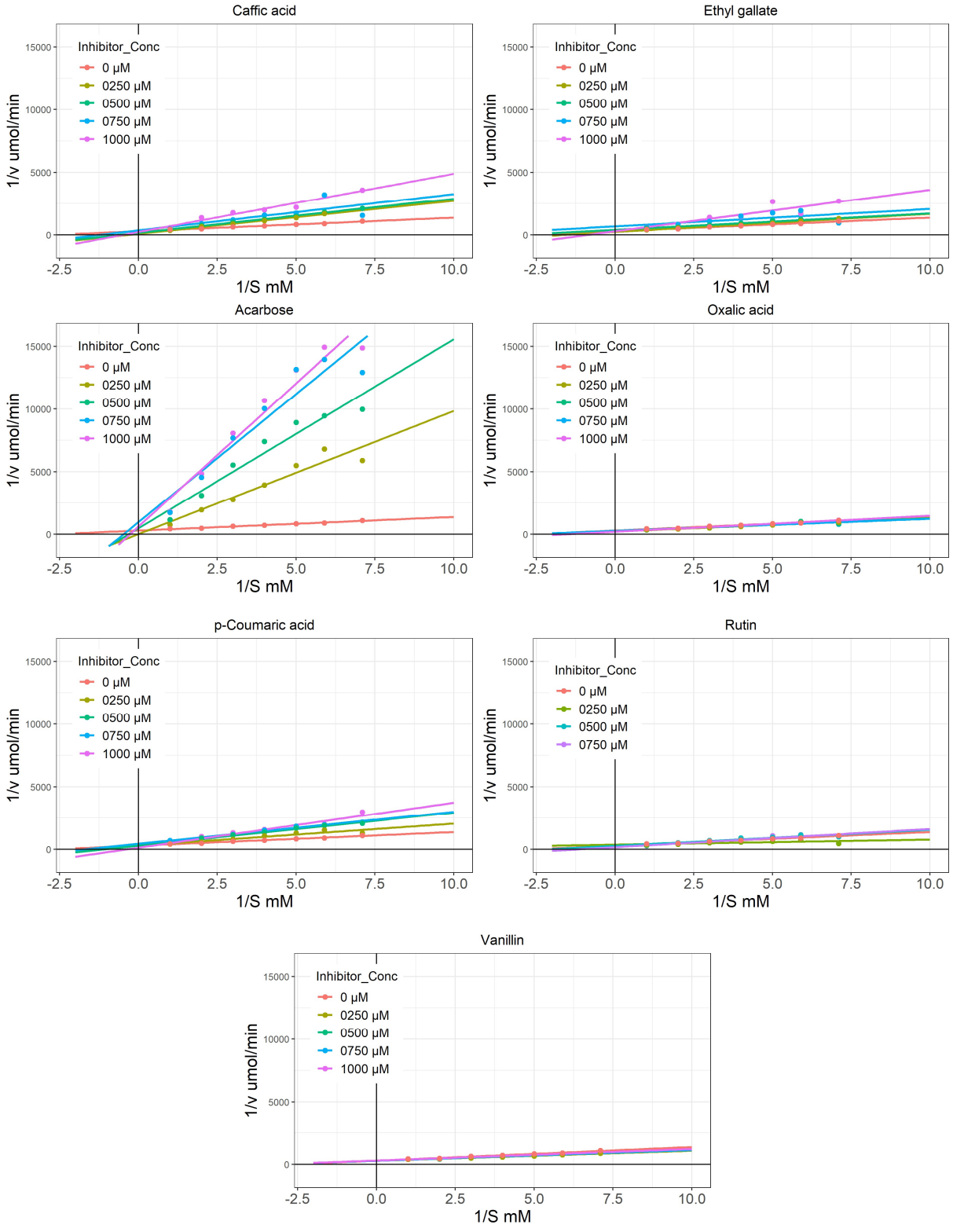

Figure 22: Lineweaver-Burk plots of acarbose and the selected compounds for alpha-glucosidase assay

The graph of 1/v (µmol/min) and 1/S (mM) where S is the *p*NPG concentration. Each compound has several plots representing different compound concentrations (µM).

Table 8: The alpha-glucosidase inhibition ability of acarbose and the selected compounds

The type of inhibition, K_i (µM), and IC_{50} (mM) of selected compounds for alpha-glucosidase.

Compound	Type of inhibition	K_i (µM)	IC_{50} (mM)
Acarbose	Competitive	481±43[a]	0.39 ±0.025[a]
Caffeic acid	Competitive	989±161[a]	1.88 ±0.204[b]
Ethyl gallate	Competitive	1630±201[b]	1.25 ±0.480[a]
***p*-Coumaric acid**	Competitive	9580±4670[a]	6.59 ±0.446[b]
Oxalic acid	None	5020±849[b]	8.36 ±0.162[b]
Rutin	None	225±78[a]	1.48 ±0.132[b]
Vanillin	None	1480±262[a]	6.44 ±0.245[b]

[a] Value is significantly similar ($p > 0.05$, n=3, two-tailed) to acarbose

[b] Value is significantly different ($p < 0.05$, n=3, two-tailed) to acarbose

3.3.3. Validation of *in silico* binding affinity analysis

The virtual docking program Maestro by Schrodinger was used to determine the docking scores of the selected compounds in the active site of pancreatic alpha-amylase and alpha-glucosidase. Both the docking score and the K_i values represent the binding affinity of the compound. A more negative docking score represents a greater binding affinity. Smaller K_i values also represent a greater binding affinity. **Figures 23 and 24** show the correlation between the docking scores and K_i values of the compounds for pancreatic alpha-amylase and alpha-glucosidase, respectivly. Pearson's correlation coefficient (r) and Spearman's rank order correlation coefficient (ρ) were calculated in Excel. The docking score and the K_i value correlates positively confirming that the compounds that had better binding affinities with *in silico* testing also had better binding affinities with *in vitro* testing.

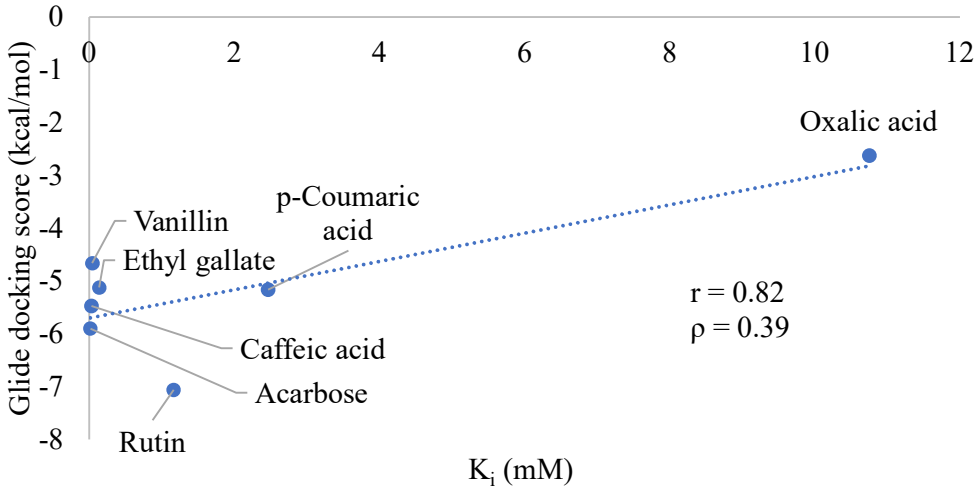

Figure 23: The correlation between Glide score and K_i for pancreatic alpha-amylase

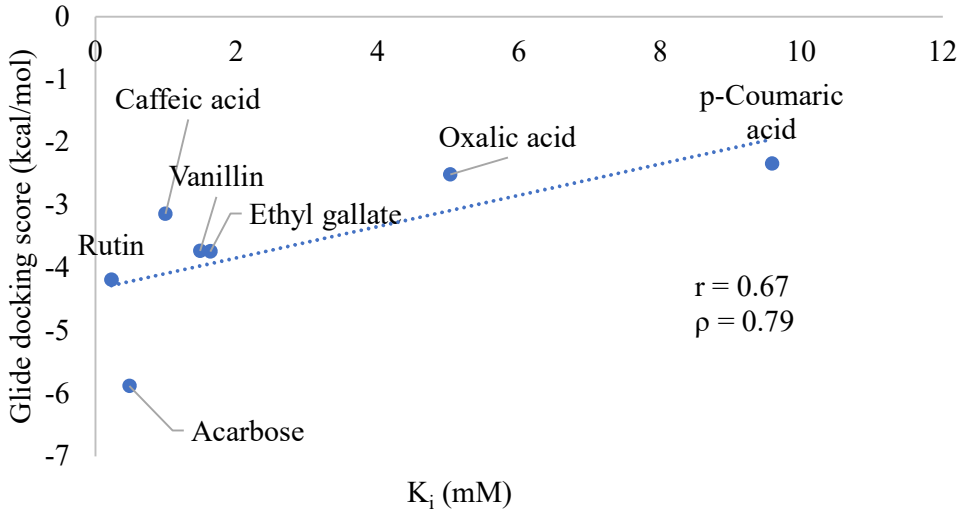

Figure 24: The correlation between Glide score and K_i for alpha-glucosidase

3.4. Discussion

Inhibition of enzymes that digest carbohydrates in the small intestine delays the postprandial increase in blood glucose concentration. The key enzymes responsible for the hydrolysis of carbohydrates are pancreatic alpha-amylase and alpha-glucosidase. These enzymes hydrolyse complex carbohydrates into monosaccharides that can be absorbed from the small intestine into the bloodstream. Delaying the absorption of monosaccharides after a meal is an effective strategy in managing T2D. Several drugs are available that inhibit these enzymes, such as, acarbose, miglitol, or voglibose. However, these drugs are expensive and have several side effects (Adefegha and Oboh, 2012). Therefore, the aim of this research was to determine whether the compounds from herbs, spices, and medicinal plants had similar inhibitory ability as acarbose for pancreatic alpha-amylase and alpha-glucosidase.

In this study, acarbose was used as a positive control for both the pancreatic alpha-amylase and alpha-glucosidase inhibition assays. Findings were that acarbose had mixed-type inhibition of pancreatic alpha-amylase, with a K_i value of 14±1 µM, and an IC_{50} of 0.03±0.003 mM. Yoon and Robyt (2003) reported that acarbose was a mixed inhibitor of porcine pancreatic alpha-amylase and had a K_i value of 0.797±0.156 µM with amylose as the substrate and acarbose concentrations were 20–80 µM. Desseaux *et al.* (2002) also reported that acarbose was a mixed inhibitor of porcine pancreatic alpha-amylase and had a K_i value of 1.6±0.7 µM with amylose as the substrate and the acarbose concentrations were 0.15–1.8 µM.

In this study, acarbose was found to be a competitive inhibitor of alpha-glucosidase, with a K_i value of 481±43 µM, and an IC_{50} of 0.39±0.025 mM. Proença *et al.* (2017) reported that acarbose was a competitive inhibitor for alpha-glucosidase (0.05 U/mL) with a K_i value of 457±11 µM with *p*NPG as a substrate and the acarbose concentrations were 0–2000 µM. Srimoon *et al.* (2020) reported that acarbose was a competitive inhibitor of alpha-glucosidase with a K_i value of 0.33 mg/mL with *p*NPG as a substrate and acarbose concentrations of 0.1–1.0 mg/mL. Differences between this experiment and the literature could be due to differences in enzyme or inhibitor concentrations, and the substrate. In this study, a direct comparison was made between acarbose and the selected compounds under identical experimental conditions.

Some plant extracts, with antidiabetic properties, have been reported to contain the compounds, or derivatives of the compounds used in this study. For example, the dried leaves of *Ventilago denticulata* inhibited alpha-amylase and alpha-glucosidase, and investigation of the phenolic and flavonoid content of these dried leaves extract revealed the presence of gallic acid, vanillic acid, and rutin (Srimoon *et al.*, 2020). *Zea mays* aqueous extract exhibited alpha-amylase and alpha-glucosidase inhibition similar to acarbose at 0.25-0.05 mg/mL and 0.25-1.0 mg/mL, respectively. Investigation of the phenol and flavanol

content revealed that *Z. mays* contained gallic acid and rutin (Sabiu *et al.*, 2016). *Elaeagnus angustifolia* leaves extract had alpha-amylase and alpha-glucosidase inhibitory activities at 10-50 µg, and investigation of the phenolic acid content revealed that *E. angustifolia* contained vanillic acid, caffeic acid, and *p*-coumaric acid (Saltan *et al.*, 2017).

Ethyl gallate, which was a compound in this study, is a derivative of gallic acid and the inhibitory effect of on alpha-amylase and alpha-glucosidase was previously studied by Oboh *et al.* (2016). Gallic acid (25 µM) had a significantly lower percentage inhibition for both alpha-amylase and alpha-glucosidase when compared with acarbose (25 µM), however the combination of gallic acid (50%) and acarbose (50%) produced significant inhibitory results for both enzymes. Dubey *et al.* (2017) reported that rutin had alpha-amylase and alpha-glucosidase inhibitory activity and the rutin concentrations were 50-250 µg/mL. Oboh *et al.* (2015) reported that caffeic acid had dose-dependent inhibitory effects on alpha-amylase and alpha-glucosidase activities. Kwon *et al.* (2008), examined the alpha-glucosidase inhibitory activity of the phenolic compounds in wine and tea and reported that caffeic acid, coumaric acid, and gallic acid had high alpha-glucosidase inhibitory activity. A recent study (Liu *et al.*, 2021) reported that vanillin had mixed inhibition mechanism for alpha-glucosidase by evaluating molecular docking simulations and fluorescence quenching experiments. No previous studies have investigated the ability of type of inhibition of rutin, caffeic acid, *p*-coumaric acid, vanillin, ethyl gallate, and oxalic acid using the K_i values and Lineweaver Burk plots for pancreatic alpha-amylase and alpha-glucosidase.

In this study, the Student's t-test might not detect significant differences between independent means. This relates to the power of the test where the greater the power of the test, the greater the chance of detecting significant differences. The test can have greater power when there is a large difference between the two means, a smaller variability, and a larger sample size (Capraro and Yetkiner, 2010). This could explain why most of the differences between the V_{max} and K_M's of the uninhibited and inhibited enzymes were not significant. The variation between these two samples was too large, and the sample size was too small. The type of inhibition was, therefore, determined by analysing how the different inhibitor concentrations relate to each other and to the uninhibited reaction. One way to overcome this limitation is to increase the sample size.

Virtual docking scoring is a useful tool to screen hundreds, even thousands, of compounds cost effectively and rapidly. However, several authors have reported that there is no significant relationship between docking scores and ligand affinity, while other authors only observed that some proteins had a strong positive correlation between *in silico* and *in vitro* studies (Warren *et al.*, 2006, Nagpal *et al.*, 2012, Gao *et al.*, 2010, Park *et al.*, 2009). In this study, there was a positive correlation between the Glide docking score and the K_i value of the selected compounds for both pancreatic alpha-amylase and alpha-

glucosidase as the Pearson's correlation coefficients (r) were 0.82 and 0.67, respectively (**Figures 23 and 24)**. The DFFITS method was performed on the correlation graphs in **Figures 23 and 24**. It appears that oxalic acid had an undue influence on the pancreatic alpha-amylase Glide- K_i correlation graph and acarbose had an undue influence on the alpha-glucosidase Glide- K_i correlation graph. Spearman's rank correlation coefficient (ρ) evaluates the rank values between the Glide docking score and K_i values instead of the actual values and this would minimize the effect of outliers, such as, oxalic acid in **Figure 23** and acarbose in **Figure 24**. The Pearson's correlation coefficient, for pancreatic alpha-amylase the Glide- K_i correlation was strong; and for alpha-glucosidase the Glide- K_i correlation was moderate. The Spearman's correlation coefficient, for pancreatic alpha-amylase the Glide- K_i correlation was weak; and for alpha-glucosidase the Glide- K_i correlation was strong. This further demonstrates the effects of outliers (Schober *et al.*, 2018, Mukaka, 2012). Future research should include the determination of the K_i value of more natural compounds that are structurally similar to acarbose and have good docking scores for pancreatic alpha-amylase and alpha-glucosidase.

3.5. Chapter summary

The inhibition ability of the selected compounds was compared with acarbose for pancreatic alpha-amylase and alpha-glucosidase by comparing their K_i values. The K_i values for caffeic acid, ethyl gallate, *p*-coumaric acid and vanillin were similar to the K_i value of acarbose for pancreatic alpha-amylase. The K_i values for caffeic acid, *p*-coumaric acid, rutin, and vanillin were similar to the K_i value of acarbose for alpha-glucosidase. Therefore, we accept the $H_0$1 for these compounds. There was a positive correlation between the Glide score and the K_i value for both pancreatic alpha-amylase and alpha-glucosidase. Thus, these two PDB codes, 4GQR and 3L4Y, can be used to screen for other inhibitors from herbs, spices, and medicinal plants. The next step was to analyse the glucose uptake inducing ability of the selected compounds in relevant cell lines.

3.5.1. Limitations and future work

Limitations to this study was the use of pancreatic alpha-amylase and alpha-glucosidase from porcine and *S. cerevisiae*, respectively, instead of from humans. Improvements to this experiment could be to use larger inhibitor concentrations for alpha-glucosidase kinetic studies, especially for vanillin and rutin, whose type of inhibition could not be determined. Future research could include the analysis of more natural compounds as pancreatic-alpha amylase and alpha-glucosidase inhibitors to better validate the *in silico – in vitro* relationship.

CHAPTER 4: Cytotoxicity and insulin-mimicking effects

4.1. Introduction

To further develop compounds for therapeutic applications, it is essential to determine if the compounds are not cytotoxic using relevant cell lines. For example, the use of rutin, caffeic acid, *p*-coumaric acid, and vanillin as inhibitors of pancreatic alpha-amylase and alpha-glucosidase in the small intestine, it is necessary to determine the cytotoxicity of these compounds using a cell line such as the Caco-2 cell line. Several of the compounds in this study were shown to be bioavailable and may target insulin dependent tissues, such as the liver and muscle. Likewise, cytotoxicity determination in representative cell lines, such as the HepG2 and C2C12 cell lines, is essential prior to determining the effects of these compounds on glucose uptake.

4.1.1. SRB assay

Sulforhodamine B (SRB) assay is a method used for *in vitro* cytotoxicity screening. The cytotoxicity of a compound is the measure of the effect a chemical agent has on the morphology, rate of cell growth, and survival of a cell (Miret *et al.*, 2006). SRB, **Figure 25**, is a dye that binds to the basic amino acid residues of cellular proteins following trichloroacetic acid (TCA) fixation (Vajrabhaya and Korsuwannawong, 2018). The SRB assay has several advantages over other protein and fluorescent dye-staining methods, as it is more sensitive, is rarely affected by the interference of the other compounds and is independent of the cellular metabolic activity (Vichai and Kirtikara, 2006). The SRB assay was used to determine whether a compound is cytotoxic to Caco2, HepG2, and C2C12 cells. The absorbance of SRB is measured at 540 nm and correlates with cell number.

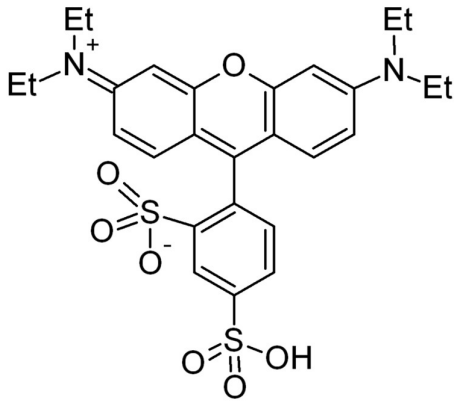

Figure 25: SRB structure
The sulfonic acid groups bind basic amino acids in cellular protein and absorbance at 540 nm is an indirect measure of cell number.

4.1.2. Glucose uptake assay

To evaluate cellular glucose uptake, 2-[N-(7nitrobenz-2-oxa-1,3-diazol-4-yl) amino]-2-deoxy-d-glucose (2NBDG), a fluorescent glucose analog, **Figure 26**, was used to determine uptake of glucose into C2C12 and HepG2 cells in the presence of insulin and the selected compounds (Zou *et al.*, 2005). Metformin was used as a positive control. The stimulation of glucose-uptake into skeletal muscle cells and hepatocytes reduces the blood glucose concentration.

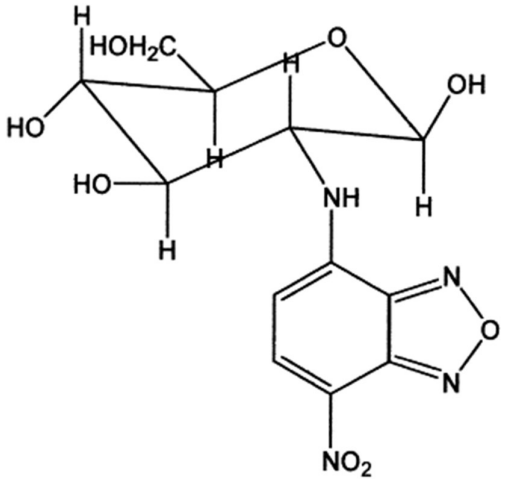

Figure 26: 2NBDG
The structure of 2NBDG, a glucose analogue, that has strong fluorescence at an excitation wavelength of 475 nm and an emission wavelength of 550 nm (Oh and Matsuoka, 2002).

The research undertaken in this chapter was to determine the cytotoxicity of the selected compounds with relevant cell lines. The cytotoxicity of a compound was quantified using the IC_{50} value. Caco2 cells were used as an intestinal epithelial model and the IC_{50} of the selected compounds were compared to acarbose. IC_{50} values significantly smaller than acarbose indicated that the compound was more cytotoxic than acarbose. The cytotoxicity of the compounds with C2C12 skeletal muscle cells and HepG2 hepatic cells were also evaluated. The ability of the selected compounds to increase glucose uptake for C2C12 and HepG2 cells as investigated.

4.2. Methods

4.2.1. Chemicals

Caco2 colorectal adenocarcinoma cells (CCAC-FL) were obtained from Cellonex (Separation Scientific, Roodepoort, South Africa). C2C12 myotubes (American Type Culture Collection [ATCC] CRL-1772) and HepG2 hepatocarcinoma cells (ATCC HB-8065) were obtained from ATCC. Dulbecco's Modified Eagle's Medium (DMEM) supplemented with 1% nonessential amino acids, 1% (w/v) L-glutamine, penicillin (100 U/mL), streptomycin (100 U/mL), dextrose (25 mM), and 10% (v/v) heat-inactivated foetal calf serum (FCS) (DMEM/10% FCS). Trichloroacetic acid (TCA), sulforhodamine B (SRB), tris buffer, glucose-free DMEM supplemented with penicillin (100 U/mL) and streptomycin (100 U/mL), and trypan blue were purchased from Sigma-Aldrich (St. Louis, Missouri, USA). Phosphate buffered saline (PBS) was purchased from BD Diagnostics (New Jersey, USA). Human insulin was purchased from European Pharmacopoeia (Strasbourg, France). 2-NBDG and trypsin were purchased from Thermo Fisher Scientific (Waltham, Massachusetts, USA).

4.2.2. SRB assay

Cell cultures were incubated in T75 culture flasks at 37°C in a humidified incubator (Binder, Tuttlingen, Germany) with a 5% CO_2 atmosphere until confluency was established. The cell cultures were trypsinized to detach the cells from the flask and the cells were collected by centrifuging the culture at 200*g* for 5 min (Beckman Coulter, California, USA). The cells were resuspended in 1 mL of DMEM/10% FCS. The appropriate cell concentration was obtained by counting the cells using 0.1% trypan blue and a hematocytometer under a microscope (Reichert-Jung, Wetlzar, Germany). The assay plates were prepared by seeding 96-well plates with the 100 µL cell suspension ($1x10^5$ cells per well) in DMEM/10% FCS and incubating the plates at 37°C for 24 h.

The cells were then exposed to 100 µL selected compounds (0.001 to 100 µM for C2C12 and HepG2 cells; and 0.1 to 1000 µM for Caco2 cells) for 72 h. The cells were then fixed overnight with 50 µL of a 50% TCA solution and incubated at 4°C. The plates were then washed four times with tap water and allowed to dry before the SRB stain was added. The cells were exposed to the 100 µL of a 0.057% SRB stain solution for 30 min and washed four times with 1% acetic acid and dried overnight in the oven (Labotec, Midrand, South Africa). To extract the dye, 200 µL of 10 mM tris buffer (pH 10.5) was added to each well and the plates were shaken at 550 rpm for 1 h (Labex, Johannesburg, South Africa). The absorbance of the extracted dye was measured at 540 nm (BioTek, Vermont, United States). For details on the method see **Annexure D**.

4.2.3. Glucose-uptake assay

The cell suspension was prepared as described for the SRB assay, and the 96-well plate was seeded with 80 µL cell suspension and incubated at 37°C for 24 h. The medium was removed, and the cells were incubated with 80 µL glucose-free DMEM/2.5% FCS at 37°C for 24 h. The medium was then removed, and the selected compounds, in glucose-free DMEM, were added to final concentrations of 10, 1, and 0.1 µM. C2C12 cells were incubated with the compounds at 37°C for 24 h and HepG2 cells were incubated for 45 min.

In a subsequent experiment, to induce insulin resistance, HepG2 cells were incubated with 100 nM insulin, in DMEM, at 37°C for 24 h. HepG2 cells were then exposed to the compounds with 50 nM insulin in glucose-free DMEM.

The cells and the compounds were then incubated with 80 µM 2-NBDG for 1 h in the dark. C2C12 cells were then washed twice with PBS and HepG2 cells were washed with glucose-free DMEM. The fluorescence was measured at an excitation wavelength of 485/40 nm and an emission wavelength of 590/35 nm (BioTek, Vermont, USA). For details on the method see **Annexure E**.

4.2.4. Statistical analysis

Three independent repeats were performed for the cytotoxicity in the Caco2 cell line, and four independent repeats were performed for the cytotoxicity in the C2C12 and HepG2 cell lines. For the glucose-uptake assay, three independent repeats in the C2C12 and HepG2 cell lines was performed. The data were expressed as the mean ± standard error of the mean (SEM). The one-tailed Student's t-test was used to determine significant differences between the control and the compound, where a p-value less than 0.05 was considered statistically significant. The IC_{50} was determined using QuestGraph™ (2020). GraphPad Prism 5 was used to produce the glucose-uptake graphs.

4.3. Results

4.3.1. Cytotoxicity

The cytotoxicity, as IC_{50} values, of the selected compounds was determined (**Table 9**) and the cytotoxicity graphs was generated (**Supplementary Figure 2**).

Table 9: The cytotoxicity of selected compounds in Caco2, HepG2, and C2C12 cells

Compound	Caco2 IC_{50} (µM)	HepG2 IC_{50} (µM)	C2C12 IC_{50} (µM)
Acarbose	715±89.1[a]	-	-
Vanillin	637±249.1[a]	>100	>100
Rutin	534±199.1[a]	>100	>100
Caffeic acid	382±243.9[a]	>100	>100
***p*-Coumaric acid**	371±13.7[a]	>100	>100
Oxalic acid	177±19.6[b]	>100	>100
Ethyl gallate	42.3±24.0[b]	63.6±13.9	39.6±13.8

[a] Caco2 IC_{50} assumed to be significantly similar ($p > 0.05$, n=3, SEM, two-tailed) to Caco2 IC_{50} of acarbose.
[b] Caco2 IC_{50} assumed to be significantly different ($p < 0.05$, n=3, SEM, two-tailed) to Caco2 IC_{50} of acarbose

In the Caco2 cell line, an IC_{50} could be determined for all the selected compounds. The order of cytotoxicity from most to least was ethyl gallate > oxalic acid > *p*-coumaric acid > caffeic acid > rutin > vanillin > acarbose. In Caco2 cells, the IC_{50} for acarbose was 715±89.10 µM and the IC_{50} of only ethyl gallate and oxalic acid was significantly less than that of acarbose. In the HepG2 and C2C12 cell lines, the IC_{50} value for all the compounds, except ethyl gallate, was greater than 100 µM, the highest concentration. In all cell lines, ethyl gallate was the most cytotoxic with the lowest IC_{50} in the Caco2 cell line. Of the cell lines evaluated, the Caco2 cell line was the most sensitive to the cytotoxic effects of the compounds evaluated.

4.3.2. Glucose-uptake ability

For the glucose uptake study (**Figures 27, 28, and 29**), concentrations that were not cytotoxic were selected (**Table 9**) and these were 10, 1, and 0.1 µM.

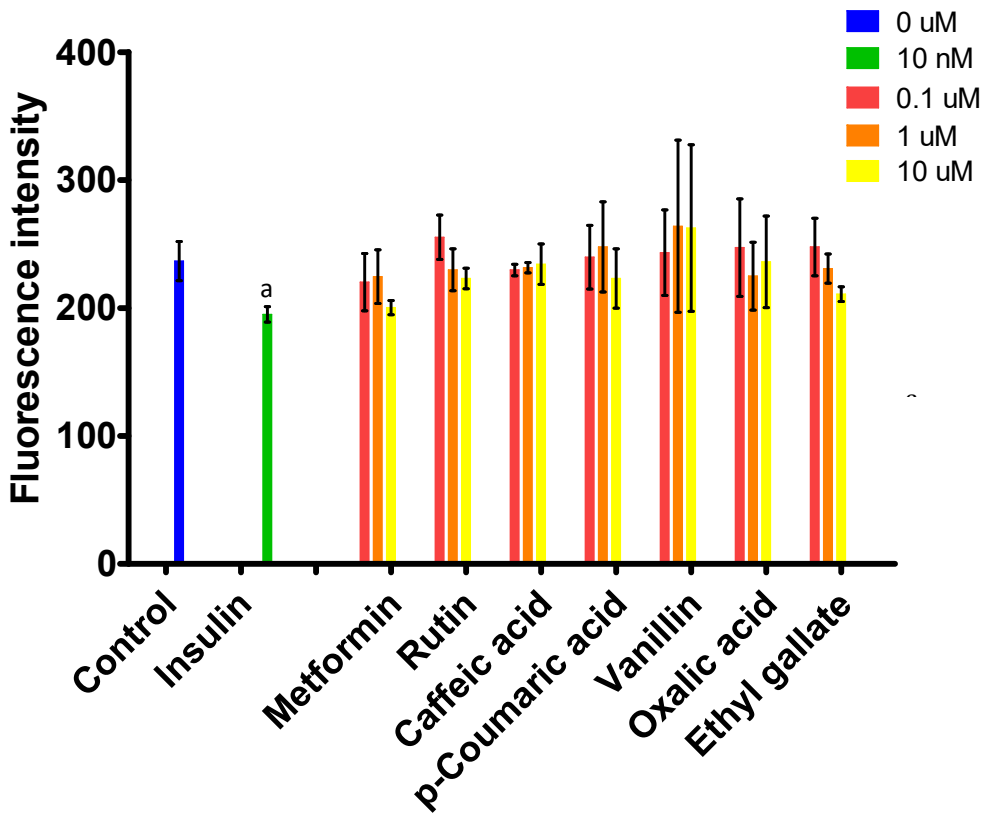

Figure 27: The glucose-uptake ability of selected compounds in HepG2 cells
HepG2 cells were exposed to 0.1, 1, and 10 µM metformin and each compound as well as 10 nM insulin at 37°C for 45 min. Glucose uptake was determined with 80 µM 2NBDG for 1 h added after the 45 min incubation with metformin and the compounds. The control was HepG2 cells not exposed to metformin or the compounds. The supernatant was removed, and the cells were washed with glucose-free DMEM, and the fluorescence was measured at an excitation wavelength of 485/40 nm and emission wavelength of 590/35 nm.
[a] Compounds that have a fluorescent intensity significantly different than the control ($p < 0.05$, n=3, error bars = SEM, one-tailed)

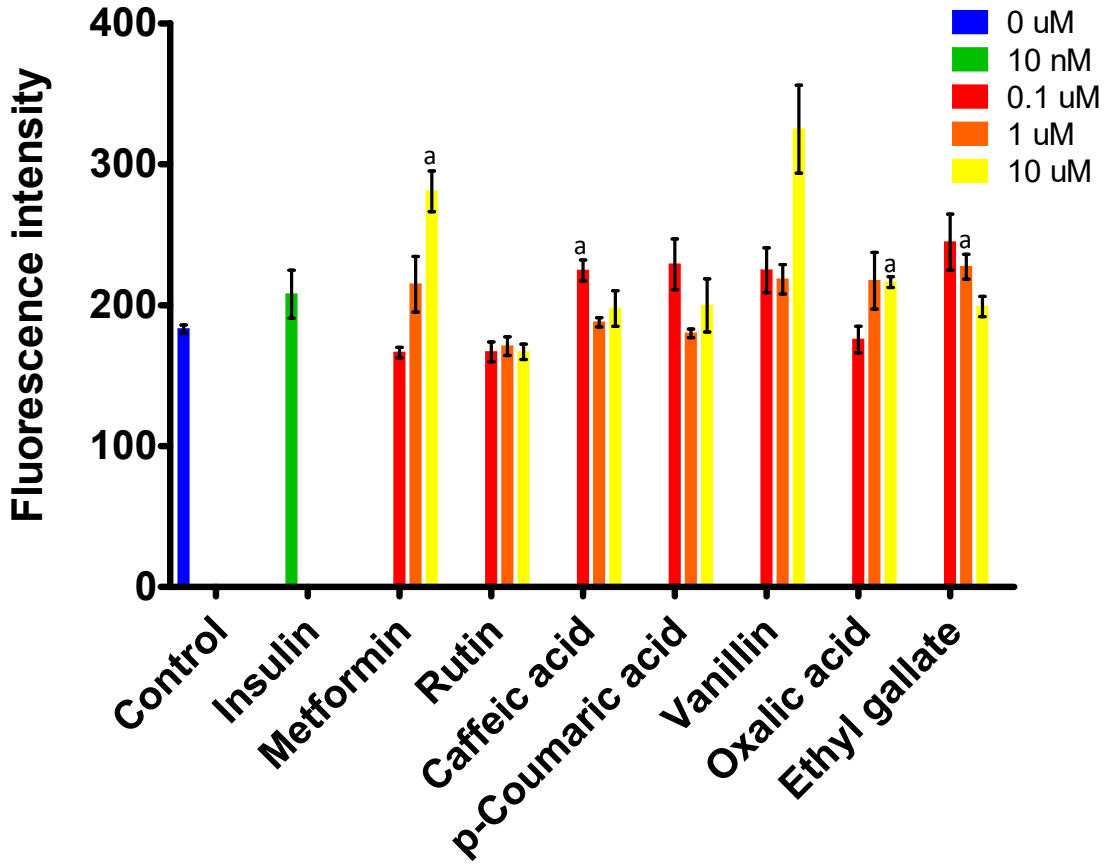

Figure 28: The glucose-uptake ability of selected compounds for C2C12 cells
C2C12 cells were exposed to 0.1, 1, and 10 µM metformin and each compound as well as 10 nM insulin at 37°C for 24 h. Glucose uptake was determined with 80 µM 2NBDG for 1 h added after the 24 h incubation with metformin and the compounds. The control was C2C12 cells not exposed to metformin or the compounds. The supernatant was removed, and the cells were washed with PBS and the fluorescence was measured at an excitation wavelength of 485/40 nm and emission wavelength of 590/35 nm.
[a] Compounds that have a fluorescent intensity significantly different than the control ($p < 0.05$, n=3, error bars = SEM, one-tailed)

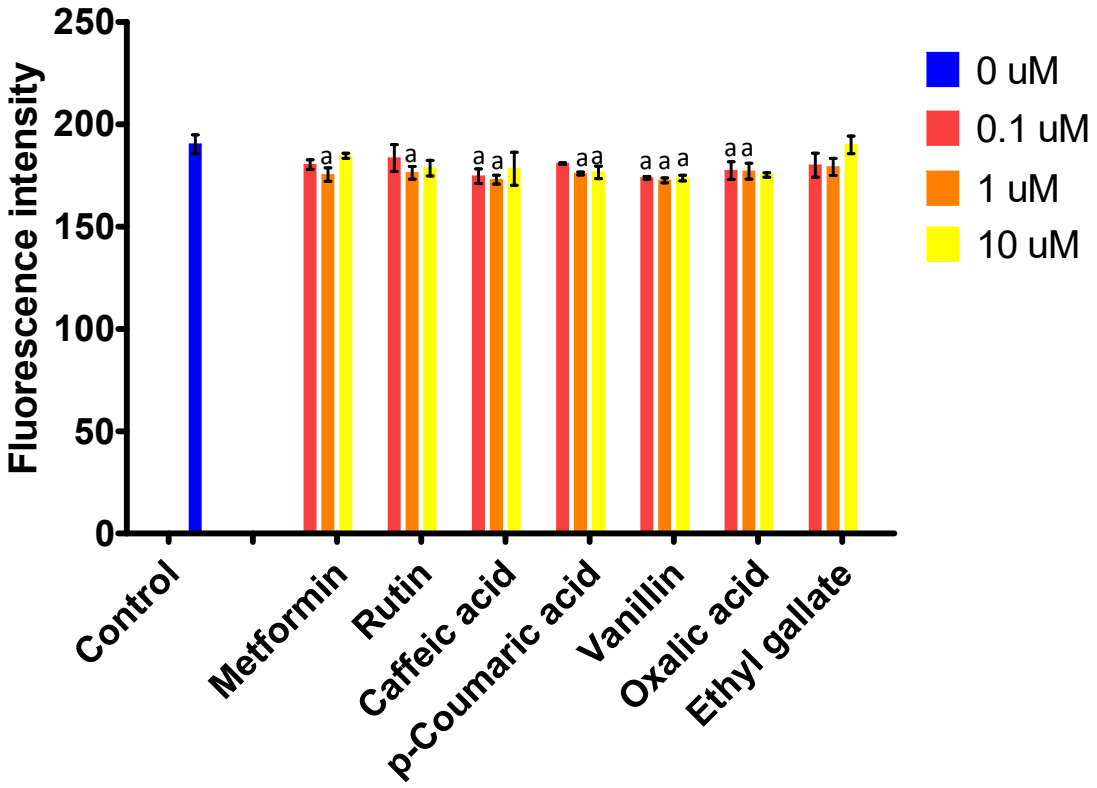

Figure 29: The glucose-uptake ability of selected compounds for insulin-resistant HepG2 cells
Insulin resistance was induced with 100 nM insulin, in DMEM, at 37°C for 24 h. Then the cells were exposed to 0.1, 1, and 10 µM metformin and each compound as well as 50 nM insulin at 37°C for 45 min. Glucose uptake was determined with 80 µM 2NBDG for 1 h added after the 45 min incubation with metformin and the compounds. The control was HepG2 insulin-resistant cells with 50 nM insulin but not exposed to metformin or the compounds. The supernatant was removed, and the cells were washed with glucose-free DMEM, and the fluorescence was measured at an excitation wavelength of 485/40 nm and emission wavelength of 590/35 nm.
[a] Compounds that have a fluorescent intensity significantly different than the control ($p < 0.05$, n=3, error bars = SEM, one-tailed)

4.4. Discussion

The ability of natural compounds to stimulate glucose-uptake in hepatocytes and skeletal muscle cells would help decrease the blood glucose concentration, especially after a meal when the blood glucose concentration spikes. Insulin is the main hormone that is released from the pancreas and stimulates these cells to take up more glucose by increasing the number of GLUT4 transporters. Metformin, a commercial drug, stimulates glucose-uptake and is used for the treatment of T2D. The signalling pathway of metformin is different from that of insulin. Instead of activating the insulin receptor to translocate the GLUT4 transporter to the cell surface, metformin stimulates AMPK to translocate GLUT1 transporters to the cell surface (Elmadhun *et al.*, 2013).

Before investigating the glucose-uptake stimulating ability of the selected compounds, it was necessary to determine the cytotoxicity in three cell lines: Caco2, HepG2 and C2C12 cell lines representative of the site of uptake and specific insulin cellular targets. The Caco2 IC_{50} of the selected compounds relates to the toxicity of the compounds in the lumen of the small intestine. Caffeic acid, *p*-coumaric acid, rutin, and vanillin all had Caco2 IC_{50} values statistically similar to acarbose. This suggests that these compounds are just as toxic in the small intestine as acarbose. These compounds can, therefore, be used as pancreatic alpha-amylase and alpha-glucosidase inhibitors as identified in **CHAPTER 3**. Ethyl gallate and oxalic acid, however, had significantly smaller Caco2 IC_{50} values than acarbose. In this study, ethyl gallate and oxalic acid were the negative controls and, therefore, are not to be used as digestive enzyme inhibitors. In the HepG2 and C2C12 cell lines, an IC_{50} could only be obtained for ethyl gallate, and all other compounds were not cytotoxic with an IC_{50} greater than 100 µM. Karakurt (2016) reported that rutin had an IC_{50} value of 52.7µM with HepG2 cells using the Alamar blue method. Magnani *et al.* (2014) reported that caffeic acid had an IC_{50} value of 781.8 µg/mL using the MTT method.

Differences in sensitivity of the cell lines tested may be related to the doubling times which according to the DSMZ website (Klaus, Accessed 2021) are 80 h for Caco2, 50-60 h for HepG2, and 20 h for C2C12. Therefore, the doubling time of Caco2 cells is longer than that of HepG2 and C2C12 cells, and Caco2 cells will have a lower growth density during the 24 h period which may make these cells more sensitive to the toxic effects of the compounds evaluated. The Caco2 cytotoxicity assay also used higher drug concentrations (0-1000 µM), whereas the HepG2 and C2C12 cytotoxicity assay used lower drug concentrations (0-100 µM) to reflect the higher drug concentrations in the gut lumen than in the liver and muscle tissue. This could possibly explain why the IC_{50} could be determined for Caco2 cells but not HepG2 or C2C12 cells. The higher drug concentrations for the Caco2 cytotoxicity assay could increase the likelihood of secondary metabolites that contribute to the cytotoxicity of the drug.

In the investigation of the effects of these compounds on glucose uptake, the effect of several insulin concentrations was evaluated, including the concentrations found in human blood which range from 0.1 to 1 nM (Mari *et al.*, 2011). Higher concentrations of insulin were also tested, with 100 nM being the highest (Park *et al.*, 2014, Semaan *et al.*, 2018). In the HepG2 cell line, insulin caused a decrease in glucose uptake. Although glucose uptake was slightly increased in the C2C12 cell line, this increase was not statistically significant. None of the compounds influenced glucose uptake in HepG2 cells. In contrast, glucose uptake in C2C12 cells was increased by 10 µM metformin, 0.1 µM caffeic acid, 10 µM oxalic acid and 1 µM ethyl gallate. None of the compounds, including insulin and metformin, were considered to significantly increase the glucose-uptake in HepG2 cells; however, insulin (10 nM) significantly decreased the fluorescent intensity compared to that of the control. Both C2C12 and HepG2 cells were grown under high glucose conditions which induced insulin resistance in these cells (Zang *et al.*, 2004).

None of the insulin concentrations that were tested had a significant effect on the glucose-uptake ability of C2C12 cells, which may indicate that the 2NBDG assay was not sensitive enough to measure glucose uptake. The fluorescent intensity of 10 µM metformin was significantly greater than the control for C2C12 cells, which was expected because metformin was a positive control. Metformin also seemed to have a dose response in C2C12 cells where the fluorescent intensity increased as the metformin concentration increased. Oxalic acid also seemed to take up a significant amount of 2-NBDG at 10 µM in C2C12 cells. However, this may be misleading as the SEM is smaller compared to the other compounds. On the other hand, 10 µM vanillin had a much larger fluorescent intensity than the control (0 µM) but it is not significant because of the SEM which is much larger than the other compounds. Caffeic acid (0.1 µM) and ethyl gallate (1 µM) had fluorescent intensities significantly greater than the control but the SEM is also small, and these compounds also appear to have a negative dose response where the higher concentrations had smaller fluorescent intensities.

Several adaptations were made to the original assay described in Zou *et al.* (2005), for example, the cells were starved of glucose for 48 h. Other methods were also tested, such as, differentiating the C2C12 cells by reducing the serum content of the media to 2% FCS (Elkalaf *et al.* (2013), however, glucose uptake by the differentiated C2C12 cells were not significantly increased in the presence of insulin. Likewise, insulin did not increase uptake of glucose in the HepG2 cells.

The possible loss of cells after washing may result in lower fluorescence measurements. By performing an SRB assay on the twice-washed cells the contribution that washing has on cell loss was evaluated. The measured absorbance of the control before washing was between 1.2 and 2.0 and after washing 0.05

to 0.10 indicating a significant loss of cells. In another experiment, the cells were washed with glucose-free DMEM, and subsequently the cells remained attached.

Kim *et al.* (2017) performed a 2NBDG uptake assay on differentiated C2C12 cells and found that tricin, a methylated flavone, significantly increases the uptake of glucose when compared to the control. The cells were incubated with 5, 10, and 20 µM drug and 100 µM 2NBDG for 24 h. Yoon *et al.* (2013) also performed a 2NBDG assay on differentiated L6 rat skeletal muscle cells and found that 100 µM *p*-coumaric acid significantly increased 2NBDG uptake compared to the control. Lim *et al.* (2021) found that 5 µM rutin induced 2NBDG uptake in differentiated 3T3-L1 adipocytes but only in the presence of 100 nM insulin. Chen *et al.* (2019) found that a 100 µg/mL phenolic acid fraction of chlorogenic acid and caffeic acid induced 2NBDG uptake in insulin resistant HepG2 cells in the presence of 500 nM insulin. Differences between the present study and previous studies may be related to the exposure time, drug concentrations, the degree of cellular differentiation for muscle cell lines and the sensitivity of the detection system. The concentrations used in these studies varied from 5 µM – 100 µM and the lack of any observed effect may be related to the concentrations of 0.1 µM – 10 µM.

Pietrzyk *et al.* (2021) evaluated glucose uptake in HepG2 cells exposed to *Viburnum opulus* L. (European guelder rose fruit) phenolic extracts. Insulin resistance was not induced but the cells were incubated with 100 nM insulin, and the HepG2 cells were exposed to 300 µM of the phenolic extract for 24 h before adding 150 µM 2NBDG for 2 h. Only some of the phenolic extracts induced 2NBDG uptake when compared to the control.

In this study, another approach was also tested in which insulin resistance was further induced by incubating HepG2 cells for 24 h in 100 nM insulin, as described by Zang *et al.* (2004). The cells were then incubated with 0.1 to 10 µM of the selected compounds and 50 nM insulin for 45 min before adding 80 µM 2-NBDG for 1 h. Most of the compounds, including metformin, decreased the fluorescent intensity compared to the control (**Figure 29**).

According to Hardy *et al.* (2017), an effect is biologically relevant if it is directly or indirectly linked to an adverse or beneficial effect, and the size of the effect must be relevant for the assessment. The increased uptake of glucose, especially in insulin resistant liver cells, would have a beneficial effect on those suffering from diabetes. However, the effect size in this experiment might not be relevant. Jiang *et al.* (2016), who also tested the glucose-uptake of HepG2 cells using 100 µM 2-NBDG for 20 min, reported a 1.5-to-2-fold increase in glucose-uptake of HepG2 cells in the presence of marein, a glucoside of okanin, a chalconoid, compared to the control (without marein), whereas the decrease in glucose-uptake in **Figure 29** was less than 1.2-fold compared to the control. Jiang *et al.* (2016) also reported a dose-dependent response to glucose-uptake, whereas **Figure 29** does not show a clear dose-dependent

response to any of the compounds. This suggests that the decreased glucose-uptake in insulin resistant HepG2 cells might be statistically significant but not biologically relevant.

Nam *et al.* (2013) tested the effect of a plant extract on the glucose uptake of differentiated C2C12 cells using the 2NBDG assay. The cells were incubated with 40 µg/mL extract, 1 µM insulin, and 10 µM 2NBDG for 1 h; and fluorescence was measured using a FACS flow cytometer. Krishna *et al.* (2015) also used FACS flow cytometry to measure 2NBDG uptake in L6 rat skeletal muscle cells in the presence of an herb extract. FACS flow cytometry is usually used to measure the fluorescence of a small sample of cells, such as, 10,000 single cell events. However, with larger cell numbers, such as, 100,000 to 1,000,000 cells, fluorescence can be measured using a fluorometer as was undertaken in the present study (Krishna *et al.*, 2015).

Giang Thanh Thi *et al.* (2017) performed a glucose uptake assay on insulin sensitive HepG2 cells and differentiated myotubes using radioactively labelled [^{14}C(U)]-glucose. Both rutin and caffeic acid increased glucose uptake in these cells. Exposure was to 10, 1, and 0.1 µM of the compounds for one to two days followed by the addition of [^{14}C(U)]-glucose for 4 h. Although effects were observed, fluorescently labelled glucose does hold several advantages over radioactively labelled glucose because fluorescent labels can be measured fast and in real-time, and are as sensitive as radioactive labels without being as hazardous as the radioisotopes (Ying *et al.*, 2007).

4.5. Chapter summary

The Caco2 IC_{50} of caffeic acid, *p*-coumaric acid, rutin, and vanillin was statistically similar to acarbose. Most of the compounds, including insulin, did not significantly increase the glucose-uptake ability of C2C12 and HepG2 cells, including insulin-resistant HepG2 cells. The $H_0 2$ is therefore accepted for these compounds. The compounds either do not increase glucose uptake, or the 2-NBDG assay is not sensitive enough to detect effects. The next step was to determine the content of the selected compounds in herbs, spices, and medicinal plants such as green tea.

4.5.1. Limitations and future work

Sinclair *et al.* (2020) suggests that 2-NBDG uptake alone is not a reliable tool for the assessment of cellular glucose transport especially if the 2-NBDG assay has no effect on the controls, which occurred in the present study. The 2-NBDG assay, therefore, requires further optimization or an alternative assay should be considered such as, a bioluminescent assay (Valley *et al.*, 2016). The detection of several proteins involved in the uptake of glucose, by Western blotting, could also be an option to measure the insulin-mimicking ability of the compounds. These proteins include AKT, IRS-1, AMPK, and PI3K all of which are involved in the increased expression of GLUT4 on the cell membrane (**Figure 5**) (Chen *et al.*, 2019).

CHAPTER 5: Green tea analysis

5.1. Introduction

Several plant species have been identified to have antidiabetic properties and these include *Cinnamomum zeylanicum* (cinnamon), *Allium sativum* (garlic), *Aloe vera* (aloe vera), *Nigella sativa* (black cumin), and *Zingiber officinale* (ginger) (Shihabudeen *et al.*, 2011, Priya Rani *et al.*, 2011, Beidokhti and Jäger, 2017). Individual plant derived compounds, such as rutin, caffeic acid, *p*-coumaric acid, and vanillin, in **CHAPTER 3**, have been found to have antidiabetic properties related to the inhibition of pancreatic alpha-amylase and alpha-glucosidase. The advantage of plants is that several of these compounds can be found in one plant species and as such, may act synergistically, resulting in increased activity.

5.1.1. *Camellia sinensis*

Camellia sinensis tea is an example of a readily available product that has many reported health benefits. Green tea is a beverage made by steeping the dried unfermented leaves of the *Camellia sinensis* plant and is the most common drink in the world after water. Tea flavanols have several beneficial properties, including antioxidant, antimutagenic, anticarcinogenic, and antibacterial activity. Thirty to forty percent of the polyphenols are water-extractable from green tea (Archana and Abraham, 2011). The most notable polyphenols in green tea are catechin, epigallocatechin gallate (EGCG), epicatechin gallate (ECG), epigallocatechin (EGC), and epicatechin (EC) (Ikbal *et al.*, 2020). Green tea also has antidiabetic activity, such as, the inhibition of alpha-glucosidase and alpha-amylase (Yilmazer-Musa *et al.*, 2012).

5.1.2. UPLC/MS

Polyphenols can be detected using ultra-performance liquid chromatography (UPLC) coupled with mass spectrometry (MS). The standard analytical approach for the identification of polyphenols in all plant material was developed by Lin and Harnly (2007). When plant material, such as green tea leaves, was extracted using aqueous acetonitrile with 0.1% formic acid, it had the best separation by liquid chromatography. The mass spectra show the relative intensity, or peak height, against the mass to charge ratio (m/z) in negative ion mode. When quantifying the concentration of a particular compound in green tea, a standard curve can be produced by plotting the peak height of different concentrations of the selected compound.

5.2. Methods

5.2.1. Chemicals

HPLC standards: epigallocatechin gallate, epicatechin, epigallocatechin, epicatechin-3-o-gallate, catechin, chlorogenic acid, rutin, caffeic acid, *p*-coumaric acid, quercetin, quinic acid, and rosmarinic acid were purchased from Sigma-Aldrich (St. Louis, Missouri, USA). The green tea brands used in this study were Five Roses, Livewell, Tetley, Eve's, and Dilmah, and were obtained from local supermarkets (Pick n Pay, Wellness Warehouse, and Spar, Pretoria, South Africa). All reagents used for the analysis of pancreatic alpha-amylase and alpha-glucosidase enzymatic activity were the same as described in **CHAPTER 3**.

5.2.2. The content of the selected compounds in herbs, spices, and green tea

Content values of different herbs and spices was obtained from Phenol-Explorer (Rothwell *et al.*, 2013), and FooDB (FooDB, 2017), except for green tea (Zhao *et al.*, 2011), and vanilla (Zhang *et al.*, 2014). The content was defined as the amount of compound (mg) in 100 g of seasoning. The equivalence was the amount (g) of seasoning that contains the amount of compound that corresponds to a 150 mg daily dose of acarbose.

5.2.3. Pancreatic alpha-amylase and alpha-glucosidase IC_{50} determination

A 20% (w/v) green tea solution was prepared for each brand by steeping two tea bags (2 x 2.5 g) in 25 mL boiling dH_2O for 10 min. The tea bags were removed, and the tea solution was centrifuged at 10 000*g* for 10 min (MiniSpin, Eppendorf, Hamburg, Germany). The supernatant was filtered using a 0.2 µm syringe filter, and the resulting filtered solution was used in the pancreatic alpha-amylase and alpha-glucosidase assay, as described in **sections 3.2.2.** and **3.2.3**. For details on the method see **Annexure F**.

5.2.4. Green tea extraction

Green tea from tea bags was ground for 20 s in a coffee grinder (Breville, Botany, Australia) and sieved with a final aperture opening of 355 µm (Labotec, Midrand, South Africa). A 0.25 g sample was mixed with 1.6 mL of 50% methanol/1% formic acid (v/v) and vortexed for 1 min. The samples were extracted in an ultrasonic bath for 1 hour and then centrifuged at 14 000*g* for 5 min. The clear supernatant was then diluted 10x with extraction solvent and transferred into 1.5 ml glass vials for analysis. A cocktail of standards was also prepared that included EGCG, EC, EGC, ECG, catechin, chlorogenic acid, rutin, caffeic acid, *p*-coumaric acid, quercetin, quinic acid, and rosmarinic acid. The concentrations ranged from 0 to 83 ppm for each standard.

5.2.5. Liquid chromatography/mass spectrometry (LC/MS) analysis

LC–MS analyses were performed on a Waters (Milford, MA, USA) Synapt G2 quadrupole time of flight mass spectrometer coupled to a Waters Acquity ultraperformance liquid chromatograph (UPLC) fitted with an Acquity photo diode array (PDA) detector. Similar to the method described by Long *et al.* (2012). Separation was achieved on a Waters HSS T3 (2.1 × 100 mm, 1.7 µm particle size) with 0.1% formic acid as mobile phase A and acetonitrile as mobile phase B. The flow rate was 0.3 mL/min, and the column temperature was maintained at 55°C. The gradient elution program was as follows: 0–28% B (0–1 min), 28–40% B (1–22 min), 40–100% B (22–23 min), held at 100% B (23–24.5 min), 100-0% B (24.5-25 min), and allowed to equilibrate for a further 4 min prior to the next injection of 5 µL. Electrospray ionization was applied in the negative ion mode at a cone voltage of 15 V, desolvation temperature of 275°C and desolvation gas setting of 650 L/h. The rest of the MS settings were optimized for best sensitivity. The instrument was calibrated with sodium formate and leucine enkaphelin was used as lock mass for accurate mass determinations. The MS acquisition method consisted of a low energy function at a trap voltage of 4 V and a high energy function where the trap collision energy was ramped from 40 to 100 V to generate fragmentation data (MS^e). For details on the method see **Annexure G**.

5.2.6. Statistical analysis

Data were processed using TargetLynx for quantitative analysis using MSDIAL and MSFINDER for unsupervised data processing (RIKEN Center for Sustainable Resource Science: Metabolome Informatics Research Team, Kanagawa, Japan) (Tsugawa *et al.*, 2015, Lai *et al.*, 2018). Data were also processed using MassLynx software version 4.1 from Waters. Principal component analysis (PCA) plots and volcano plots (adjusted p-value using false discovery rate (FDR)) were produced using MetaboAnalyst 5.0 (https://www.metaboanalyst.ca/) (Xia and Wishart, 2011). Mass fragmentation patterns produced using ChemSketch MassSpec Scissors.

5.3. Results

5.3.1. The content of the selected compounds in herbs, spices, and green tea

Rutin, caffeic acid, and *p*-coumaric acid were present in green tea. The highest content of caffeic acid was in common verbena, tarragon, and sweet basil. The highest content of rutin was in parsley, sorrel, and capers. Vanillin was only present in vanilla. The equivalence dosages are listed in **Table 10.**

Table 10: The content (mg/100 g) of selected compounds in a variety of seasonings

Caffeic acid		
Seasoning	**Content (mg/100 g)**	**Equiv (g)**
Common verbena (*Verbena officinalis*)	1000	4
Tarragon (*Artemisia dracunculus*)	764	5
Sweet basil (*Ocimum basilicum*)	634	7
Green tea (*Camellia sinensis*)[a]	257	16
Anise (*Pimpinella anisum*)	103	40
Common sage (*Salvia officinalis*), dried	26	158
Spearmint (*Mentha spicata*), dried	25	167
Ceylon cinnamon (*Cinnamomum burmannii*)	24	173
Common thyme (*Thymus vulgaris*), dried	21	196
Star anise (*Illicium verum*)	20	207
Cumin (*Cuminum cyminum*)	17	252
Caraway (*Carum carvi*)	16	255
Nutmeg (*Myristica fragrans*)	16	256
Ginger (*Zingiber officinale*), dried	16	270
Common thyme (*Thymus vulgaris*), fresh	12	357
***p*-Coumaric acid**		
Seasoning	**Content (mg/100 g)**	**Equiv (g)**
Green tea (*Camellia sinensis*)[a]	399	10
Pepper (*Capsicum frutescens*)	54	71
Cloves (*Syzygium aromaticum*)	8	449
Oregano (*Origanum vulgare*), fresh	6	662
Common sage (*Salvia officinalis*), dried	5	769
Common thyme (*Thymus vulgaris*), dried	5	769
Rosemary (*Salvia Rosmarinus*), dried	4	1038
Marjoram (*Origanum majorana*), dried	2	1587
Rutin		
Seasoning	Content (mg/100 g)	Equiv (g)
Parsley (*Petroselinum crispum*)	3000	5
Sorrel (*Rumex acetosa*)	1280	11
Capers (*Capparis spinosa*)	332	43
Red tea (*Aspalathus linearis*)	120	118
Green tea (*Camellia sinensis*)[a]	53	270
Marjoram (*Origanum majorana*), dried	3	5457
Vanillin		
Seasoning	Content (mg/100 g)	Equiv (g)
Vanilla (*Vanilla planifolia*)[b]	1980	2

Content values obtained from Phenol-Explorer (Rothwell *et al.*, 2013) and FooDB (FooDB, 2017), except for green tea (Zhao *et al.*, 2011)[a], and vanilla (Zhang *et al.*, 2014)[b]
Content = the amount of compound (mg) in 100 g of seasoning, Equiv = the amount (g) of seasoning that contains the amount of compound that corresponds to a 150 mg daily dose of acarbose

5.3.2. Untargeted metabolomics

The Waters Synapt G2 UPLC/MS data were quantified using TargetLynx which provided information about the peak height and retention time of the peaks. These data were used to produce chromatograms for each green tea sample as well as the standards. **Figure 30** represents the base peak intensity (BPI) chromatogram of the Dilmah green tea brand showing the chemical structures of some of the highest peaks: gallocatechin (8.57 min, 305.07 m/z), epigallocatechin (11.03 min, 305.07 m/z), catechin (11.83 min, 289.07 m/z), epicatechin (13.90 min, 289.07 m/z), assamicain A (14.13 min, 915.16 m/z), EGCG (14.27 min, 457.08 m/z), and epicatechin gallate dimer (17.38, 883.17 m/z). **Supplementary Figure 3** represents the BPI chromatogram of the other four green tea brands.

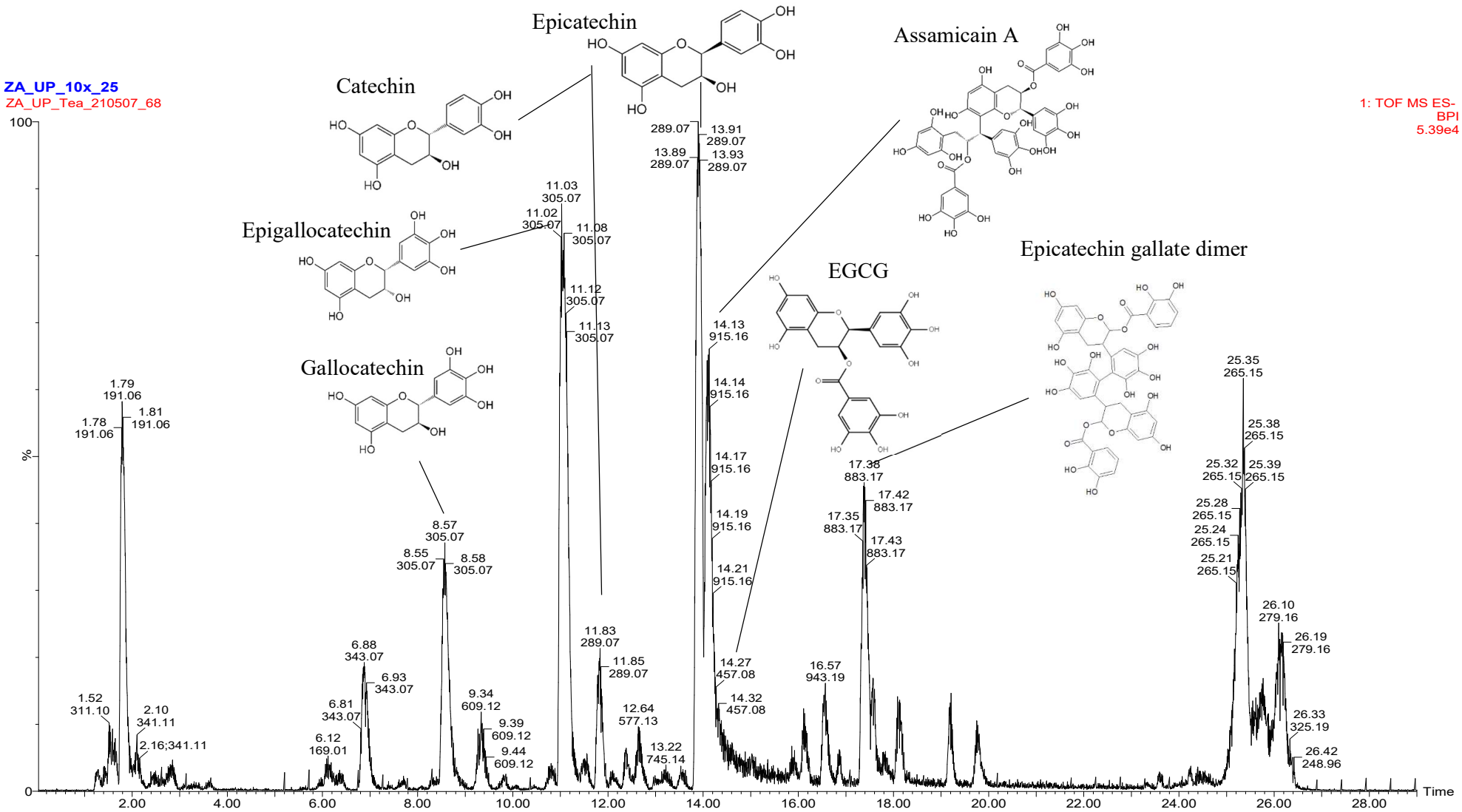

Figure 30: BPI chromatogram of Dilmah green tea brand

Figure 31 represents a PCA of all five green tea brands produced using MassLynx based on the original profile matrix. The first principal component (PC1) explains 32.7% and the second principal component (PC2) explains 27.7% of the variation.

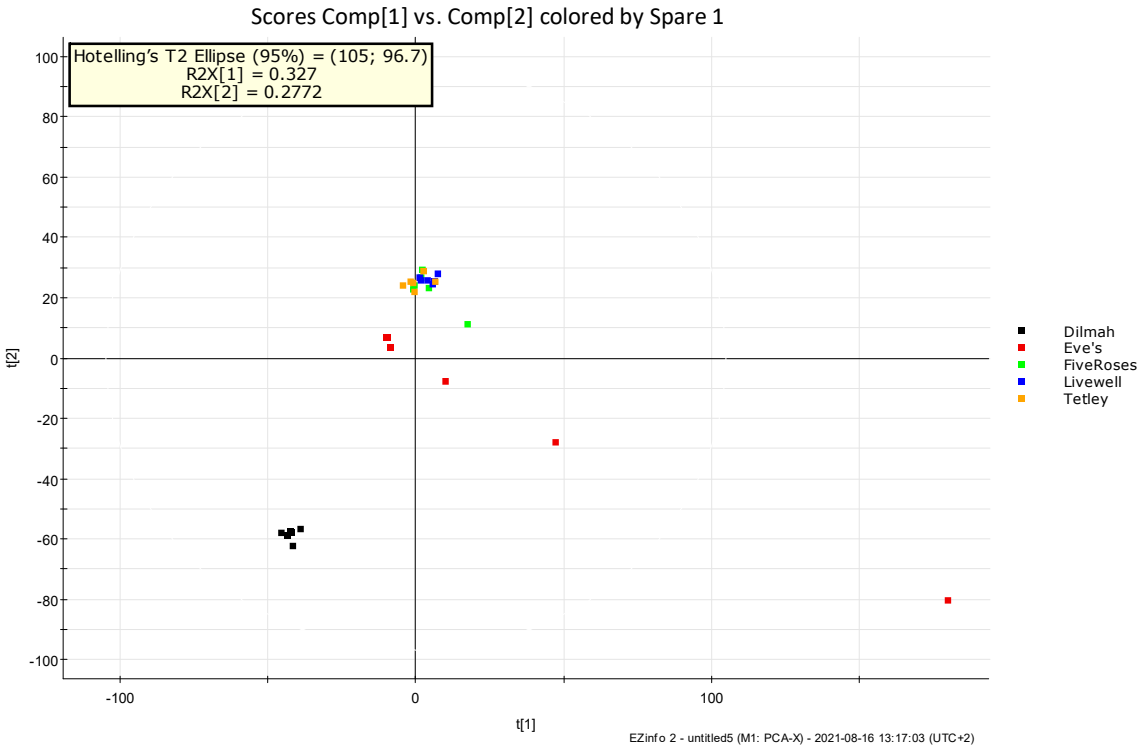

Figure 31: The PCA plot of all five green tea brands based on the original profile matrix exported from MassLynx

PCA was performed on the 139 putatively annotated compounds in all five green tea brands, **Figure 32**. **Supplementary Table 6** summarises the compounds that were annotated with a high level of confidence. According to the PCA, Five Roses, Livewell, and Tetley have similar peak heights for the putatively annotated compounds. Eve's and Dilmah had different peak heights of the putatively annotated compounds when compared with each other and the other three green tea brands. Eve's had a large variation within the sample when evaluating the PCA plot in **Figure 31** and the raw data. The outliers were removed and the PCA in **Figure 32** was produced with MetaboAnalyst. PC1 explains 64.6% and PC2 explains 15.3% of the variation.

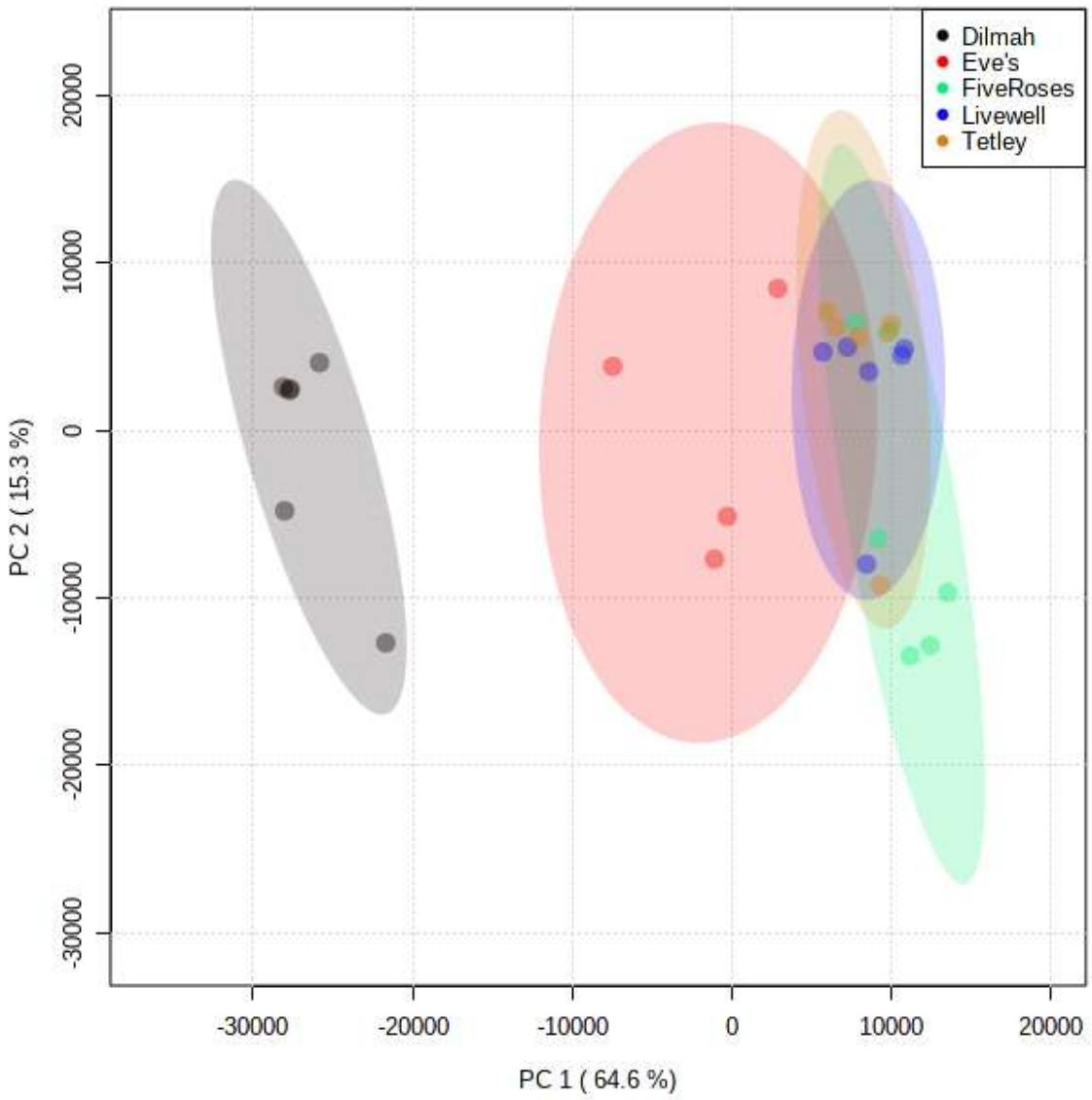

Figure 32: PCA of the putatively annotated compounds in the five green tea brands

5.3.3. Targeted metabolomics

Figure 33 shows the Waters Synapt G2 TOF MS of the selected standards in negative ion mode (ES-). The TOF MS ES- chromatogram is represented as the BPI chromatogram which is a variant of a total ion current (TIC) chromatogram, but the BPI chromatogram only shows the most intense peaks and therefore has greater apparent resolution, (Waters, 2005). The standards identified in **Figure 33**, with their monoisotopic masses in negative ion mode are: quinic acid (1.84 min, 191.06 m/z), epigallocatechin (11.06 min, 305.07 m/z), catechin (11.78 min, 289.07 m/z), chlorogenic acid (12.23 min, 353.09 m/z), caffeic acid (12.97 min, 179.04 m/z), epicatechin (13.90 min, 289.07 m/z), EGCG (14.07 min, 457.08 m/z), *p*-coumaric acid (15.75 min, 163.05 m/z), epicatechin-3-O-gallate (17.40 min, 441.08 m/z), rutin (17.66 min, 609.14 m/z), rosmarinic acid (20.70 min, 359.08 m/z), and quercetin (24.20 min, 301.04 m/z). Any peaks after 24 min were ignored as this represent the washing step with 100% solvent B as well as re-calibration back to solvent A.

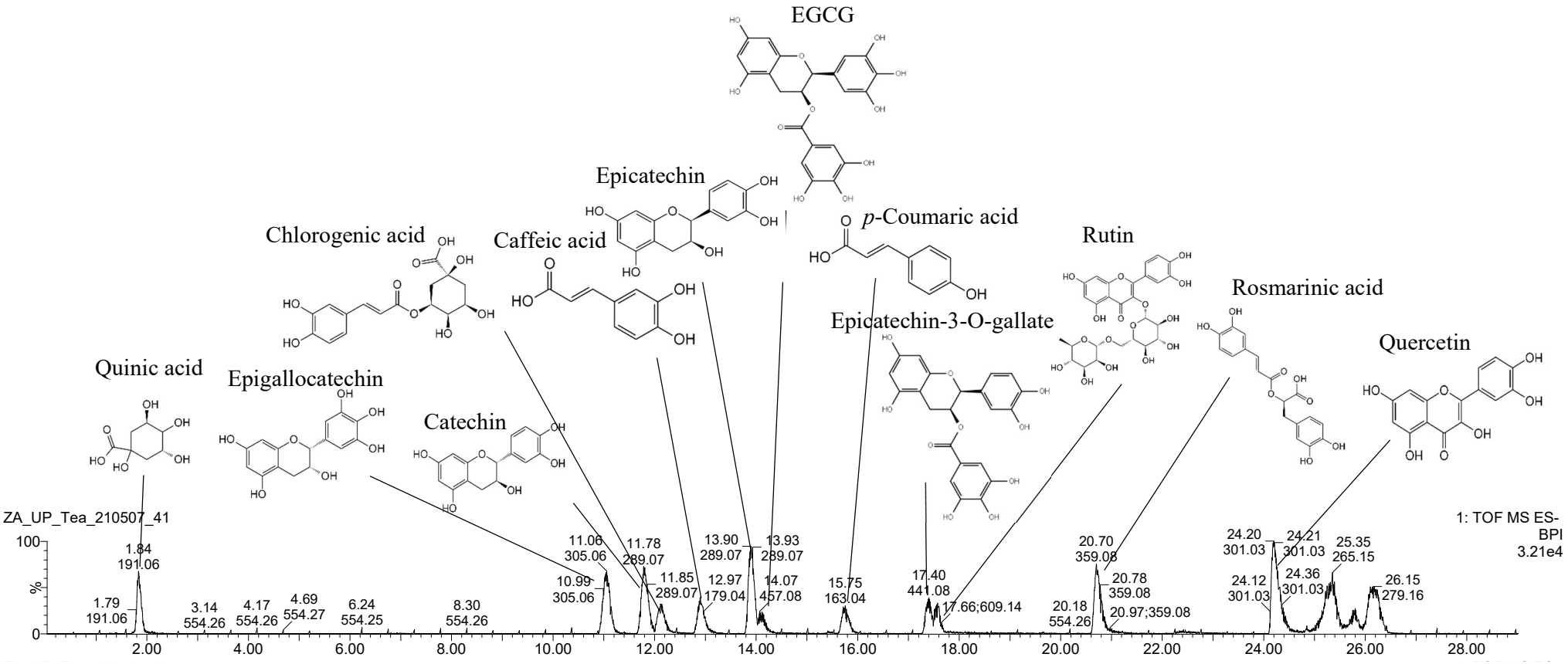

Figure 33: Chromatogram of standards
The TOF MS ES- BPI chromatogram of the standard cocktail (17 ppm)

The standard curve of each standard in the cocktail was generated and the % dry weight was determined. **Table 11** shows the % dry weight of each standard in the five green tea brands. Dilmah had the largest overall percentage of standards. EGC and EGCG had the largest % dry weight in all five green tea brands. Caffeic acid, *p*-coumaric acid, and rosmarinic acid had the smallest % dry weight in all five green tea brands.

Table 11: The % dry weight (mean±SD, n=6) of the standards in the five green tea brands

Standards	Dilmah	Eve's	Five Roses	Livewell	Tetley
Caffeic acid	<0.01	<0.01	<0.01	<0.01	<0.01
Catechin	1.68±0.01	0.76±0.06	0.38±0.02	0.58±0.01	0.62±0.01
Chlorogenic acid	0.27±0.01	0.04±0.01	0.04±0.01	0.03±0.01	0.06±0.01
Epicatechin	6.26±0.02	3.78±0.19	3.75±0.01	3.58±0.02	3.68±0.01
Epicatechin 3-O-gallate	5.61±0.02	4.51±0.22	5.04±0.01	4.01±0.14	4.84±0.02
Epigallocatechin	8.35±0.03	5.02±0.02	7.55±0.02	7.36±0.04	7.62±0.04
Epigallocatechin gallate	8.66±0.05	7.16±0.35	9.01±0.01	8.57±0.04	8.35±0.04
***p*-Coumaric acid**	<0.01	<0.01	<0.01	<0.01	<0.01
Rosmarinic acid	<0.01	<0.01	<0.01	<0.01	<0.01
Rutin	2.85±0.03	0.57±0.06	0.44±0.05	0.60±0.02	0.70±0.03
Quinic acid	0.42±0.01	0.06±0.01	0.07±0.01	0.10±0.01	0.11±0.01

5.3.4. Enzyme inhibition of green tea brands

The pancreatic alpha-amylase inhibitory ability of the five green tea brands was investigated. The IC_{50} of each green tea brand was determined for pancreatic alpha-amylase and was compared with acarbose (**Table 12**). Dilmah, Eve's, Five Roses, and Livewell had IC_{50} values significantly greater than acarbose. Tetley had an IC_{50} value significantly similar to acarbose. Eve's and Tetley had IC_{50} values that were lower than Dilmah, Five roses, and Livewell. The putatively annotated compounds in the low and high IC_{50} green tea groups were analysed using MetaboAnalyst. The PCA of high vs low pancreatic alpha-amylase IC_{50} is represented in **Figure 34**. There is a large variation within the high IC_{50} green tea brands compared to the low IC_{50} green tea brands.

Table 12: The inhibition of pancreatic alpha-amylase by the five green tea brands

Green tea brand	IC_{50} (mg/mL)
Acarbose	0.02±0.002[a]
Dilmah	25.36±2.931[b]
Eve's	14.42±2.618[b]
Five Roses	22.64±1.006[b]
Livewell	26.13±3.856[b]
Tetley	14.40±3.648[a]

IC_{50} is the mean ± SEM (n = 3)

[a] Value is significantly similar, ($p > 0.05$, n=3, two-tailed) to acarbose

[b] Value is significantly different ($p < 0.05$, n=3, two-tailed) to acarbose

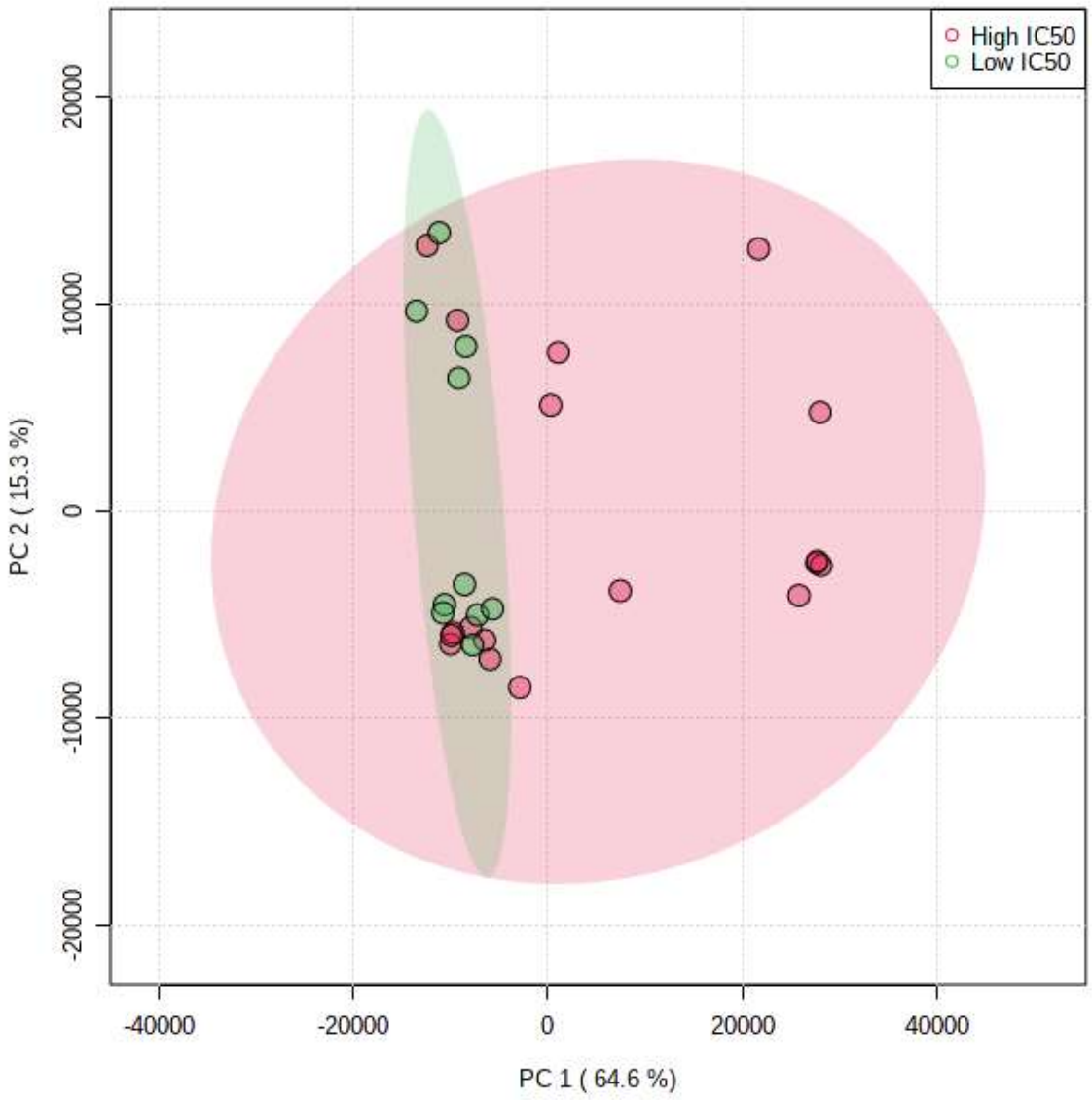

Figure 34: PCA of high vs low pancreatic alpha amylase IC_{50}

Figure 35 shows the volcano plot of the 139 putatively annotated compounds where none of these compounds were significantly more abundant in the green tea brands that had low or high pancreatic alpha-amylase IC_{50}.

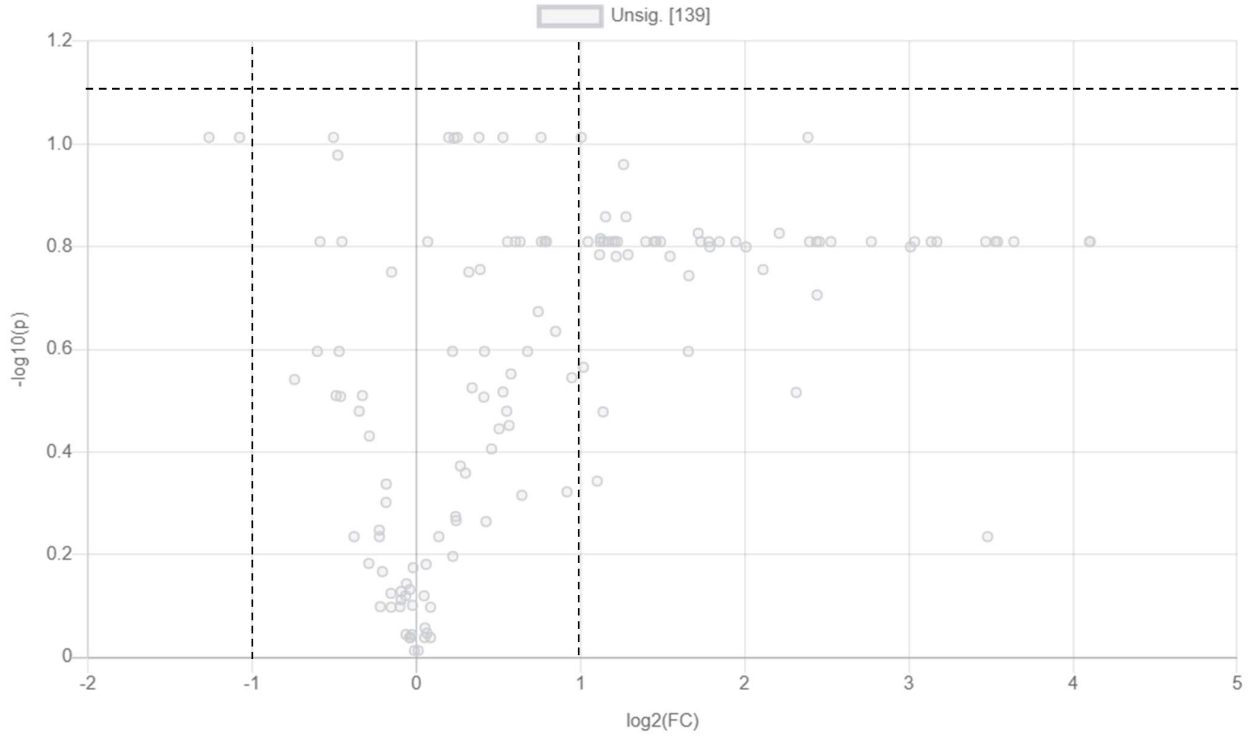

Figure 35: Volcano plot of high vs low pancreatic alpha-amylase IC_{50}

Fold change threshold of 2.0, p-value threshold of 0.05 (log(p) = 1.12), and direction of comparison is high IC_{50}/low IC_{50}

The alpha-glucosidase inhibitory ability of the five green tea brands was investigated. The IC_{50} of each green tea brand was determined for alpha-glucosidase and compared to acarbose (**Table 13**). All five green tea brands had IC_{50} values significantly smaller than acarbose. Dilmah and Eve's had IC_{50} values that were considered to be low when compared with Five Roses, Livewell, and Tetley green tea brands. The putatively annotated compounds in the low and high IC_{50} green tea groups were analysed using MetaboAnalyst. The PCA of high vs low alpha-glucosidase IC_{50} is represented in **Figure 36**.

Table 13: The inhibition of alpha-glucosidase by the five green tea brands

Green tea brand	IC_{50} (mg/mL)
Acarbose	0.2524±0.0164[a]
Dilmah	0.0094±0.0005[b]
Eve's	0.0128±0.0005[b]
Five Roses	0.0275±0.0012[b]
Livewell	0.0233±0.0019[b]
Tetley	0.0227±0.0005[b]

IC_{50} is the mean ± SEM (n = 3)

[a] Value is significantly similar ($p > 0.05$, n=3, two-tailed) to acarbose

[b] Value is significantly different ($p < 0.05$, n=3, two-tailed) to acarbose

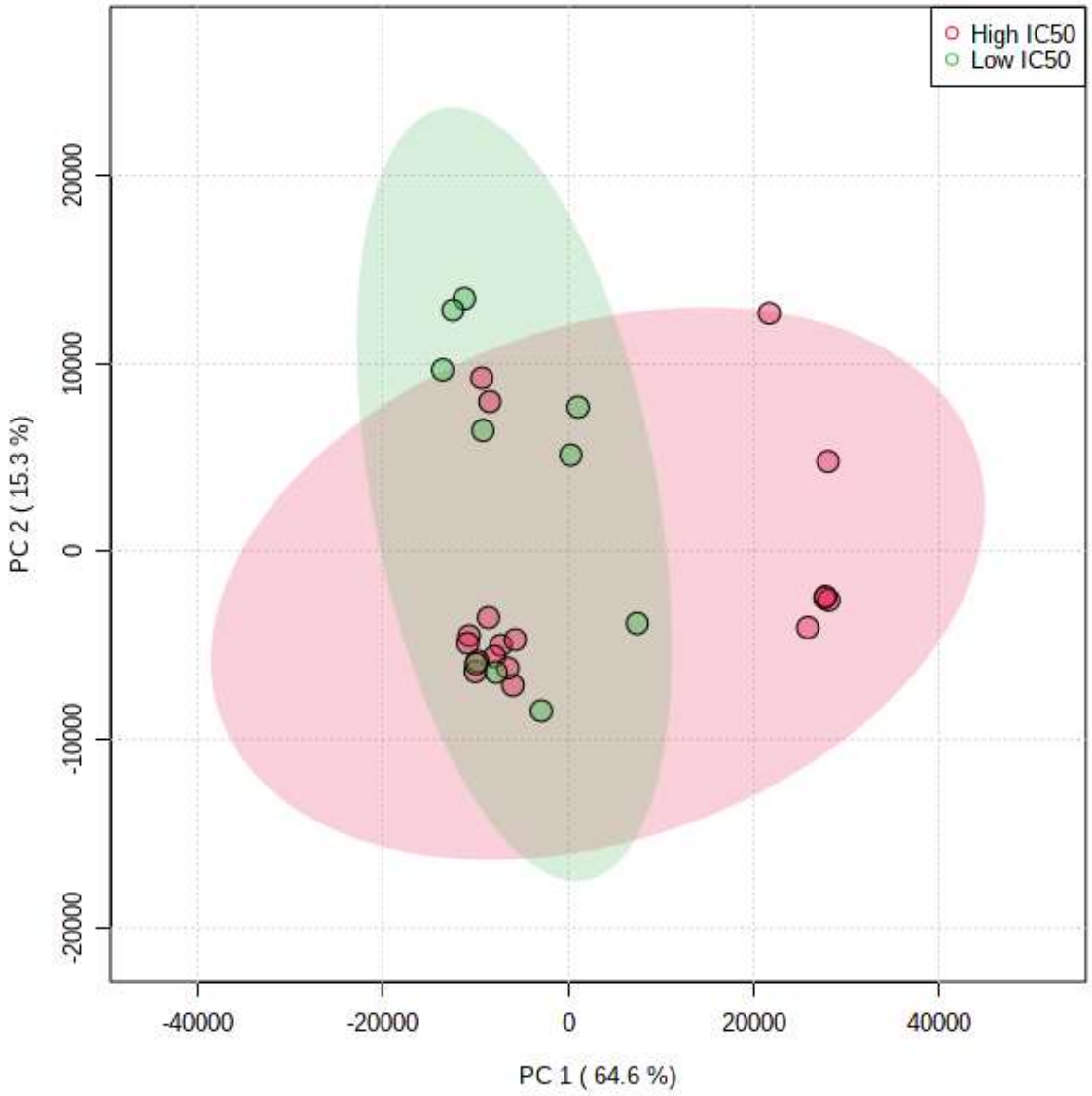

Figure 36: PCA of high vs low alpha-glucosidase IC_{50}

Figure 37 shows the volcano plot of the 139 putatively annotated compounds where 2 of these compounds were significantly more abundant in green tea brands that had a low alpha-glucosidase IC_{50}.

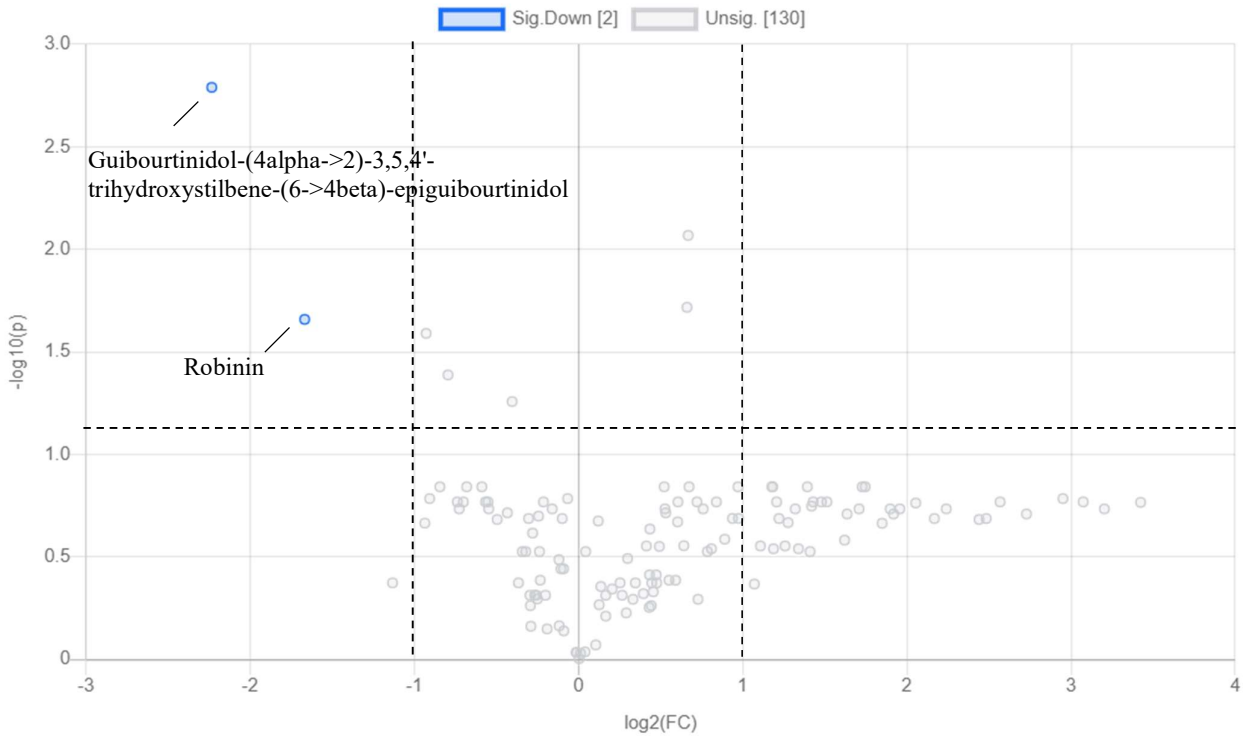

Figure 37: Volcano plot of high vs low alpha-glucosidase IC_{50}

Fold change threshold of 2.0, p-value threshold of 0.05 (log(p) = 1.12), and direction of comparison is high IC_{50}/low IC_{50}

The compounds that were significantly more abundant in green tea brands with a low IC_{50} value for alpha-glucosidase were putatively identified as guibourtinidol-(4alpha->2)-3,5,4'-trihydroxystilbene-(6->4beta)-epiguibourtinidol and robinin. **Figure 38** shows the MS/MS spectra for these compounds and EGCG indicating the fragmentation pattern. The red lines that fragment the chemical structures represent the fragments present in the *in silico* MS/MS spectra obtained from the databases in MSFINDER.

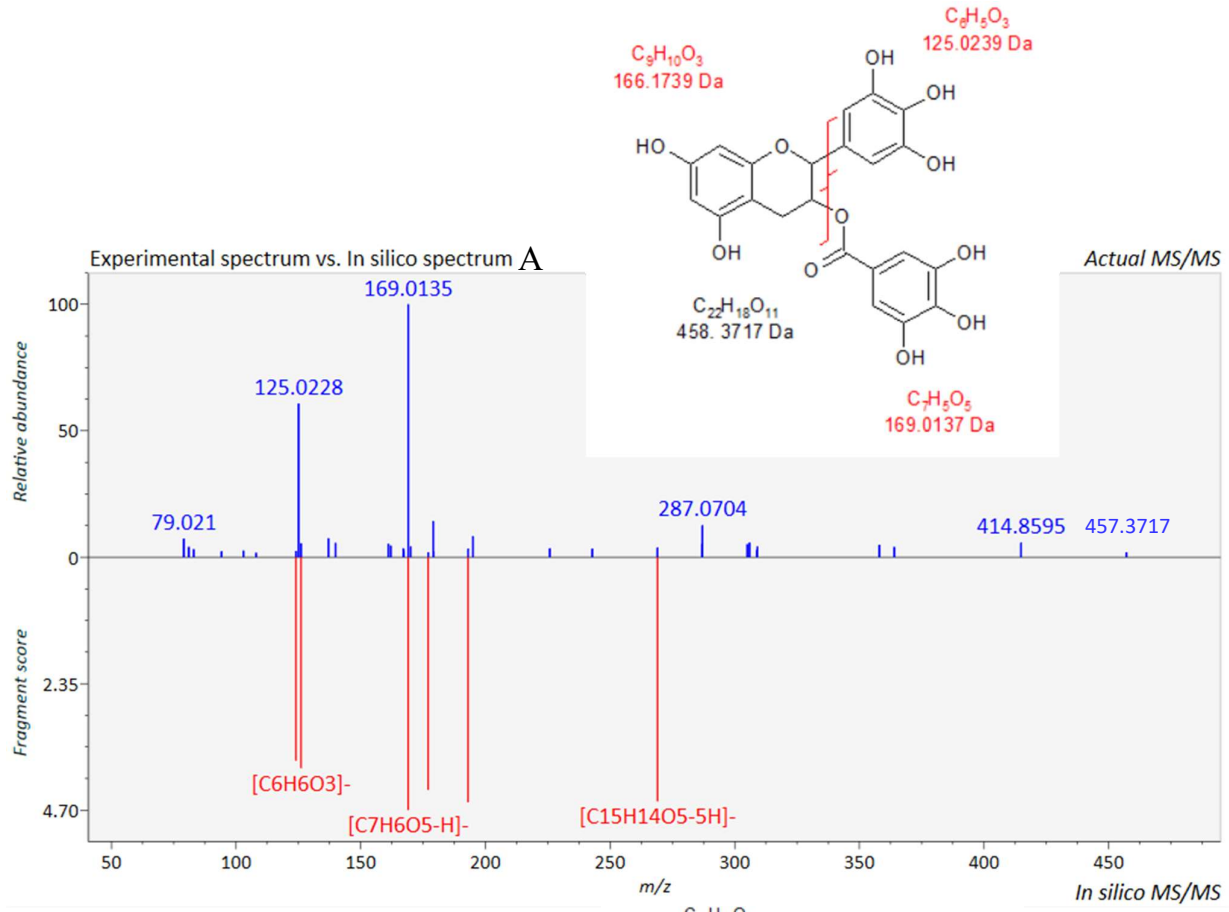
Experimental spectrum vs. In silico spectrum A
Actual MS/MS
In silico MS/MS
Relative abundance
Fragment score
m/z
169.0135
125.0228
79.021
287.0704
414.8595
457.3717
[C6H6O3]-
[C7H6O5-H]-
[C15H14O5-5H]-
C9H10O3
166.1739 Da
C6H5O3
125.0239 Da
C22H18O11
458. 3717 Da
C7H5O5
169.0137 Da

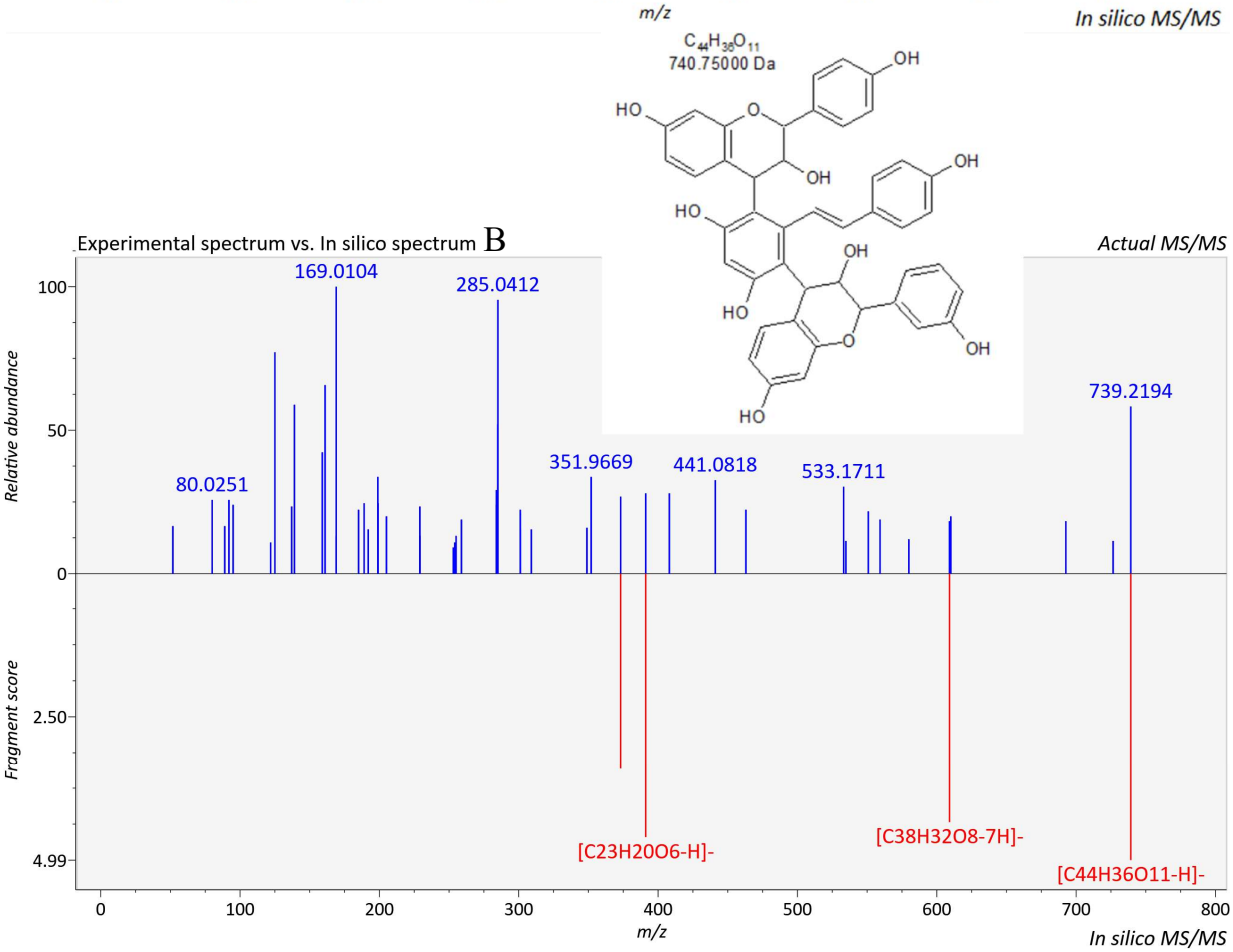
Experimental spectrum vs. In silico spectrum B
Actual MS/MS
In silico MS/MS
Relative abundance
Fragment score
m/z
169.0104
285.0412
80.0251
351.9669
441.0818
533.1711
739.2194
[C23H20O6-H]-
[C38H32O8-7H]-
[C44H36O11-H]-
C44H36O11
740.75000 Da

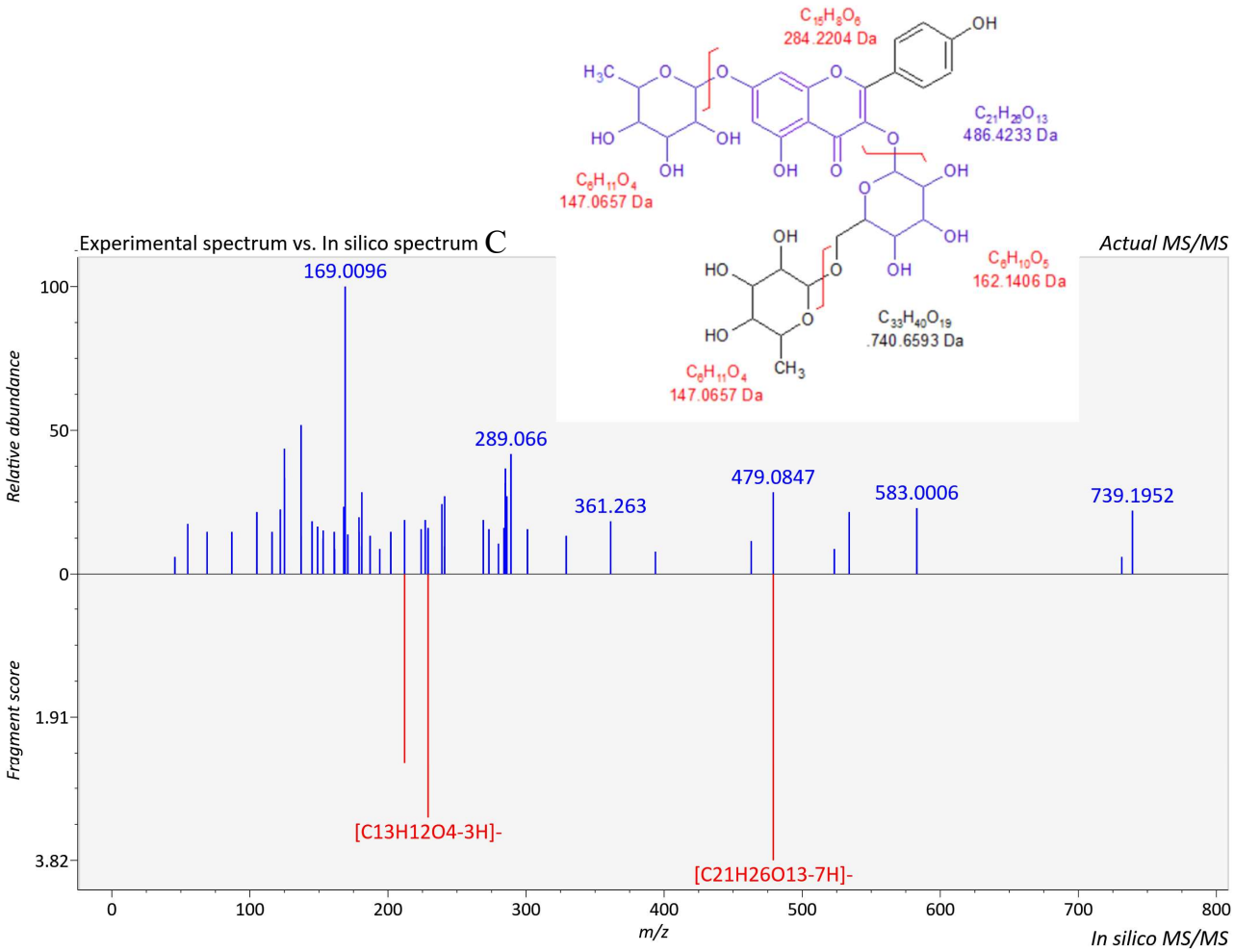

Figure 38: MS/MS spectra of compounds significantly abundant in green tea brands with low digestive enzyme IC_{50} values and EGCG

A: EGCG (fragmentation pattern according to MassBank), B: guibourtinidol-(4alpha->2)-3,5,4'-trihydroxystilbene-(6->4beta)-epiguibourtinidol, C: robinin (fragmentation pattern based on pattern obtained by Ju *et al.* (2018))

5.4. Discussion

Green tea (*Camellia sinensis*) has several beneficial properties, including antioxidant, antimutagenic, anticarcinogenic, and antibacterial activities. Green tea is widely available and can be consumed daily. The most notable polyphenols in green tea are catechin, EGCG, ECG, EGC and EC (Ikbal *et al.*, 2020). Caffeic acid, *p*-coumaric acid, and rutin which were investigated in **CHAPTER 3 and 4** were also present in green tea (Zhao *et al.*, 2011). Untargeted metabolomics was used to compare the polyphenol content between five commercial green teas. Green tea was extracted with 50% methanol, separated using a Waters Acquity UPLC column and analysed using a Waters Synapt TOF MS in negative ion mode. The UPLC/MS data were analysed using TargetLynx, an application manager that automates sample data acquisition, processing and reporting for quantitative results. MassLynx could then be used to visualize the data as chromatograms as shown in **Figure 30** and **Supplementary Figure 3**.

Catechin and EC both have a m/z value of 289 Da and the same molecular formula, $C_{15}H_{14}O_6$, the only difference being that they are stereoisomers. The same for EGC and GC, which both have a m/z value of 305 Da and a molecular formula of $C_{15}H_{14}O_7$. These stereoisomers have different retention times and can, therefore, be identified on a chromatogram. According to Abbas and Wink (2014), catechin elutes from the column before EC; and GC elutes before EGC, which is apparent in **Figure 30**. An ECG dimer (17.38 min, 883 Da) with a m/z value two times that of ECG (441.5 Da) was observed in the chromatogram. These peaks are present in all five green tea brands. The main polyphenols were, therefore, detected in these green tea brands as described in the literature (Friedman *et al.*, 2006).

The raw UPLC/MS data were imported into MassLynx where statistical analysis could be performed. A PCA plot was produced showing the variation between all five green tea brands based on the original profile matrix, **Figure 31**. According to this PCA, the PC1 was 32.7% and the PC2 was 27.7%. The percentage variation explained by these two principal components was 60.4%. Evaluation of the PCA plot (**Figure 31**) reveals that there was a large variation in the Eve's tea sample. The repeats that contribute the most to the variation were removed. **Supplementary table 6** summarises the compounds that were annotated with a high level of confidence. Schymanski *et al.* (2014) defines 5 levels of confidence, level 1 being the highest level of confidence and applies to the compounds annotated with a standard. Level 2 applies to the compounds annotated using a library spectrum match.

Compound annotation was performed on the Waters raw data using MSDIAL and MSFINDER. The Waters raw file was converted to an ABF file that could be imported into MSDIAL. The alignment results were then imported into MSFINDER which putatively annotated the compounds by matching MS/MS spectra from library databases. The peak height file from MSDIAL and the structure file from MSFINDER were combined. These data were then sorted by removing peaks that were not annotated

which left 139 compounds that were putatively annotated. The variation between the five green tea brands based on the peak height of the putatively annotated compounds was analysed using MetaboAnalyst. A PCA was produced, **Figure 32** which shows separation between Dilmah and the other four green tea brands as well as some separation between Eve's and the other three green tea brands (Five Roses, Livewell, and Tetley). The PC1 for the PCA in **Figure 32** is 64.6% and the PC2 is 15.3%. The percentage variation explained by these two principal components is 79.9%. The change in percentage variation between the PCA in **Figure 31** and the PCA in **Figure 32** is because the first PCA evaluated the original profile matrix whereas the second PCA evaluated the 139 compounds that were putatively annotated in the five green brands. The second PCA also had the two Eve's outliers removed. There is, therefore, a larger percentage variation between Dilmah, Eve's and the other three green tea brands when evaluating the peak height of the putatively annotated compounds rather than the original profile matrix. Subsequent PCAs were plotted using the putatively annotated compounds.

Targeted metabolomics was also performed to determine the amount of the selected standards present in the five green tea brands. The selected standards were: EGCG, EC, EGC, epicatechin-3-o-gallate, catechin, and chlorogenic acid, which are common compounds found in green tea (Yu *et al.*, 2020). Included were rutin, caffeic acid, and *p*-coumaric acid, which had pancreatic alpha-amylase and alpha-glucosidase inhibitory activity (**CHAPTER 3**). Quercetin, quinic acid, and rosmarinic acid that were part of another study were also investigated. The chromatogram of these standards was produced by MassLynx, **Figure 33**. All 12 standards were identified in this BPI chromatogram. The peak height of each standard for five different concentrations (ppm) was used to generate a standard curve for each standard. The % (m/m) dry weight of each standard in each green tea brand is shown in **Table 11**. Many of the standards were more abundant in Dilmah green tea than in the other four green tea brands. EGCG had the highest % dry weight for all five green tea brands, between 7% and 9% dry weight. Caffeic acid, *p*-coumaric acid, and rosmarinic acid had % dry weight values less than 0.01. Quercetin was not detected in the green tea samples. Zhao *et al.* (2011) was able to quantify these standards where EGCG was the most abundant catechin with a % dry weight of 14.4 and a total content of the relevant catechins was 20.8%. The total catechin content for the five green tea brands in this study ranged from 16% to 25% which was similar to the amount quantified by Zhao *et al.* (2011). Lin *et al.* (1998) observed similar trends in Chinese green tea compared with Zhao *et al.* (2011), with a total catechin content of approximately 20% and EGCG had the largest % dry weight of all the catechins. EGCG is the most abundant bioactive compound in green tea and has several health benefits such as antioxidant activity, antimutagenic activity, and antimicrobial effects (Pastoriza *et al.*, 2017). The antidiabetic effects of green tea and EGCG decreased digestive enzyme activity, and intestinal GLUT activity, while they increased insulin sensitivity (Kao *et al.*, 2006).

Green tea also has antidiabetic properties, such as, the inhibition of alpha-glucosidase and alpha-amylase (Archana and Abraham, 2011). The IC_{50} of the five green teas for these two enzymes was evaluated using the assays described in **CHAPTER 3**. The green tea for these assays was extracted with boiling water. In fact, 30 -40% of the dry weight of a tea bag is extracted as soluble solids (Archana and Abraham, 2011). Dilmah, Eve's, Five Roses, and Livewell had pancreatic alpha-amylase IC_{50} values significantly greater than that of acarbose; and Tetley had an IC_{50} significantly similar to acarbose, **Table 12**. The pancreatic alpha-amylase IC_{50} of Eve's and Tetley was approximately 14 mg/mL, but the SD of Tetley was larger than Eve's which is a possible reason for the significant similarity of Tetley to acarbose but not Eve's to acarbose. Both Eve's and Tetley were considered to have low IC_{50} values compared with Dilmah, Five Roses, and Livewell which had high IC_{50} values. The metabolomic difference between the green teas with low IC_{50} values for pancreatic alpha-amylase inhibition was further investigated, **Figures 34 and 35**. Yilmazer-Musa *et al.* (2012) reported a green tea extract with an alpha-amylase IC_{50} value of 34.9 ± 0.9 μg/mg that was significantly smaller than the IC_{50} value of acarbose (6.9 ± 0.8 μg/mg).

All five green tea brands had alpha-glucosidase IC_{50} values significantly smaller than acarbose, which suggests that these green tea brands are better alpha-glucosidase inhibitors than acarbose, **Table 13**. Dilmah and Eve's had lower IC_{50} values compared to Five Roses, Livewell, and Tetley which had higher IC_{50} values. The metabolomic difference between the low and high alpha-glucosidase IC_{50} green teas was further investigated, **Figures 36 and 37**. Yilmazer-Musa *et al.* (2012) reported a green extract with an alpha-glucosidase IC_{50} value of 0.5 ± 0.1 μg/mg that was significantly smaller than the IC_{50} value of acarbose (91.0 ± 10.8 μg/mg). Yilmazer-Musa *et al.* (2012) also investigated the alpha-glucosidase IC_{50} of key catechins in green tea, where ECG, EGCG, and GCG had alpha-glucosidase IC_{50} values significantly less than acarbose. The IC_{50} of ECG, EGCG, and GCG reported by Yilmazer-Musa *et al.* (2012) were 3.5 ± 1.1, 0.3 ± 0.1, 1.4 ± 0.1 μg/mg, respectively.

Another study determined that the combination of green tea extract with acarbose or EGCG with acarbose had a synergistic effect on alpha-amylase and alpha-glucosidase at low concentrations (below the IC_{50}). This implies that green tea and acarbose potentially could be used as a combination treatment for the treatment of T2D (Gao *et al.*, 2013).

The green tea brands were grouped into low IC_{50} and high IC_{50} for pancreatic alpha-amylase and alpha-glucosidase as previously described. The peak height files with the putatively annotated compounds were uploaded into MetaboAnalyst and PCA and volcano plots were produced. The PCA in **Figure 34** represents the variation between high vs low pancreatic alpha-amylase IC_{50} based on the relative peak heights of the previously putatively annotated compounds. A volcano plot was subsequently produced

to visualize the compounds that were significantly different ($p < 0.05$) between high and low IC_{50} values, **Figure 35**. None of the putatively annotated compounds were significantly more abundant in green tea brands with low or high pancreatic alpha-amylase IC_{50} values.

The PCA in **Figure 36** represents the variation between high vs low alpha-glucosidase IC_{50} values also based on the relative peak heights of the putatively annotated compounds. The volcano plot for these data presented the compounds that were significantly ($p < 0.05$) more abundant in green tea brands with low alpha-glucosidase IC_{50} values, **Figure 37**. These compounds were guibourtinidol-(4alpha->2)-3,5,4'-trihydroxystilbene-(6->4beta)-epiguibourtinidol and robinin having the adjusted p-value of 0.002 and 0.023, respectively.

The MS/MS spectra from MSFINDER for these compounds and EGCG are represented in **Figure 38**. The MS/MS spectrum A represents EGCG which was identified by several databases on MSFINDER. The fragmentation pattern was confirmed by comparing the MS/MS spectrum to that on MassBank (https://massbank.eu/MassBank/). The fragmentation pattern in MS/MS spectrum A was also reported by Spacil *et al.* (2010) who performed Waters UHPLC-MS/MS ESI^- on non-fermented tea samples. The examination of the MS/MS spectrum of EGCG, a common green tea constituent, and the comparison to mass spectrum databases, confirmed the ability of MSFINDER to putatively annotate the compounds in this study. The similarity score for EGCG between the actual MS/MS and the *in silico* MS/MS was 5.73/10.

The MS/MS spectrum B represents guibourtinidol-(4alpha->2)-3,5,4'-trihydroxystilbene-(6->4beta)-epiguibourtinidol which was identified by KNApSAcK, UNPD, and COCONUT (CNP0146201). The actual MS/MS spectrum matched these databases with a similarity score of 4.60/10. This compound is classified as a linear diarylheptanoid and COCONUT predicted that this compound has alpha-glucosidase inhibitory ability (Sorokina *et al.*, 2021). The actual MS/MS spectrum B has fragments that are present in the *in silico* MS/MS as well as other smaller fragments that do not match the *in silico* MS/MS and explains the low similarity score of 4.60/10. The mass fragmentation pattern was not available on any database, nor were there any reports featuring this compound.

MS/MS spectrum C represents robinin also known as kaempferol 3-O-robinoside-7-O-rhamnoside or kaempferol 3-rutinoside-7-rhamnoside was identified by KNApSAcK, CHEBI, FooDB, NANPDB, UNPD, and COCONUT (CNP0171942). The actual MS/MS spectrum matched these databases with a similarity score of 5.09/10. This compound is classified as a flavonoid glycoside and COCONUT predicted that this compound has both amylase and alpha-glucosidase inhibitory ability (Sorokina *et al.*, 2021). The actual MS/MS spectrum C has fragments that are present in the *in silico* MS/MS as well as other smaller and larger fragments that do not match the *in silico* MS/MS and explains the low similarity

score of 5.09/10. The fragment represented in blue shows a possible fragment in the *in silico* MS/MS ($C_{21}H_{26}O_{13}$). Kaempferol 3-rutinoside-7-rhamnoside was detected in mulberry leaves by Ju *et al.* (2018) and the fragmentation pattern is represented in **Figure 38C**. However, mass spectrum C does not correlate to the mass spectrum reported by Ju *et al.* (2018), nor does it correlate to the mass spectrum library known as MassBank.

Guibourtinidol-(4alpha->2)-3,5,4'-trihydroxystilbene-(6->4beta)-epiguibourtinidol and robinin, which were more abundant in green tea brands that had low pancreatic alpha-glucosidase IC_{50} values, were also predicted by COCONUT to have amylase and/or alpha-glucosidase inhibitory ability. The presence of several inhibitory compounds in a single plant (*Camellia sinensis*) is advantageous when it comes to complementary and alternative medicines because each compound could have different modes of action and act synergistically in combination. Further research will provide greater insight into the inhibitory activity and the role of these compounds in green tea. Targeted metabolomics of the promising compounds will allow the quantification of the content in green tea. Metabolic networking of the putatively annotated compounds would also provide information about the metabolism and interactions in both *Camellia sinensis* and humans.

5.5. Chapter summary

In general, green tea had better alpha-glucosidase inhibitory activity than acarbose. The catechin content in green tea had a total percentage dry weight of approximately 20% which was calculated to be 500 mg per 2.5 g tea bag. The daily dose of acarbose is 75 to 150 mg (with a meal), and a single tea bag has enough catechins to be equivalent to the daily dose of acarbose. Green tea can, therefore, be used to complement the treatment of T2D.

5.5.1. Limitations and future work

Six repeats per green tea brand were used, however, only from one box each. The limitations of using only one box are that there were no independent replicates for the green tea brands. Electrospray ionization was applied in the negative ion mode, improvements would be to use the positive ion mode. The UV-detection data can also be used to further validate the annotation of the compounds. Future work could be to synthesise compounds from green tea to better inhibit antidiabetic targets.

CHAPTER 6: Conclusion

Diabetes mellitus is a disease that affects millions of people all over the world. Diabetes is characterised as having a persistent increased blood glucose level in a condition known as hyperglycemia. Diabetes can lead to many serious complications, such as hypertension, stroke, coma, or even death. Many of the commercially available treatments are expensive, and often have side effects. It is, therefore, important to discover new and more effective treatments, such as natural compounds from edible plants, which are less expensive, easier to obtain, and could have fewer side effects.

This study focused on natural compounds as potential pancreatic alpha-amylase and alpha-glucosidase inhibitors as well as their ability to stimulate glucose-uptake into liver and skeletal muscle cells. The inhibition of pancreatic alpha-amylase and alpha-glucosidase would slow down the hydrolysis of starch and maltose and thereby decrease the amount of glucose that enters the bloodstream after a meal. The stimulation of glucose uptake into the relevant cells would decrease the glucose concentration in the bloodstream. Both the decreased absorption of glucose from the small intestine into the bloodstream, and the increased uptake of glucose into the relevant cells; would lower the blood glucose concentration in individuals with T2D, **Figure 39**.

The compounds that were previously identified in herbs, spices, and medicinal plants were selected using *in silico* studies and further analysed *in vitro* for pancreatic alpha-amylase and alpha-glucosidase inhibition. The *in silico* studies that were used to filter for possible antidiabetic candidates were, virtual docking simulations using Glide and AutoDock Vina algorithms, ADMET property analysis using pKCSM, and cross reaction studies using SwissTargetPrediction.

The selected compounds, based on their docking score and commercial availability, were rutin, caffeic acid, and *p*-coumaric acid. The negative controls, with poor docking scores, were vanillin, ethyl gallate, and oxalic acid. The *in vitro* studies determined the antidiabetic properties of the selected compounds. The assays used for enzyme inhibition analysis were the DNSA assay for pancreatic alpha-amylase assay and the *p*NPG assay for alpha-glucosidase, with acarbose as the positive control. Then the cytotoxicity of the compounds was determined in the Caco2, HepG2, and C2C12 cells representing the gastrointestinal tract and specific insulin targets; liver and muscle, using the SRB assay. The effect on glucose uptake was determined in the HepG2 and C2C12 cell lines with the 2NBDG glucose uptake assay with metformin, a commercial antidiabetic drug, as the positive control.

The enzyme inhibition assays determined the K_i values using Lineweaver-Burk and secondary plots. The K_i values of the selected compounds which represents the binding ability of the compound to the active site of the selected enzyme, were compared to acarbose. For pancreatic alpha-amylase; caffeic

acid, vanillin, *p*-coumaric acid, and ethyl gallate had K_i values that were significantly similar to the K_i value of acarbose. For alpha-glucosidase; rutin, caffeic acid, *p*-coumaric acid, and vanillin had K_i values significantly similar to acarbose. The first null hypothesis was accepted for these compounds because there was no statistically significant difference in the K_i values between acarbose and these compounds. When the docking score which also represents binding affinity, and the K_i values were compared there was a positive correlation between the Glide docking score and the K_i values for both selected enzymes. This correlation trend can be further validated by including more natural compounds in the study.

The glucose uptake stimulating ability of the selected compounds was determined by evaluating their ability to stimulate glucose uptake into HepG2 and C2C12 cell lines. The HepG2 cells were also exposed to a high concentration of insulin to induce insulin resistance. The selected cell lines were exposed to the selected compounds in the presence of 2NBDG, a fluorescent glucose analog. The measured fluorescent intensity represents intracellular glucose levels in the presence of the compounds. None of the compounds, including metformin, significantly increased the glucose uptake in the HepG2 cells or insulin resistant HepG2 cells when compared to the vehicle control (no drugs). Some of the compounds, including metformin, significantly increased the glucose uptake in C2C12 cells when compared to the control (no drugs). However, these findings might not be biologically relevant and further investigation related to the sensitivity of the assay, concentration of the compounds and incubation time is warranted. The second null hypothesis is therefore rejected because the selected compounds did not significantly increase the glucose uptake ability of the selected cell lines in this study.

The content of each compound evaluated in this study was determined in common seasonings and green tea. Caffeic acid, *p*-coumaric acid, and rutin were all present in green tea. Caffeic acid is in a wide range of seasonings which provides a variety of ways for caffeic acid to be consumed. Rutin is most abundant in parsley and vanillin is most abundant in vanilla. Incorporation of these seasonings into the diet could possibly complement standard treatment of T2D. The presence of identified polyphenols such as ECG, EGCG, and GCG is an excellent source of antidiabetic compounds. In addition, green tea is widely and usually regularly consumed throughout the day and is an inexpensive source of these compounds.

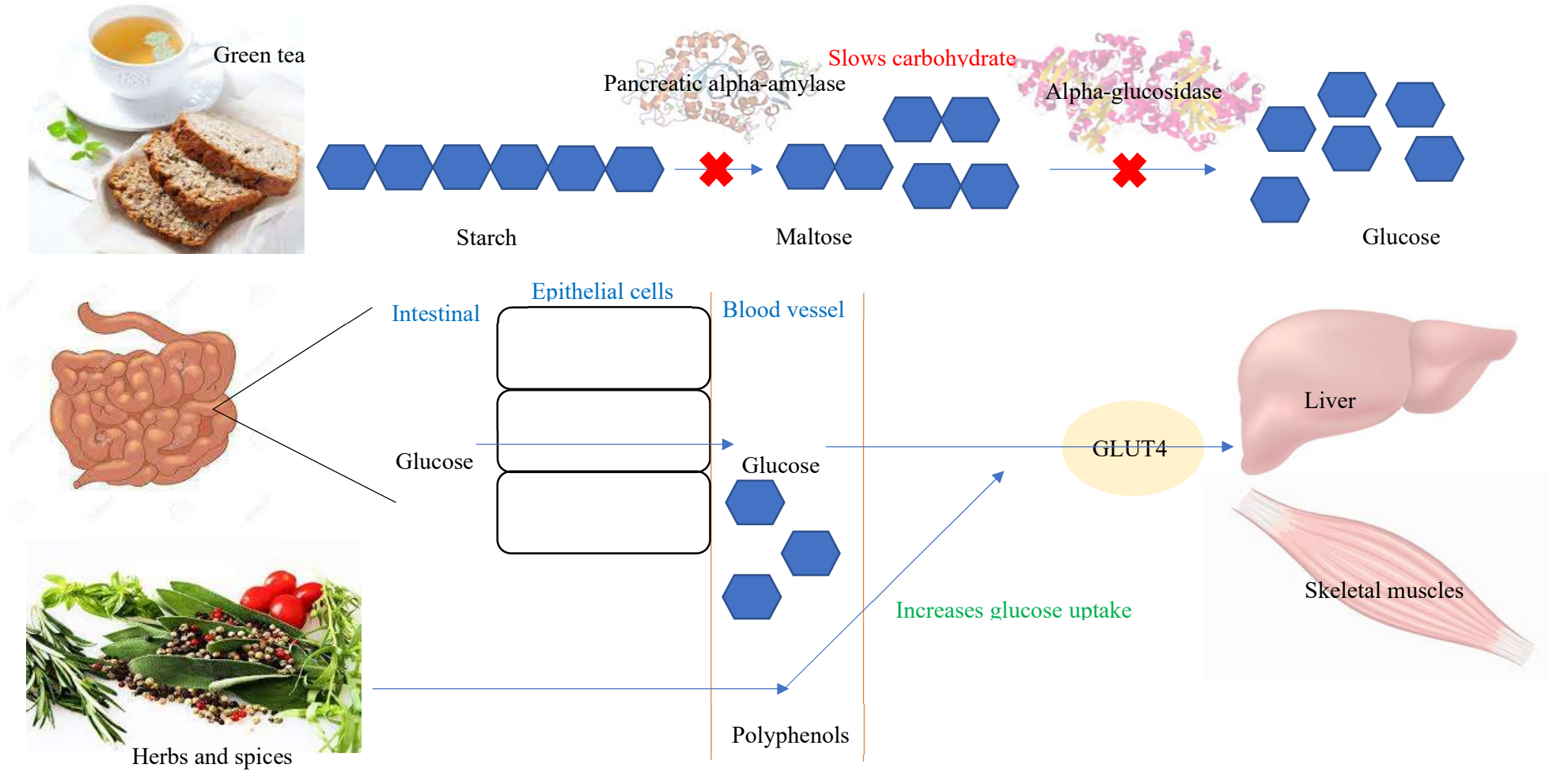

Figure 39: The effects of natural compounds on starch digestion and glucose uptake
Consuming a carbohydrate-rich meal with green tea, herbs, and spices would provide beneficial polyphenols such as rutin, caffeic acid, *p*-coumaric acid, and vanillin. These polyphenols slow the digestion of carbohydrates by inhibiting pancreatic alpha-amylase and alpha-glucosidase in the small intestine. Only monosaccharides, such as glucose, are absorbed into the bloodstream; therefore, the inhibition of these digestive enzymes would prevent a rapid increase in blood glucose concentration after a meal. Stimulation of glucose uptake into liver and skeletal muscle cells via the GLUT4 transporter decreases the blood glucose concentration. Some polyphenols such as caffeic acid could possibly stimulate glucose uptake in C2C12 skeletal muscle cells.

Untargeted metabolomic analysis was performed on five commercial green tea brands (Dilmah, Eve's, Livewell, Tetley, and Five Roses) using UPLC/MS analysis. The data were analysed using MassLynx, MSDIAL, and MSFINDER. MSFINDER uses several metabolomic databases to annotate the peaks detected by Waters UPLC/MS. Targeted metabolomic analysis was performed to determine the content of the selected standards in each green tea sample. The most abundant standards were EGC (5 - 8.5% dry weight), and EGCG (7 - 9% dry weight). The pancreatic alpha-amylase and alpha-glucosidase inhibitory activity of the five green tea brands was determined using *in vitro* enzyme inhibition assays and the IC_{50} was compared to acarbose. Tetley was the only brand that had a pancreatic alpha-amylase IC_{50} value that was significantly similar to that of acarbose, whereas the other four brands had significantly higher pancreatic alpha-amylase IC_{50} values when compared with acarbose. All five green tea brands had significantly lower alpha-glucosidase IC_{50} values than acarbose. Green tea brands with lower IC_{50} values are good pancreatic alpha-amylase and alpha-glucosidase inhibitors. The green tea brands with low IC_{50} values were compared with the green tea brands with high IC_{50} values based on the putatively annotated compounds. MetaboAnalyst identified two compounds that were significantly more abundant in the green tea brands with a low IC_{50} value which indicates that these two compounds are potentially responsible for the enhanced enzyme inhibition by the green tea brands. The MS/MS spectra of these two compounds and EGCG were evaluated, and the fragmentation patterns was investigated. The fragmentation pattern of EGCG correlated to the fragmentation pattern in MassBank. The fragmentation pattern of the actual MS/MS and the *in silico* MS/MS for the other two compounds had similarity scores less than 5/10. All the fragments present in the *in silico* MS/MS were also present in the actual MS/MS, but the actual MS/MS also contained other mass fragments. These promising compounds which were more abundant in green tea brand with low alpha-glucosidase IC_{50} values, were also predicted by the COCONUT database to have amylase and/or alpha-glucosidase inhibitory ability.

The presence of several inhibitory compounds in a single plant (*Camellia sinensis*) is most advantageous when it comes to complementary and alternative medicines because each compound could have different modes of action and act synergistically with each other or potentially with other antidiabetics. Further investigation of the *in vitro* inhibition of these compounds will provide greater insight into the inhibitory activity and the role of these compounds in green tea. Targeted metabolomics of the compounds will provide information on the content in green tea. Metabolic networking of the putatively annotated compounds would also provide information about the metabolism and interactions in both *Camellia sinensis* and humans. Future research will require the evaluation of the effect of these compounds, and the plant sources of these compounds in an animal model of T2D.

ReferencesDirect cAMP ELISA kit.

Abbas, S. & Wink, M. 2014. Green tea extract induces the resistance of *Caenorhabditis elegans* against oxidative stress. *Antioxidants,* 3**,** 129-143.

Adefegha, S. A. & Oboh, G. 2012. Inhibition of key enzymes linked to type 2 diabetes and sodium nitroprusside-induced lipid peroxidation in rat pancreas by water extractable phytochemicals from some tropical spices. *Pharmaceutical Biology,* 50**,** 857-865.

Ahmed, F., Ansari, J., Ansari, Z., Alam, Q., Kamal, M. & Ahmad, E. 2013. A molecular bridge: Connecting type 2 diabetes and Alzheimer's disease. *CNS & Neurological Disorders Drug Targets,* 13**,** 312-321.

Alam, A., Kowal, J., Broude, E., Roninson, I. & Locher, K. P. 2019a. Structural insight into substrate and inhibitor discrimination by human P-glycoprotein. *Science (New York, N.Y.),* 363**,** 753-756.

Alam, M. D. B., Bajpai, V. K., Ra, J.-S., Lim, J.-Y., An, H., Shukla, S., Quan, K., Khan, I., Huh, Y. S., Han, Y.-K., Na, M. & Lee, S.-H. 2019b. Anthraquinone-type inhibitor of α-glucosidase enhances glucose uptake by activating an insulin-like signaling pathway in C2C12 myotubes. *Food and Chemical Toxicology,* 129**,** 337–343.

Alejandro, A., S. Eliza, H., Colin G, N. & Monica, S.-R. 2009. Molecular biology of KATP channels and implications for health and disease. *IUBMB Life,* 61**,** 971-978.

Archana, S. & Abraham, J. 2011. Comparative analysis of antimicrobial activity of leaf extracts from fresh green tea, commercial green tea and black tea on pathogens. *Journal of Applied Pharmaceutical Science,* 1**,** 149.

Atlas, D. 2003. International diabetes federation. *IDF Diabetes Atlas, 2nd edn. Brussels, Belgium: International Diabetes Federation*.

Atlas, D. 2019. International diabetes federation. *IDF Diabetes Atlas, 9th edn. Brussels, Belgium: International Diabetes Federation*.

Beidokhti, M. N. & Jäger, A. K. 2017. Review of antidiabetic fruits, vegetables, beverages, oils and spices commonly consumed in the diet. *Journal of Ethnopharmacology,* 201**,** 26-41.

Belsley, D. A., Kuh, E. & Welsch, R. E. 1980. *Regression diagnostics: Identifying influential data and sources of collinearity*, John Wiley & Sons.

Berezhkovskiy, L. M. 2010. On the influence of protein binding on pharmacological activity of drugs. *Journal of Pharmaceutical Sciences,* 99**,** 2153-2165.

Bi, X., Lim, J. & Henry, C. J. 2017. Spices in the management of *diabetes mellitus*. *Food Chemistry,* 217**,** 281-293.

Birkedal-Hansen, H., Moore, W., Bodden, M., Windsor, L., Birkedal-Hansen, B., DeCarlo, A. & Engler, J. 1993. Matrix metalloproteinases: a review. *Critical Reviews in Oral Biology & Medicine,* 4**,** 197-250.

Capraro, R. & Yetkiner, Z. 2010. p-Value. *In:* SAGE (ed.) *Encyclopedia of research design.* Thousand Oaks, California.

Cavalli, A., Poluzzi, E., De Ponti, F. & Recanatini, M. 2002. Toward a pharmacophore for drugs inducing the long QT syndrome: insights from a CoMFA study of HERG K(+) channel blockers. *Journal of Medicinal Chemistry,* 45**,** 3844-53.

Chagas, C. M., Moss, S. & Alisaraie, L. 2018. Drug metabolites and their effects on the development of adverse reactions: Revisiting Lipinski's Rule of Five. *International Journal of Pharmaceutics,* 549**,** 133-149.

Chen, L., Teng, H. & Cao, H. 2019. Chlorogenic acid and caffeic acid from *Sonchus oleraceus Linn* synergistically attenuate insulin resistance and modulate glucose uptake in HepG2 cells. *Food and Chemical Toxicology,* 127**,** 182-187.

Chiou, W. L. 1982. The physiological significance of total body clearance in pharmacokinetic studies. *Journal of Clinical Pharmacy and Therapeutics,* 7**,** 25-30.

Daina, A., Michielin, O. & Zoete, V. 2019. SwissTargetPrediction: updated data and new features for efficient prediction of protein targets of small molecules. *Nucleic Acids Research,* 47**,** W357-W364.

Desseaux, V., Koukiekolo, R., Moreau, Y., Santimone, M. & Marchis-Mouren, G. 2002. Mechanism of porcine pancreatic alpha-amylase: inhibition of amylose and maltopentaose hydrolysis by various inhibitors. *Biologia Bratislava,* 57**,** 163-170.

Dimitriadis, G., Mitrou, P., Lambadiari, V., Maratou, E. & Raptis, S. A. 2011. Insulin effects in muscle and adipose tissue. *Diabetes Research and Clinical Practice,* 93**,** S52-S59.

Dubey, S., Ganeshpurkar, A., Ganeshpurkar, A., Bansal, D. & Dubey, N. 2017. Glycolytic enzyme inhibitory and antiglycation potential of rutin. *Future Journal of Pharmaceutical Sciences,* 3**,** 158-162.

Eldridge, M. D., Murray, C. W., Auton, T. R., Paolini, G. V. & Mee, R. P. 1997. Empirical scoring functions: I. The development of a fast empirical scoring function to estimate the binding affinity of ligands in receptor complexes. *Journal of Computer-Aided Molecular Design,* 11**,** 425-445.

Elkalaf, M., Anděl, M. & Trnka, J. 2013. Low glucose but not galactose enhances oxidative mitochondrial metabolism in C2C12 myoblasts and myotubes. *PloS one,* 8**,** e70772-e70772.

Elmadhun, N. Y., Lassaletta, A. D., Chu, L. M. & Sellke, F. W. 2013. Metformin alters the insulin signaling pathway in ischemic cardiac tissue in a swine model of metabolic syndrome. *The Journal of Thoracic and Cardiovascular Surgery,* 145**,** 258-266.

Federation, I. D. 2019. IDF Diabetes Atlas, 9th edn. Belgium International Diabetes Federation.

FooDB 2017. The Metabolomics Innovation Centre: FooDB (Version 1.0).

Database. Canada: The Metabolomics Innovation Centre.

Friedman, M., Levin, C. E., Choi, S.-H., Kozukue, E. & Kozukue, N. 2006. HPLC analysis of catechins, theaflavins, and alkaloids in commercial teas and green tea dietary supplements: comparison of water and 80% ethanol/water extracts. *Journal of Food Science,* 71**,** C328-C337.

Friesner, R. A., Banks, J. L., Murphy, R. B., Halgren, T. A., Klicic, J. J., Mainz, D. T., Repasky, M. P., Knoll, E. H., Shelley, M., Perry, J. K., Shaw, D. E., Francis, P. & Shenkin, P. S. 2004. Glide: A new approach for rapid, accurate docking and scoring. 1. Method and assessment of docking accuracy. *Journal of Medicinal Chemistry,* 47**,** 1739-1749.

Gao, C., Park, M.-S. & Stern, H. A. 2010. Accounting for ligand conformational restriction in calculations of protein-ligand binding affinities. *Biophysical Journal,* 98**,** 901-910.

Gao, J., Xu, P., Wang, Y., Wang, Y. & Hochstetter, D. 2013. Combined effects of green tea extracts, green tea polyphenols or epigallocatechin gallate with acarbose on inhibition against α-amylase and α-glucosidase *in vitro*. *Molecules (Basel, Switzerland),* 18**,** 11614-11623.

Garriga, M., Almaraz, M. & Marchiaro, A. 2017. Determination of reducing sugars in extracts of *Undaria pinnatifida* (harvey) algae by UV-visible spectrophotometry (DNS method). *Actas De Ingenieria,* 3**,** 173-179.

Gates, R. 2010. Enzymes and reagents for alternative energy. *In:* SIGMA-ALDRICH (ed.). St. Louis: Sigma-Aldrich.

Gfeller, D., Michielin, O. & Zoete, V. 2013. Shaping the interaction landscape of bioactive molecules. *Bioinformatics,* 29**,** 3073-3079.

Giang Thanh Thi, H., Kase, E. T., Wangensteen, H. & Barsett, H. 2017. Effect of phenolic compounds from elderflowers on glucose- and fatty acid uptake in human myotubes and HepG2-cells. *Molecules,* 22**,** 1-15.

Girgis, C. & Gunton, J. 2012. Pancreatic beta-cell failure in the pathogenesis of type 2 diabetes. *A Modern Epidemic.* Australia

Hardy, A., Benford, D., Halldorsson, T., Jeger, M. J., Knutsen, H. K., More, S., Naegeli, H., Noteborn, H., Ockleford, C., Ricci, A., Rychen, G., Schlatter, J. R., Silano, V., Solecki, R., Turck, D., Younes, M., Bresson, J.-L., Griffin, J., Hougaard Benekou, S., van Loveren, H., Luttik, R., Messean, A., Penninks, A., Ru, G., Stegeman, J. A., van der Werf, W., Westendorf, J., Woutersen, R. A., Barizzone, F., Bottex, B., Lanzoni, A., Georgiadis, N. & Alexander, J. 2017. Guidance on the assessment of the biological relevance of data in scientific assessments. *EFSA Journal,* 15**,** e04970.

Hatting, M., Tavares, C. D. J., Sharabi, K., Rines, A. K. & Puigserver, P. 2018. Insulin regulation of gluconeogenesis. *Annals of the New York Academy of Sciences,* 1411**,** 21-35.

Hodgkin, D. C. 1971. X-rays and the structure of insulin. *The British Medical Journal,* 4**,** 447-451.

Holmes, R. 1971. Carbohydrate digestion and absorption. *Journal of Clinical Pathology,* 3-5**,** 10-13.

Ikbal, A., Roy, S. & Pat, K. 2020. Health benefits of green tea: A mini review. *Journal of Entomology and Zoology Studies,* 8**,** 1424-1430.

Jensen, J. & Lai, Y.-C. 2009. Regulation of muscle glycogen synthase phosphorylation and kinetic properties by insulin, exercise, adrenaline and role in insulin resistance. *Archives of Physiology and Biochemistry,* 115**,** 13-21.

Jhong, C.-H., Riyaphan, J., Lin, S.-H., Chia, Y.-C. & Weng, C.-F. 2015. Screening alpha-glucosidase and alpha-amylase inhibitors from natural compounds by molecular docking *in silico*. *BioFactors,* 41**,** 242-251.

Jiang, B., Le, L., Zhai, W., Wan, W., Hu, K., Yong, P., He, C., Xu, L. & Xiao, P. 2016. Protective effects of marein on high glucose-induced glucose metabolic disorder in HepG2 cells. *Phytomedicine,* 23**,** 891-900.

Jingchun, S., Min, Z., Peilin, J., Lily, W., Yonghui, W., Carissa, I., Yubo, Z., Erica, B., Dan, M. R., Joshua, C. D., Melinda, C. A., Hua, X. & Zhongming, Z. 2015. Deciphering signaling pathway networks to understand the molecular mechanisms of metformin action. *PLoS Computational Biology* [Online], 6.

Jorgensen, W. L. & Duffy, E. M. 2000. Prediction of drug solubility from Monte Carlo simulations. *Chemical Data Analysis in the Large,* 10**,** 1155–1158.

Ju, W.-T., Kwon, O. C., Kim, H.-B., Sung, G.-B., Kim, H.-W. & Kim, Y.-S. 2018. Qualitative and quantitative analysis of flavonoids from 12 species of Korean mulberry leaves. *Journal of Food Science and Technology,* 55**,** 1789-1796.

Kao, Y.-H., Chang, H.-H., Lee, M.-J. & Chen, C.-L. 2006. Tea, obesity, and diabetes. *Molecular Nutrition & Food Research,* 50**,** 188-210.

Karakurt, S. 2016. Modulatory effects of rutin on the expression of cytochrome P450s and antioxidant enzymes in human hepatoma cells. *Acta Pharmaceutica,* 66**,** 491-502.

Kelder, J., Grootenhuis, P. D. J., Bayada, D. M., Delbressine, L. P. C. & Ploemen, J.-P. 1999. Polar molecular surface as a dominating determinant for oral absorption and brain penetration of drugs. *Pharmaceutical Research : An Official Journal of the American Association of Pharmaceutical Scientists,* 16**,** 1514-1519.

Kelly, J. L. 2014. Continuous insulin infusion: when, where, and how? *Diabetes spectrum : a publication of the American Diabetes Association,* 27**,** 218-223.

Kim, M.-J., Lee, S.-B., Lee, H.-S., Lee, S.-Y., Baek, J.-S., Kim, D., Moon, T.-W., Robyt, J. F. & Park, K.-H. 1999. Comparative study of the inhibition of α-glucosidase, α-amylase, and cyclomaltodextrin glucanosyltransferase by acarbose, isoacarbose, and acarviosine-glucose. *Archives of Biochemistry and Biophysics,* 371**,** 277-283.

Kim, S., Go, G.-W. & Imm, J.-Y. 2017. Promotion of glucose uptake in C2C12 myotubes by cereal flavone Tricin and its underlying molecular mechanism. *Journal of Agricultural and Food Chemistry,* 65**,** 3819-3826.

Klaus, S. Accessed 2021. *DSMZ-German collection of microorganisms and cell cultures* [Online]. Germany. Available: https://www.dsmz.de/collection/catalogue [Accessed].

Koepsell, H. 2020. Glucose transporters in the small intestine in health and disease. *European Journal of Physiology,* 472**,** 1207-1248.

Krishna, M. S., Joy, B. & Sundaresan, A. 2015. Effect on oxidative stress, glucose uptake level and lipid droplet content by Apigenin 7, 4'-dimethyl ether isolated from *Piper longum L*. *Journal of Food Science and Technology,* 52**,** 3561-3570.

Kwon, Y., Apostolidis, E. & Shetty, K. 2008. Inhibitory potential of wine and tea against α-Amylase and α-Glucosidase for management of hyperglycemia linked to type 2 diabetes. *Journal of Food Biochemistry,* 32**,** 15-31.

Lai, Z., Tsugawa, H., Wohlgemuth, G., Mehta, S., Mueller, M., Zheng, Y., Ogiwara, A., Meissen, J., Showalter, M., Takeuchi, K., Kind, T., Beal, P., Arita, M. & Fiehn, O. 2018. Identifying metabolites by integrating metabolome databases with mass spectrometry cheminformatics. *Nature Methods,* 15**,** 53-56.

Lim, S. H., Yu, J. S., Lee, H. S., Choi, C.-I. & Kim, K. H. 2021. Antidiabetic flavonoids from fruits of *Morus alba* promoting insulin-stimulated glucose uptake via Akt and AMP-activated protein kinase activation in 3T3-L1 adipocytes. *Pharmaceutics,* 13**,** 526.

Lin, J.-K., Lin, C.-L., Liang, Y.-C., Lin-Shiau, S.-Y. & Juan, I. M. 1998. Survey of catechins, gallic acid, and methylxanthines in green, oolong, pu-erh, and black teas. *Journal of Agricultural and Food Chemistry,* 46**,** 3635-3642.

Lin, L.-Z. & Harnly, J. M. 2007. A screening method for the identification of glycosylated flavonoids and other phenolic compounds using a standard analytical approach for all plant materials. *Journal of Agricultural and Food Chemistry,* 55**,** 1084-1096.

Lindskog, S. 1997. Structure and mechanism of carbonic anhydrase. *Pharmacology and Therapeutics,* 74**,** 1-20.

Lipinski, C. A., Lombardo, F., Dominy, B. W. & Feeney, P. J. 2012. Experimental and computational approaches to estimate solubility and permeability in drug discovery and development settings. *Advanced Drug Delivery Reviews,* 64**,** 4-17.

Liu, J. J., Payza, K., Huang, J., Liu, R., Chen, T., Coupal, M., Laird, J. M., Cao, C.-Q., Butterworth, J. & Lapointe, S. 2009. Discovery and pharmacological characterization of a small-molecule antagonist at neuromedin U receptor NMUR2. *Journal of Pharmacology and Experimental Therapeutics,* 330**,** 268-275.

Liu, Y., Zhu, J., Yu, J., Chen, X., Zhang, S., Cai, Y. & Li, L. 2021. A new functionality study of vanillin as the inhibitor for α-glucosidase and its inhibition kinetic mechanism. *Food Chemistry,* 353**,** 129448.

Long, H., Stander, M. & Van Wyk, B.-E. 2012. Notes on the occurrence and significance of triterpenoids (asiaticoside and related compounds) and caffeoylquinic acids in *Centella* species. *South African Journal of Botany,* 82**,** 53-59.

Luo, J., Rossouw, J., Tong, E., Giovino, G. A., Lee, C. C., Chen, C., Ockene, J. K., Qi, L. & Margolis, K. L. 2013. Smoking and diabetes: does the increased risk ever go away? *American Journal of Epidemiology,* 178**,** 937-945.

Magnani, C., Chiari, B. G., Isaac, V. L. B., Correa, M. A. & Salgado, H. 2014. *In vitro* safety evaluation of caffeic acid. *Athens Journal of Health***,** 181-188.

Mari, A., Tura, A., Natali, A., Anderwald, C., Balkau, B., Lalic, N., Walker, M., Ferrannini, E. & Investigators, R. 2011. Influence of hyperinsulinemia and insulin resistance on in vivo β-cell function: their role in human β-cell dysfunction. *Diabetes,* 60**,** 3141-3147.

Milkani, E., Lambert, C. R. & McGimpsey, W. G. 2011. Direct detection of acetylcholinesterase inhibitor binding with an enzyme-based surface plasmon resonance sensor. *Analytical Biochemistry,* 408**,** 212-219.

Miret, S., De Groene, E. & Klaffke, W. 2006. Comparison of *in vitro* assays of cellular toxicity in the human hepatic cell line HepG2. *Journal of Biomolecular Screening,* 11**,** 184-193.

Mohiuddin, M., Arbain, D., Islam, A. K. M., Ahmad, M. S. & Ahmad, M. 2016. Alpha-glucosidase enzyme biosensor for the electrochemical measurement of antidiabetic potential of medicinal plants. *Nanoscale Research Letters,* 11**,** 95.

Muka, T., Vargas, K. G., Jaspers, L., Wen, K.-x., Dhana, K., Vitezova, A., Nano, J., Brahimaj, A., Colpani, V., Bano, A., Kraja, B., Zaciragic, A., Bramer, W. M., Dijk, G. M. v., Kavousi, M. & Franco, O. H. 2016. Estrogen receptor β actions in the female cardiovascular system: A systematic review of animal and human studies. *Maturitas,* 86**,** 28-43.

Mukaka, M. M. 2012. Statistics corner: A guide to appropriate use of correlation coefficient in medical research. *Malawi Medical Journal : The Journal of Medical Association of Malawi,* 24**,** 69-71.

Nagpal, I., Raj, I., Subbarao, N. & Gourinath, S. 2012. Virtual screening, identification and *in vitro* testing of novel inhibitors of O-acetyl-L-serine sulfhydrylase of *Entamoeba histolytica*. *PLoS One,* 7**,** e30305.

Nam, J. S., Chung, H. J., Jang, M. K., Jung, I. A., Park, S. H., Cho, S. I. & Jung, M. H. 2013. *Sasa borealis* extract exerts an antidiabetic effect via activation of the AMP-activated protein kinase. *Nutrition research and practice,* 7**,** 15-21.

NCBI 2020. PubChem Compound Summary. National Center for Biotechnology Information

Ntie-Kang, F., Onguéné, P. A., Scharfe, M., Owono Owono, L. C., Megnassan, E., Mbaze, L. M. a., Sippl, W. & Efange, S. M. N. 2014. ConMedNP: a natural product library from Central African medicinal plants for drug discovery. *RSC Advances,* 4**,** 409-419.

Oboh, G., Agunloye, O. M., Adefegha, S. A., Akinyemi, A. J. & Ademiluyi, A. O. 2015. Caffeic and chlorogenic acids inhibit key enzymes linked to type 2 diabetes (*in vitro*): a comparative study. *Journal of Basic and Clinical Physiology and Pharmacology,* 26**,** 165-170.

Oboh, G., Ogunsuyi, O. B., Ogunbadejo, M. D. & Adefegha, S. A. 2016. Influence of gallic acid on α-amylase and α-glucosidase inhibitory properties of acarbose. *Journal of Food and Drug Analysis,* 24**,** 627-634.

Obrezanova, O., Csányi, G., Gola, J. M. & Segall, M. D. 2007. Gaussian processes: a method for automatic QSAR modeling of ADME properties. *Journal of Chemical Information and Modeling,* 47**,** 1847-1857.

Ogu, C. C. & Maxa, J. L. 2000. Drug interactions due to cytochrome P450. *Proceedings (Baylor University. Medical Center),* 13**,** 421-423.

Oh, K.-B. & Matsuoka, H. 2002. Rapid viability assessment of yeast cells using vital staining with 2-NBDG, a fluorescent derivative of glucose. *International Journal of Food Microbiology,* 76**,** 47-53.

Palmer, T. & Bonner, P. L. R. 2008. *Enzymes : biochemistry, biotechnology and clinical chemistry,* Chichester, Horwood.

Pantazis, D. A. 2013. Maltase reaction. *Wikimedia Commons.*

Park, M.-S., Dessal, A. L., Smrcka, A. V. & Stern, H. A. 2009. Evaluating docking methods for prediction of binding affinities of small molecules to the g protein βγ subunits. *Journal of Chemical Information and Modeling,* 49**,** 437-443.

Park, S. Y., Kim, M. H., Ahn, J. H., Lee, S. J., Lee, J. H., Eum, W. S., Choi, S. Y. & Kwon, H. Y. 2014. The stimulatory effect of essential fatty acids on glucose uptake involves both Akt and AMPK activation in C2C12 skeletal muscle cells. *The Korean Journal of Physiology & Pharmacology* 18**,** 255-261.

Pastoriza, S., Mesías, M., Cabrera, C. & Rufián-Henares, J. 2017. Healthy properties of green and white teas: an update. *Food & Function,* 8**,** 2650-2662.

Patel, D., Kumar, R., Laloo, D. & Hemalatha, S. 2012. *Diabetes mellitus*: an overview on its pharmacological aspects and reported medicinal plants having antidiabetic activity. *Asian Pacific Journal of Tropical Biomedicine,* 2**,** 411-420.

Pereira, A. S., Banegas-Luna, A. J., Peña-García, J., Pérez-Sánchez, H. & Apostolides, Z. 2019. Evaluation of the anti-diabetic activity of some common herbs and spices: Providing new insights with inverse virtual screening. *Molecules,* 24**,** 4030.

Perez-Sanchez, H., den-Haan, H., Peña-García, J., Lozano-Sánchez, J. s., Moreno, M. E. n. M. n., Sánchez-Pérez, A., Muñoz, A. s., Ruiz-Espinosa, P., Pereira, A. S. P., Katsikoudi, A., Gabaldón Hernández, J. A., Stojanovic, I., Segura-Carretero, A. & Tzakos, A. 2020. DIA-DB: A database and web server for the prediction of diabetes drugs. *Journal of Chemical Information and Modeling*.

Petrash, J. M. 2004. All in the family: aldose reductase and closely related aldo-keto reductases. *Cellular and Molecular Life Sciences CMLS,* 61**,** 737-749.

Pietrzyk, N., Zakłos-Szyda, M., Koziołkiewicz, M. & Podsędek, A. 2021. *Viburnum opulus L*. fruit phenolic compounds protect against FFA-induced steatosis of HepG2 cells via AMPK pathway. *Journal of Functional Foods,* 80**,** 104437.

Pires, D. E. V., Blundell, T. L. & Ascher, D. B. 2015. pkCSM: Predicting small-molecule pharmacokinetic and toxicity properties using graph-based signatures. *Journal of Medicinal Chemistry,* 58**,** 4066-4072.

Pollier, J., Vancaester, E., Kuzhiumparambil, U., Vickers, C. E., Vandepoele, K., Goossens, A. & Fabris, M. 2019. A widespread alternative squalene epoxidase participates in eukaryote steroid biosynthesis. *Nature Microbiology,* 4**,** 226-233.

Prachayasittikul, V. & Prachayasittikul, V. 2016. P-glycoprotein transporter in drug development. *EXCLI Journal,* 15**,** 113.

Priya Rani, M., Padmakumari, K. P., Sankarikutty, B., Lijo Cherian, O., Nisha, V. M. & Raghu, K. G. 2011. Inhibitory potential of ginger extracts against enzymes linked to type 2 diabetes, inflammation and induced oxidative stress. *International Journal of Food Sciences and Nutrition,* 62**,** 106-110.

Proença, C., Freitas, M., Ribeiro, D., Oliveira, E. F. T., Sousa, J. L. C., Tomé, S. M., Ramos, M. J., Silva, A. M. S., Fernandes, P. A. & Fernandes, E. 2017. α-Glucosidase inhibition by flavonoids: an *in vitro* and *in silico* structure–activity relationship study. *Journal of Enzyme Inhibition and Medicinal Chemistry,* 32**,** 1216-1228.

QuestGraph™ 2020. IC50 Calculator. AAT Bioquest, Inc.

Rochlani, Y., Pothineni, N. V., Kovelamudi, S. & Mehta, J. L. 2017. Metabolic syndrome: pathophysiology, management, and modulation by natural compounds. *Therapeutic Advances in Cardiovascular Disease,* 11**,** 215-225.

Roglic, G. 2016. *Global Report on Diabetes*, World Health Organization.

Ross, S. A., Gulve, E. A. & Wang, M. 2004. Chemistry and biochemistry of type 2 diabetes. *Chemical Reviews,* 104**,** 1255.

Rothwell, J. A., Pérez-Jiménez, J., Neveu, V., Medina-Ramon, A., M'Hiri, N., Garcia Lobato, P., Manach, C., Knox, K., Eisner, R., Wishart, D. & Scalbert, A. 2013. Phenol-Explorer 3.0: a major update of the Phenol-Explorer database to incorporate data on the effects of food processing on polyphenol content.

Sabiu, S., O'Neill, F. H. & Ashafa, A. O. T. 2016. Kinetics of α-amylase and α-glucosidase inhibitory potential of *Zea mays Linnaeus* (Poaceae), *Stigma maydis* aqueous extract: An in vitro assessment. *Journal of Ethnopharmacology,* 183**,** 1-8.

Saeedi, P., Petersohn, I., Salpea, P., Malanda, B., Karuranga, S., Unwin, N., Colagiuri, S., Guariguata, L., Motala, A. A., Ogurtsova, K., Shaw, J. E., Bright, D. & Williams, R. 2019. Global and regional diabetes prevalence estimates for 2019 and projections for 2030 and 2045: Results from the International Diabetes Federation Diabetes Atlas, 9th edition. *Diabetes Research and Clinical Practice,* 157**,** 107843.

Saltan, F. Z., Okutucu, B., Canbay, H. S. & Özel, D. 2017. *In vitro* alpha-glucosidase and alpha-amylase enzyme inhibitory effects in *Elaeagnus angustifolia* leaves extracts. *Eurasian Journal of Analytical Chemistry,* 12**,** 117-126.

Saunders, C. & Limbird, L. E. 1999. Localization and trafficking of α2-adrenergic receptor subtypes in cells and tissues. *Pharmacology & Therapeutics,* 84**,** 193-205.

Schinner, S., Scherbaum, W., Bornstein, S. & Barthel, A. 2005. Molecular mechanisms of insulin resistance. *Diabetic Medicine,* 22**,** 674-682.

Schober, P., Boer, C. & Schwarte, L. A. 2018. Correlation coefficients: appropriate use and interpretation. *Anesthesia & Analgesia,* 126**,** 1763-1768.

Schrödinger 2015a. LigPrep, version 3.4. *New York, NY*.

Schrödinger 2015b. QikProp properties and descriptors. Schrodinger Press.

Schrödinger 2021. Schrödinger Release 2021-4: Glide. *New York, NY*.

Schymanski, E. L., Jeon, J., Gulde, R., Fenner, K., Ruff, M., Singer, H. P. & Hollender, J. 2014. Identifying small molecules via high resolution mass spectrometry: communicating confidence. ACS Publications.

Seetaloo, A. D., Aumeeruddy, M. Z., Rengasamy Kannan, R. R. & Mahomoodally, M. F. 2019. Potential of traditionally consumed medicinal herbs, spices, and food plants to inhibit key digestive enzymes geared towards *diabetes mellitus* management — A systematic review. *South African Journal of Botany,* 120**,** 3-24.

Semaan, D., Igoli, J., Young, L., Gray, A., Rowan, E. & Marrero, E. 2018. *In vitro* anti-diabetic effect of flavonoids and pheophytins from *Allophylus cominia Sw*. on the glucose uptake assays by HepG2, L6, 3T3-L1 and fat accumulation in 3T3-L1 adipocytes. *Journal of Ethnopharmacology,* 216**,** 8-17.

Sharma, S. 2018. *Diabetes mellitus*: An overview. *Journal of Advanced Scientific Research,* 92**,** 10-13.

Shelley, J. C., Cholleti, A., Frye, L. L., Greenwood, J. R., Timlin, M. R. & Uchimaya, M. 2007. Epik: a software program for pKa prediction and protonation state generation for drug-like molecules. *Journal of Computer-Aided Molecular Design: Incorporating Perspectives in Drug Discovery and Design,* 21**,** 681-691.

Shihabudeen, H. M. S., Priscilla, D. H. & Thirumurugan, K. 2011. Cinnamon extract inhibits α-glucosidase activity and dampens postprandial glucose excursion in diabetic rats. *Nutrition & Metabolism,* 8**,** 1-11.

Sinclair, L. V., Barthelemy, C. & Cantrell, D. A. 2020. Single cell glucose uptake assays: A cautionary tale. *Immunometabolism,* 2**,** e200029-e200029.

Singh, J., Dartois, A. & Kaur, L. 2010. Starch digestibility in food matrix: a review. *Trends in Food Science & Technology,* 21**,** 168-180.

Sorokina, M., Merseburger, P. & Rajan, K. 2021. *COCONUT online: Collection of open natural products database* [Online]. Germany: Steinbeck group. Available: https://doi.org/10.1186/s13321-020-00478-9 [Accessed].

Spacil, Z., Nováková, L. & Solich, P. 2010. Comparison of positive and negative ion detection of tea catechins using tandem mass spectrometry and ultra high performance liquid chromatography. *Food Chemistry,* 123**,** 535-541.

Srimoon, R., Anartgnam, P. & Tilarux, P. 2020. *In vitro* inhibitory efficiency of *Ventilago denticulata Willd*. dried leaves extract on alpha-glucosidase, alpha-amylase and lipase and antioxidant activities. *Science & Technology Asia***,** 135-149.

Tendulkar, R. N. & Mahajan, S. S. 2014. Molecular docking studies of novel flavones as cyclooxygenase-2 (Cox 2) Inhibitors. *Journal of Advanced Pharmacy Education & Research,* 4**,** 330-338.

Trott, O. & Olson, A. J. 2010. AutoDock Vina: improving the speed and accuracy of docking with a new scoring function, efficient optimization, and multithreading. *Journal of Computational Chemistry,* 31**,** 455-461.

Tsugawa, H., Cajka, T., Kind, T., Ma, Y., Higgins, B., Ikeda, K., Kanazawa, M., VanderGheynst, J., Fiehn, O. & Arita, M. 2015. MS-DIAL: data-independent MS/MS deconvolution for comprehensive metabolome analysis. *Nature Methods,* 12**,** 523-6.

Vajrabhaya, L.-o. & Korsuwannawong, S. 2018. Cytotoxicity evaluation of a Thai herb using tetrazolium (MTT) and sulforhodamine B (SRB) assays. *Journal of Analytical Science and Technology,* 9**,** 15.

Valley, M. P., Karassina, N., Aoyama, N., Carlson, C., Cali, J. J. & Vidugiriene, J. 2016. A bioluminescent assay for measuring glucose uptake. *Analytical Biochemistry,* 505**,** 43-50.

Van De Laar, F. A., Lucassen, P. L., Akkermans, R. P., Van De Lisdonk, E. H., Rutten, G. E. & Van Weel, C. 2005. α-Glucosidase inhibitors for patients with type 2 diabetes: results from a Cochrane systematic review and meta-analysis. *Diabetes Care,* 28**,** 154-163.

Vertzoni, M., Augustijns, P., Grimm, M., Koziolek, M., Lemmens, G., Parrott, N., Pentafragka, C., Reppas, C., Rubbens, J., Van Den Abeele, J., Vanuytsel, T., Weitschies, W. & Wilson, C. G. 2019. Impact of regional differences along the gastrointestinal tract of healthy adults on oral drug absorption: An UNGAP review. *European Journal of Pharmaceutical Sciences,* 134**,** 153-175.

Vichai, V. & Kirtikara, K. 2006. Sulforhodamine B colorimetric assay for cytotoxicity screening. *Nature protocols,* 1**,** 1112-1116.

Visakh, P. M. 2014. Starch-based bionanocomposites: processing and properties polysaccharide building blocks: A sustainable approach to the development of renewable biomaterials.

Wang, H., Provan, G. J. & Helliwell, K. 2004. Determination of rosmarinic acid and caffeic acid in aromatic herbs by HPLC. *Food Chemistry,* 87**,** 307-311.

Wang, Q., Liang, X. & Wang, S. 2013. Intra-islet glucagon secretion and action in the regulation of glucose homeostasis. *Frontiers in Pysiology,* 3**,** 485-485.

Warren, G. L., Andrews, C. W., Capelli, A. M., Clarke, B., LaLonde, J., Lambert, M. H., Lindvall, M., Nevins, N., Semus, S. F., Senger, S., Tedesco, G., Wall, I. D., Woolven, J. M., Peishoff, C. E. & Head, M. S. 2006. A critical assessment of docking programs and scoring functions. *Journal of Medicinal Chemistry,* 49**,** 5912-31.

Waters 2005. MassLynx 4.1 Getting Started Guide. *Waters Corporation*.

Werz, O. & Steinhilber, D. 2006. Therapeutic options for 5-lipoxygenase inhibitors. *Pharmacology and Therapeutics,* 112**,** 701-718.

WHO 2013. Diagnostic criteria and classification of hyperglycaemia first detected in pregnancy. World Health Organization.

Wilcox, G. 2005. Insulin and insulin resistance. *The Clinical Biochemist,* 26**,** 19-39.

Wu, C., Khan, S. A. & Lange, A. 2005. Regulation of glycolysis - Role of insulin. *Experimental Gerontology,* 40**,** 894-9.

Xia, J. & Wishart, D. S. 2011. Web-based inference of biological patterns, functions and pathways from metabolomic data using MetaboAnalyst. *Nature Protocols,* 6**,** 743-60.

Yates, J. W. T. & Arundel, P. A. 2008. On the volume of distribution at steady state and its relationship with two-compartmental models. *Journal of Pharmaceutical Sciences,* 97**,** 111-122.

Yazdanian, M., Glynn, S. L., Wright, J. L. & Hawi, A. 1998. Correlating partitioning and Caco-2 cell permeability of structurally diverse small molecular weight compounds. *Journal of the American Association of Pharmaceutical Scientists,* 15**,** 1490-1494.

Yilmazer-Musa, M., Griffith, A. M., Michels, A. J., Schneider, E. & Frei, B. 2012. Grape seed and tea extracts and catechin 3-gallates are potent inhibitors of α-amylase and α-glucosidase activity. *Journal of Agricultural and Food Chemistry,* 60**,** 8924-8929.

Ying, B.-W., Fourmy, D. & Yoshizawa, S. 2007. Substitution of the use of radioactivity by fluorescence for biochemical studies of RNA. *RNA (New York, N.Y.),* 13**,** 2042-2050.

Yoon, S.-A., Kang, S.-I., Shin, H.-S., Kang, S.-W., Kim, J.-H., Ko, H.-C. & Kim, S.-J. 2013. p-Coumaric acid modulates glucose and lipid metabolism via AMP-activated protein kinase in L6 skeletal muscle cells. *Biochemical and Biophysical Research Communications,* 432**,** 553-557.

Yoon, S.-H. & Robyt, J. F. 2003. Study of the inhibition of four alpha amylases by acarbose and its 4IV-α-maltohexaosyl and 4IV-α-maltododecaosyl analogues. *Carbohydrate Research,* 338**,** 1969-1980.

Yu, X., Xiao, J., Chen, S., Yu, Y., Ma, J., Lin, Y., Li, R., Lin, J., Fu, Z. & Zhou, Q. 2020. Metabolite signatures of diverse *Camellia sinensis* tea populations. *Nature Communications,* 11**,** 1-14.

Zang, M., Zuccollo, A., Hou, X., Nagata, D., Walsh, K., Herscovitz, H., Brecher, P., Ruderman, N. B. & Cohen, R. A. 2004. AMP-activated protein kinase is required for the lipid-lowering effect of metformin in insulin-resistant human HepG2 cells. *The Journal of Biological Chemistry,* 279**,** 47898-905.

Zhang, Y., Mo, L., Chen, F., Lu, M., Dong, W., Wang, Q., Xu, F. & Gu, F. 2014. Optimized production of vanillin from green vanilla pods by enzyme-assisted extraction combined with pre-freezing and thawing. *Molecules (Basel, Switzerland),* 19**,** 2181-2198.

Zhao, Y., Chen, P., Lin, L., Harnly, J. M., Yu, L. L. & Li, Z. 2011. Tentative identification, quantitation, and principal component analysis of green pu-erh, green, and white teas using UPLC/DAD/MS. *Food Chemistry,* 126**,** 1269-1277.

Zou, C., Wang, Y. & Shen, Z. 2005. 2-NBDG as a fluorescent indicator for direct glucose uptake measurement. *Journal of Biochemical and Biophysical Methods,* 64**,** 207-215.

Supplementary Table 1: The docking scores of selected compounds for 4GQR and 3L4Y as well as the number of interaction points between the ligand and the protein binding pocket

	4GQR (Pancreatic alpha-amylase)			3L4Y (Alpha-glucosidase)		
Compound	**Glide (kcal/mol)**	**Number of interactions**	**AutoDock Vina (kcal/mol)**	**Glide (kcal/mol)**	**Number of interactions**	**AutoDock Vina (kcal/mol)**
Acarbose	-5.61	7	-8.10	-5.88	4	-7.00
Caffeic acid	-5.69	3	-6.50	-3.70	2	-6.80
Ethyl gallate	-5.24	3	-5.80	-4.96	2	-5.80
Oxalic acid	-2.49	0	-3.40	-1.68	0	-4.20
***p*-Coumaric acid**	-5.26	2	-6.10	-3.27	2	-6.90
Rutin	-6.62	5	-8.80	-5.47	7	-7.90
Vanillin	-4.46	4	-5.20	-4.92	0	-5.50

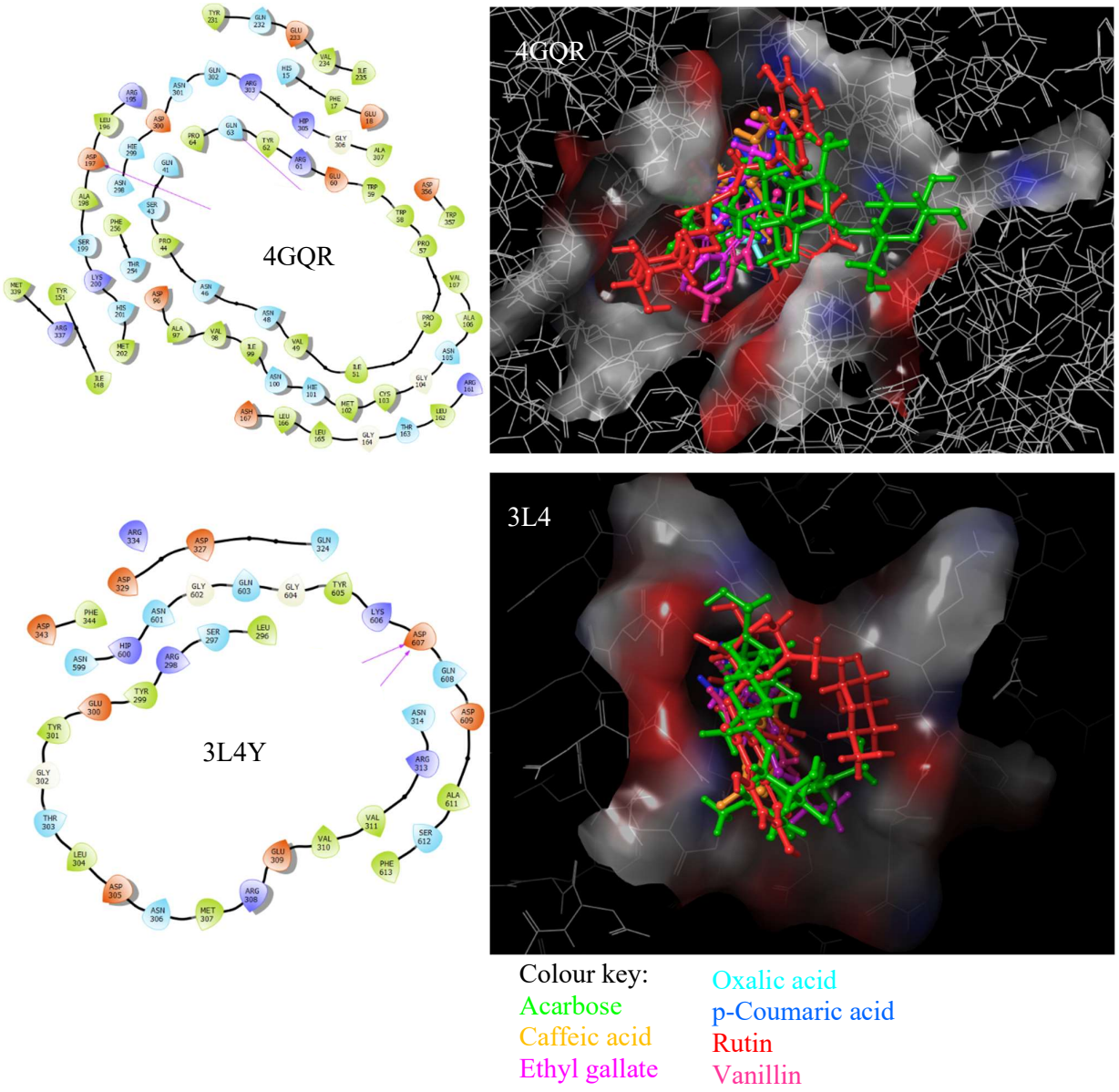

Supplementary Figure 1: The binding pocket of 4GQR (pancreatic alpha-amylase) and 3L4Y (alpha-glucosidase) and the selected compounds docked into the active site of 4GQR and 3L4Y

Supplementary Table 2: SwissTargetPrediction of selected compounds

Target	Acarbose
AMY1C	0.9997
Lysosomal alpha-glucosidase	0.9997
Pancreatic alpha-amylase	0.7678
Maltase-glucoamylase	0.4166
Sucrase-isomaltase	0.2642
Cyclin-dependent kinase 1	0.0746
Trehalase	0.0746
Target	**Metformin**
Thrombin	0.0238
Target	**Rutin**
Acetylcholinesterase	1.0000
Adrenergic receptor alpha-2	1.0000
Alpha-2a adrenergic receptor	1.0000
Neuromedin-U receptor 2	1.0000
Aldose reductase	0.6126
Carbonic anhydrase IV	0.4872
Carbonic anhydrase VII	0.4872
Carbonic anhydrase XII	0.4872
NADPH oxidase 4	0.3921
Carbonic anhydrase II	0.3438
Quinone reductase 2	0.2003
Ribosomal protein S6 kinase alpha 3	0.2003
Xanthine dehydrogenase	0.1140
Cyclooxygenase-2	0.0949
Lymphocyte differentiation antigen CD38	0.0949
Adenosine A1 receptor (by homology)	0.0661
Arachidonate 5-lipoxygenase	0.0661
Interleukin-2	0.0661
Phosphodiesterase 5A	0.0661
Telomerase reverse transcriptase	0.0661
TNF-alpha	0.0661
Target	***p*-Coumaric acid**
Aldose reductase	1.0000
Carbonic anhydrase II	1.0000
Carbonic anhydrase VII	1.0000
Estrogen receptor beta	1.0000
Carbonic anhydrase I	1.0000
Carbonic anhydrase III	1.0000
Carbonic anhydrase VI	1.0000
Carbonic anhydrase XII	1.0000
Carbonic anhydrase XIV	1.0000
Carbonic anhydrase IX	1.0000

Carbonic anhydrase IV	1.0000
Carbonic anhydrase VB	1.0000
Carbonic anhydrase VA	1.0000
Macrophage migration inhibitory factor	0.2585
Arachidonate 5-lipoxygenase	0.2250
Matrix metalloproteinase 9	0.2250
Matrix metalloproteinase 1	0.2250
Matrix metalloproteinase 2	0.2250
Protein-tyrosine phosphatase 1B	0.2250
Aldo-keto reductase family 1 member B10	0.1584
Hydroxycarboxylic acid receptor 2	0.1501
Toll-like receptor 4 (by homology)	0.1334
Carbonic anhydrase XIII (by homology)	0.1334
Coagulation factor VII/tissue factor	0.1251
11-beta-hydroxysteroid dehydrogenase 1	0.1251
Transient receptor potential cation channel subfamily A member 1	0.1167
Estrogen receptor alpha	0.1167
Progesterone receptor	0.1167
Aldo-keto-reductase family 1 member C3	0.1167
Target	**Caffeic acid**
Carbonic anhydrase II	1.0000
Arachidonate 5-lipoxygenase	1.0000
Carbonic anhydrase VII	1.0000
Carbonic anhydrase I	1.0000
Carbonic anhydrase VI	1.0000
Matrix metalloproteinase 9	1.0000
Carbonic anhydrase XII	1.0000
Matrix metalloproteinase 1	1.0000
Matrix metalloproteinase 2	1.0000
Protein-tyrosine phosphatase 1B	1.0000
Carbonic anhydrase XIV	1.0000
Carbonic anhydrase IX	1.0000
Carbonic anhydrase VB	1.0000
Carbonic anhydrase VA	1.0000
Carbonic anhydrase III	0.2124
Aldose reductase	0.1684
Estrogen receptor beta	0.1684
Carbonic anhydrase IV	0.1684
Aldo-keto reductase family 1 member B10	0.0806
Hydroxycarboxylic acid receptor 2	0.0806
Macrophage migration inhibitory factor	0.0806
Carbonic anhydrase XIII	0.0806
Quinone reductase 2	0.0718
Toll-like receptor 4 (by homology)	0.0718
Receptor protein-tyrosine kinase erbB-2	0.0718

Estrogen receptor alpha	0.0718
Norepinephrine transporter	0.0718
Transthyretin	0.0718
MAP kinase ERK2	0.0718
Aldo-keto-reductase family 1 member C3	0.0718
Aldo-keto reductase family 1 member C4	0.0718
Aldo-keto reductase family 1 member C2	0.0718
Tyrosine-protein kinase SYK	0.0718
Beta amyloid A4 protein	0.0718
Epidermal growth factor receptor erbB1	0.0718
Tyrosine-protein kinase FYN	0.0718
Tyrosine-protein kinase LCK	0.0718
Cyclooxygenase-1	0.0718
PI3-kinase p110-beta subunit	0.0718
Cytochrome P450 1A2	0.0718
Cytochrome P450 2C9	0.0718
Cytochrome P450 3A4	0.0718
Cytochrome P450 2C19	0.0718
PI3-kinase p110-alpha subunit	0.0718
Leukocyte elastase	0.0718
Coagulation factor VII/tissue factor	0.0718
11-beta-hydroxysteroid dehydrogenase 1	0.0718
Monoamine oxidase B	0.0718
Nuclear factor erythroid 2-related factor 2	0.0718
Signal transducer and activator of transcription 3	0.0718
Target	**Vanillin**
Serine/threonine-protein kinase/endoribonuclease IRE1	0.2742
Carbonic anhydrase II	0.1778
Carbonic anhydrase VII	0.0630
Carbonic anhydrase I	0.0630
Carbonic anhydrase XII	0.0630
Carbonic anhydrase XIV	0.0630
Carbonic anhydrase IX	0.0630
Carbonic anhydrase IV	0.0630
Carbonic anhydrase III	0.0535
Carbonic anhydrase VI	0.0535
Carbonic anhydrase VA	0.0535
Dual specificity phosphatase Cdc25B	0.0535
Transthyretin	0.0439
Arylamine N-acetyltransferase 1	0.0439
Alkaline phosphatase placental-like	0.0439
Phospholipase A-2-activating protein	0.0439
Leukocyte common antigen	0.0439
Histone acetyltransferase p300	0.0439
Target	**Ethyl gallate**
Squalene monooxygenase (by homology)	1.0000

Carbonic anhydrase II	0.3486
Carbonic anhydrase VII	0.3486
Carbonic anhydrase I	0.3486
Carbonic anhydrase XII	0.3486
Carbonic anhydrase XIV	0.3486
Carbonic anhydrase IX	0.3486
Carbonic anhydrase XIII	0.0823
Alpha-(1,3)-fucosyltransferase 7	0.0517
Plasminogen activator inhibitor-1	0.0415
Estrogen receptor beta	0.0415
Vascular endothelial growth factor receptor 2	0.0415
Carbonic anhydrase III	0.0415
Carbonic anhydrase IV	0.0415
Tyrosinase	0.0415
Carbonic anhydrase VA	0.0312
Insulin-like growth factor I receptor	0.0312
ALK tyrosine kinase receptor	0.0312
Serine/threonine-protein kinase Aurora-B	0.0312
Tyrosine-protein kinase SRC	0.0312
Focal adhesion kinase 1	0.0312
Hepatocyte growth factor receptor	0.0312
Serine/threonine-protein kinase NEK2	0.0312
Tyrosine-protein kinase receptor UFO	0.0312
Carbonic anhydrase VI	0.0312
Carbonic anhydrase VB	0.0312
Apoptosis regulator Bcl-X	0.0312
Platelet-derived growth factor receptor beta	0.0312
Fibroblast growth factor receptor 1	0.0312
Myoglobin	0.0312
Alpha-synuclein	0.0312
Xanthine dehydrogenase	0.0312
Target	**Oxalic acid**
Tyrosine-protein kinase FYN	0.0238
Tyrosine-protein kinase LCK	0.0238

Supplementary Table 3: The proteins that interact with the selected compounds and the natural substrates of these proteins with the corresponding probability (%)

Protein	Substrate -- %	Compound
Amylase	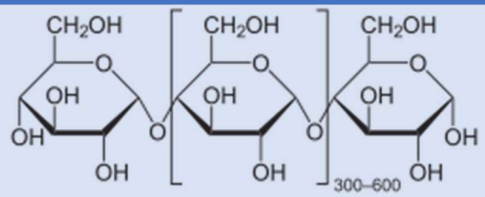 Starch – n/a	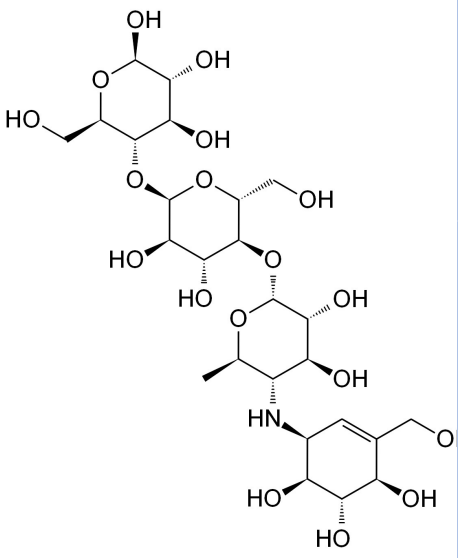 Acarbose
Glucosidase	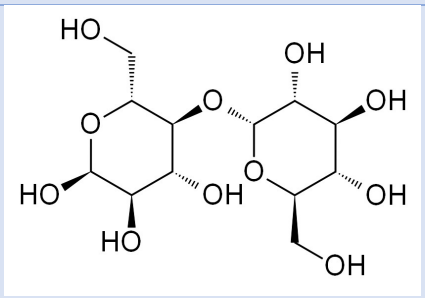 Maltose – 0	
Acetylcholinesterase	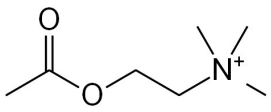 Acetlycholine – 3	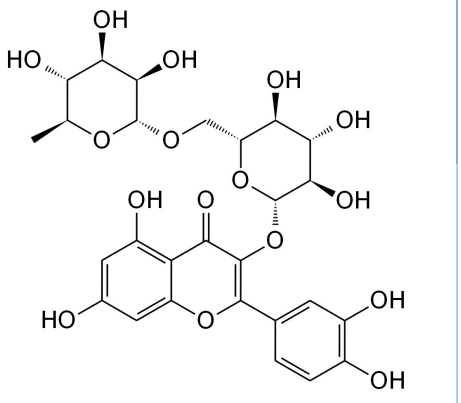 Rutin
Adrenergic receptor	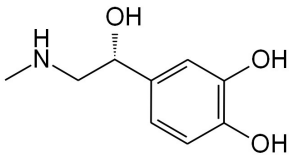 Epinephrine – 75	
Neuromedin-U receptor 2	H-Tyr-Lys-Val-Asn-Glu-Tyr-Gln-Gly-Pro-Val-Ala-Pro-Ser-Gly-Gly-Phe-Phe-Leu-Phe-Arg-Pro-Arg-Asn-NH2 Neuromedin U – n/a	
Aldose reductase	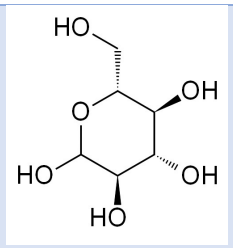 Glucose – 0	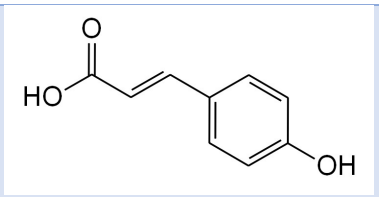 *p*-Coumaric acid
Estrogen receptor	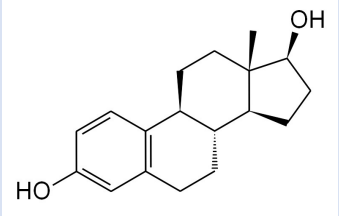 Estrogen – 94	

Carbonic anhydrase	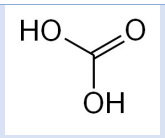 $CO_2 + H_2O = H_2CO_3$ – n/a	
Matrix metalloproteinase	H-Gly-DL-Glu-DL-Pro-Gly-DL-xiIle-DL-Ala-Gly-DL-Phe-DL-Lys-Gly-DL-Glu-DL-Gln-Gly-DL-Pro-DL-Lys-OH Extracellular proteins such as collagen – n/a	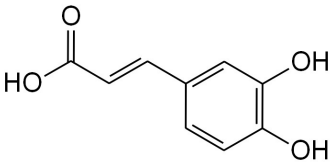 Caffeic acid
Arachidonate 5-lipoxygenase	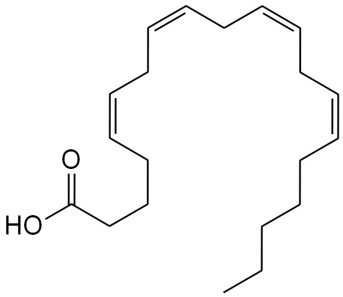 Arachidonic acid – 24	
Protein tyrosine phosphatase 1B	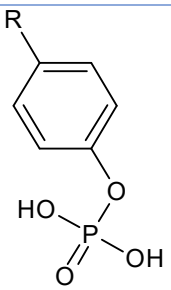 Phosphorylated protein such as IRS – n/a	
Squalene monooxygenase	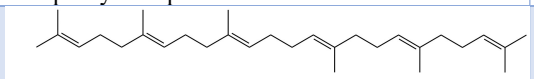 Squalene -- 0	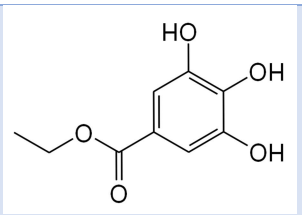 Ethyl gallate

The proteins identified by SwissTargetPrediction that had a high probability (100%) of interacting with the corresponding compounds as well as the protein's natural substrate found in the body as well as the percentage probability of the natural substrate interacting with the corresponding protein
The structures were sourced from PubChem (**https://pubchem.ncbi.nlm.nih.gov/**)
n/a = the probaility could not be determined because the structure is too large or too small

Supplementary Table 4: The V_{max} and K_m of the selected compounds for pancreatic-alpha amylase

Concentration (µM)	V_{max} (µmol/min)	K_m (mg/mL)
Acarbose		
40	0.046±0.0083	1.936±0.0001
20	0.056±0.0056*	1.168±0.1077
10	0.083±0.0178	1.453±0.4229
5	0.092±0.0061	1.332±0.1028
0	0.109±0.0018	1.480±0.1207
Caffeic acid		
40	0.076±0.0329	2.775±0.4239
20	0.078±0.0342	1.910±0.3685
10	0.073±0.0311	1.435±0.1241
5	0.075±0.0315	1.329±0.0059
0	0.109±0.0018	1.480±0.1207
Ethyl gallate		
40	0.100±0.0233	2.359±0.6448
20	0.098±0.0170	1.994±0.8094
10	0.093±0.0112	1.545±0.4353
5	0.075±0.0124	0.887±0.0087*
0	0.109±0.0018	1.480±0.1207
Oxalic acid		
400	0.173±0.0258	2.551±0.1734*
200	0.150±0.0331	1.982±0.4744
100	0.182±0.0972	2.604±1.7000
50	0.104±0.0083	1.380±0.1932
0	0.109±0.0018	1.480±0.1207
***p*-Coumaric acid**		
1000	0.124±0.0136	1.684±0.5510
750	0.135±0.0396	1.616±0.7662
500	0.147±0.0423	1.971±1.1331
250	0.140±0.0385	1.503±0.6909
0	0.109±0.0018	1.480±0.1207
Rutin		
200	0.101±0.0116	1.468±0.3399
100	0.092±0.0113	1.201±0.3271
50	0.096±0.0063	1.242±0.2203
0	0.109±0.0018	1.480±0.1207
Vanillin		
20	0.094±0.0092	2.100±0.5165
10	0.085±0.0050*	2.516±1.2864
5	0.098±0.0131	3.924±2.6384
0	0.109±0.0018	1.480±0.1207

*Significantly different ($p < 0.05$) to 0 µM

Supplementary Table 5: The Vmax and Km of the selected compounds for alpha glucosidase

Concentration (µM)	V_{max} (nmol/min)	K_m (mM)
Acarbose		
1000	1.66±0.277*	3.98±1.875
750	2.08±1.089	2.87±1.015
500	3.03±1.051	3.65±0.582*
250	6.35±1.047	4.34±0.844
0	4.08±0.314	0.45±0.038
Caffeic acid		
1000	2.19±0.800	0.64±0.060
750	4.22±1.942	0.73±0.395
500	6.03±1.675	1.55±0.529
250	6.71±1.537	1.21±0.609
0	4.08±0.314	0.45±0.038
Ethyl gallate		
1000	3.37±1.643	0.92±0.344
750	4.90±2.251	1.64±0.993
500	3.65±0.813	0.69±0.349
250	4.93±1.410	0.83±0.583
0	4.08±0.314	0.45±0.038
Oxalic acid		
1000	9.95±6.119	1.89±1.577
750	25.55±20.960	5.80±5.442
500	24.74±20.607	5.51±5.181
250	6.19±2.211	0.87±0.606
0	4.08±0.314	0.45±0.038
***p*-Coumaric acid**		
1000	3.70±2.608	0.84±0.540
750	8.59±3.895	2.35±0.996
500	6.40±2.870	1.73±1.060
250	15.15±2.343	3.58±0.636
0	4.08±0.314	0.45±0.038
Rutin		
750	9.27±4.354	1.34±0.771
500	18.86±10.93	4.25±3.237
250	4.14±0.469	0.36±0.260
0	4.08±0.314	0.45±0.038
Vanillin		
1000	3.99±0.280	0.39±0.035
750	4.03±0.146	0.36±0.021
500	3.78±0.326	0.33±0.052
250	3.58±0.066	0.28±0.072
0	4.08±0.314	0.45±0.038

*Significantly different ($p < 0.05$) to 0 µM

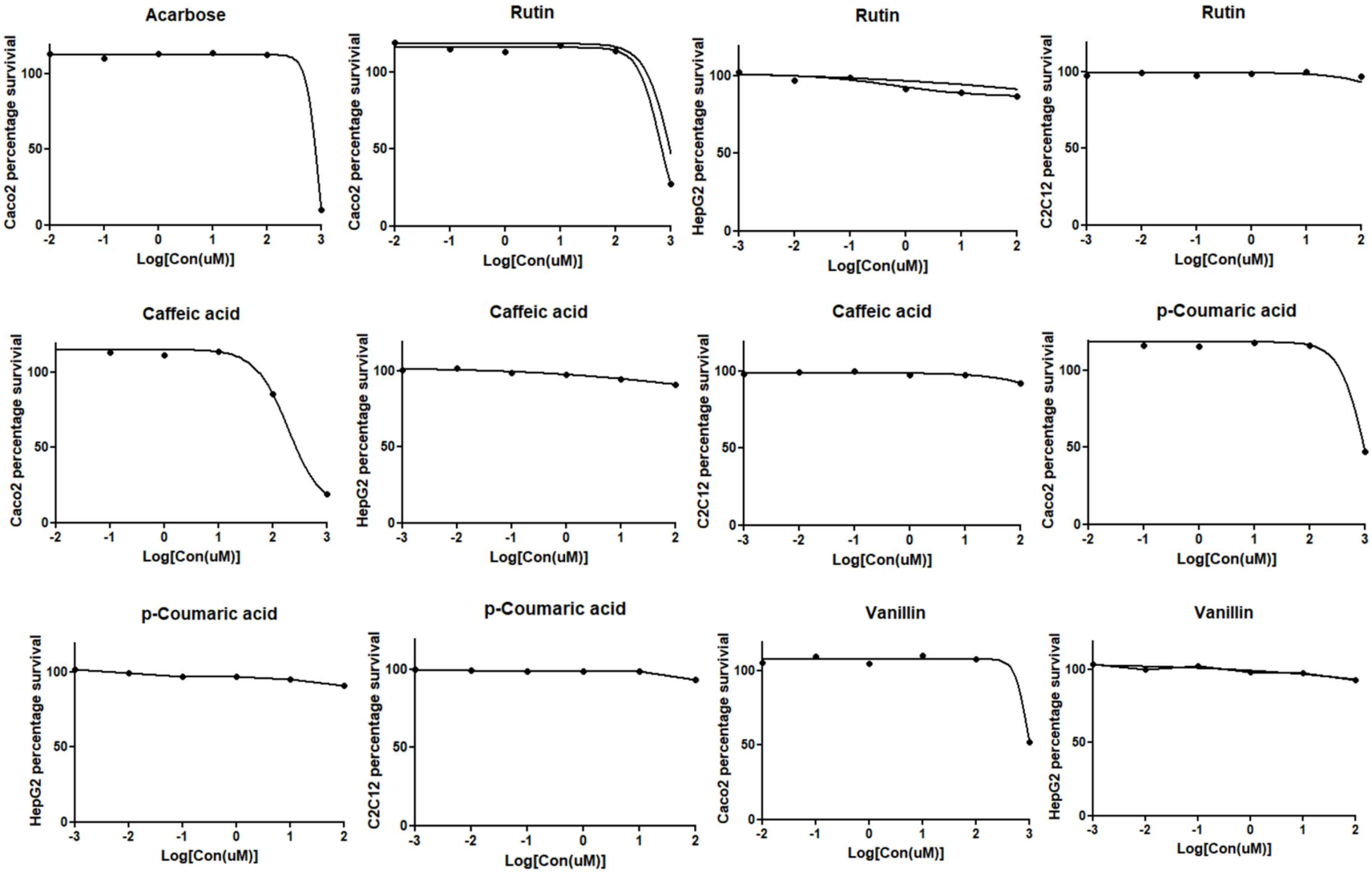
Acarbose
Caco2 percentage survival
Log[Con(uM)]
Rutin
Caco2 percentage survival
Log[Con(uM)]
Rutin
HepG2 percentage survival
Log[Con(uM)]
Rutin
C2C12 percentage survival
Log[Con(uM)]
Caffeic acid
Caco2 percentage survival
Log[Con(uM)]
Caffeic acid
HepG2 percentage survival
Log[Con(uM)]
Caffeic acid
C2C12 percentage survival
Log[Con(uM)]
p-Coumaric acid
Caco2 percentage survival
Log[Con(uM)]
p-Coumaric acid
HepG2 percentage survival
Log[Con(uM)]
p-Coumaric acid
C2C12 percentage survival
Log[Con(uM)]
Vanillin
Caco2 percentage survival
Log[Con(uM)]
Vanillin
HepG2 percentage survival
Log[Con(uM)]

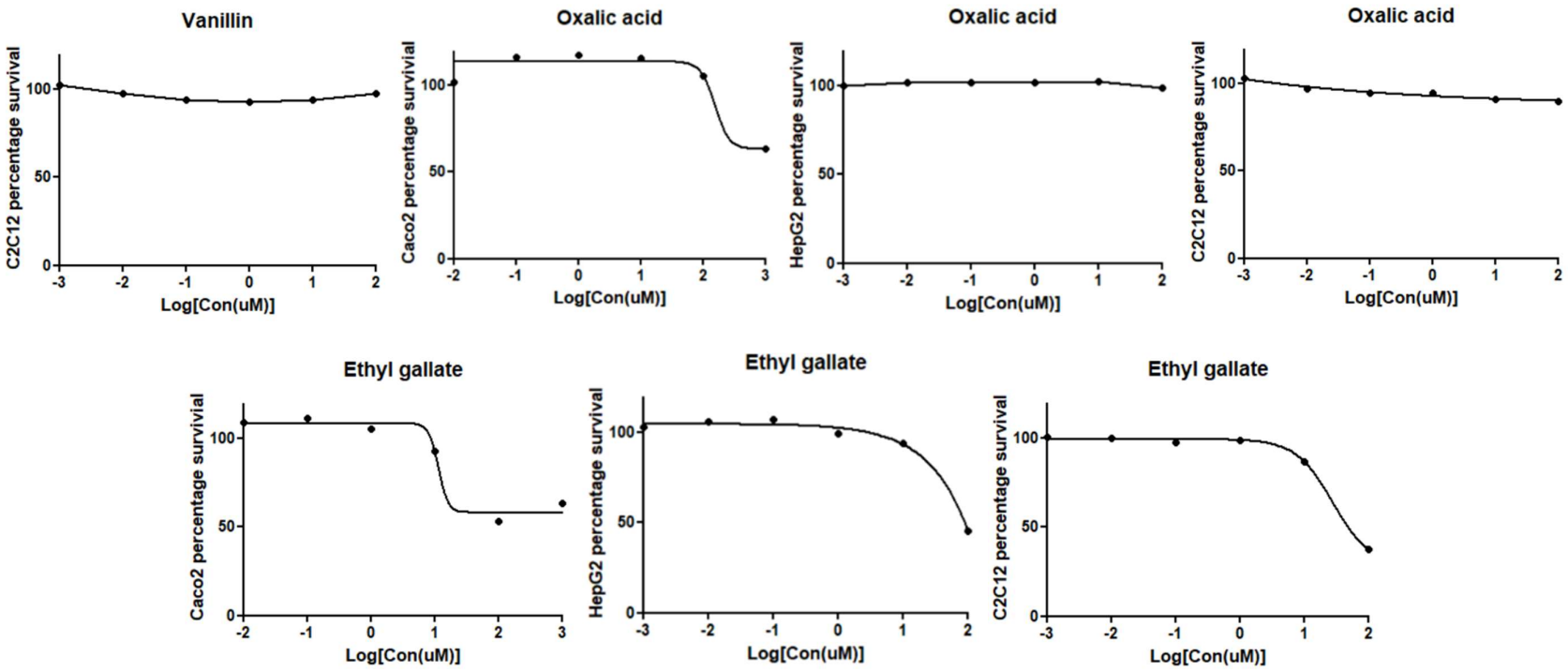

Supplementary Figure 2: Cytotoxicity of selected compounds for Caco2, HepG2, and C2C12 cells

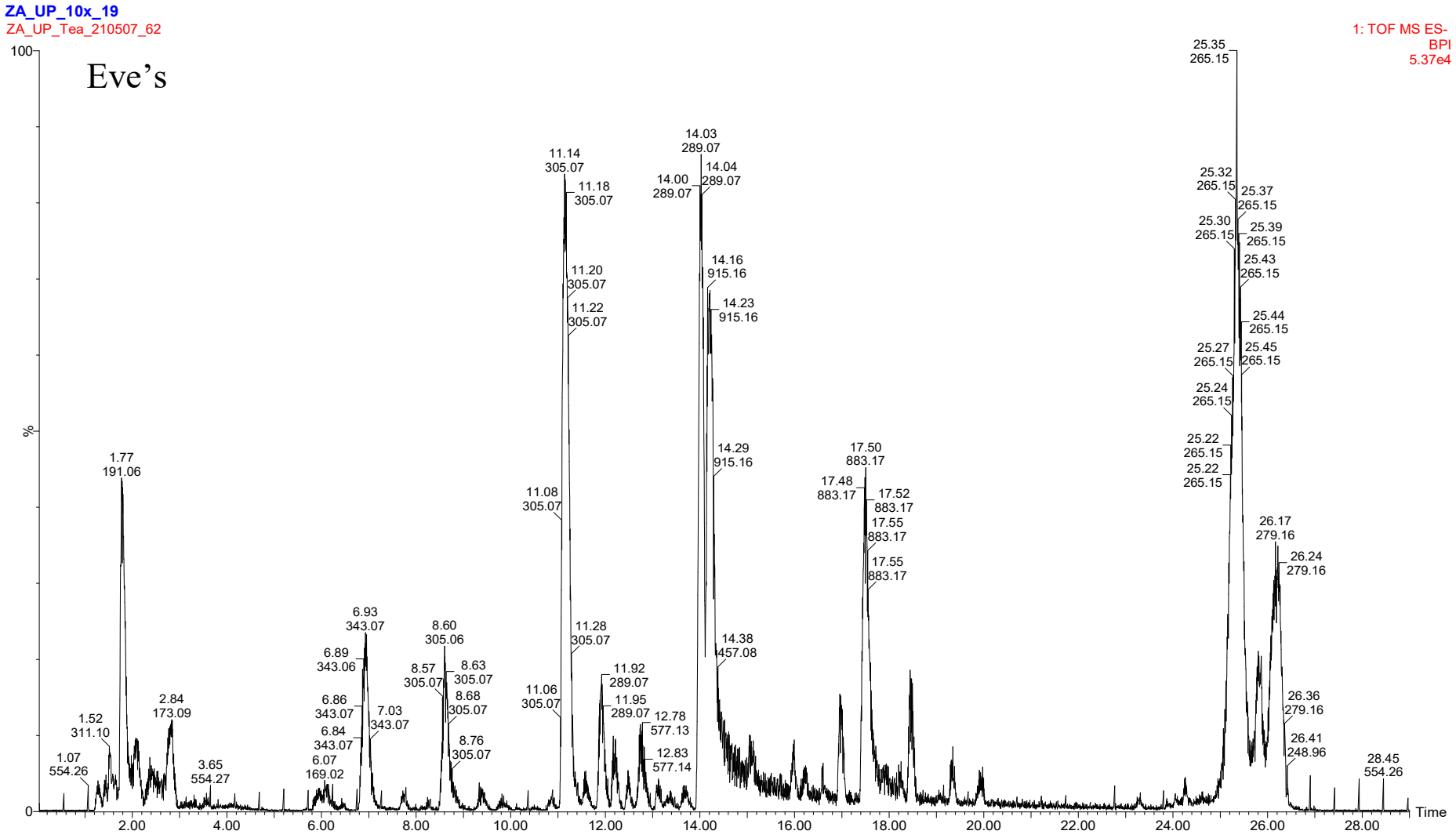
ZA_UP_10x_19
ZA_UP_Tea_210507_62
1: TOF MS ES-
BPI
5.37e4
Eve's
100
%
0
Time
2.00
4.00
6.00
8.00
10.00
12.00
14.00
16.00
18.00
20.00
22.00
24.00
26.00
28.00
1.77
191.06
1.52
311.10
1.07
554.26
2.84
173.09
3.65
554.27
6.93
343.07
6.89
343.06
6.86
343.07
6.84
343.07
6.07
169.02
7.03
343.07
8.60
305.06
8.57
305.07
8.63
305.07
8.68
305.07
8.76
305.07
11.14
305.07
11.18
305.07
11.20
305.07
11.22
305.07
11.08
305.07
11.28
305.07
11.06
305.07
14.03
289.07
14.04
289.07
14.00
289.07
14.16
915.16
14.23
915.16
14.29
915.16
14.38
457.08
11.92
289.07
11.95
289.07
12.78
577.13
12.83
577.14
17.50
883.17
17.48
883.17
17.52
883.17
17.55
883.17
17.55
883.17
25.35
265.15
25.32
265.15
25.37
265.15
25.30
265.15
25.39
265.15
25.43
265.15
25.44
265.15
25.27
265.15
25.45
265.15
25.24
265.15
25.22
265.15
25.22
265.15
26.17
279.16
26.24
279.16
26.36
279.16
26.41
248.96
28.45
554.26

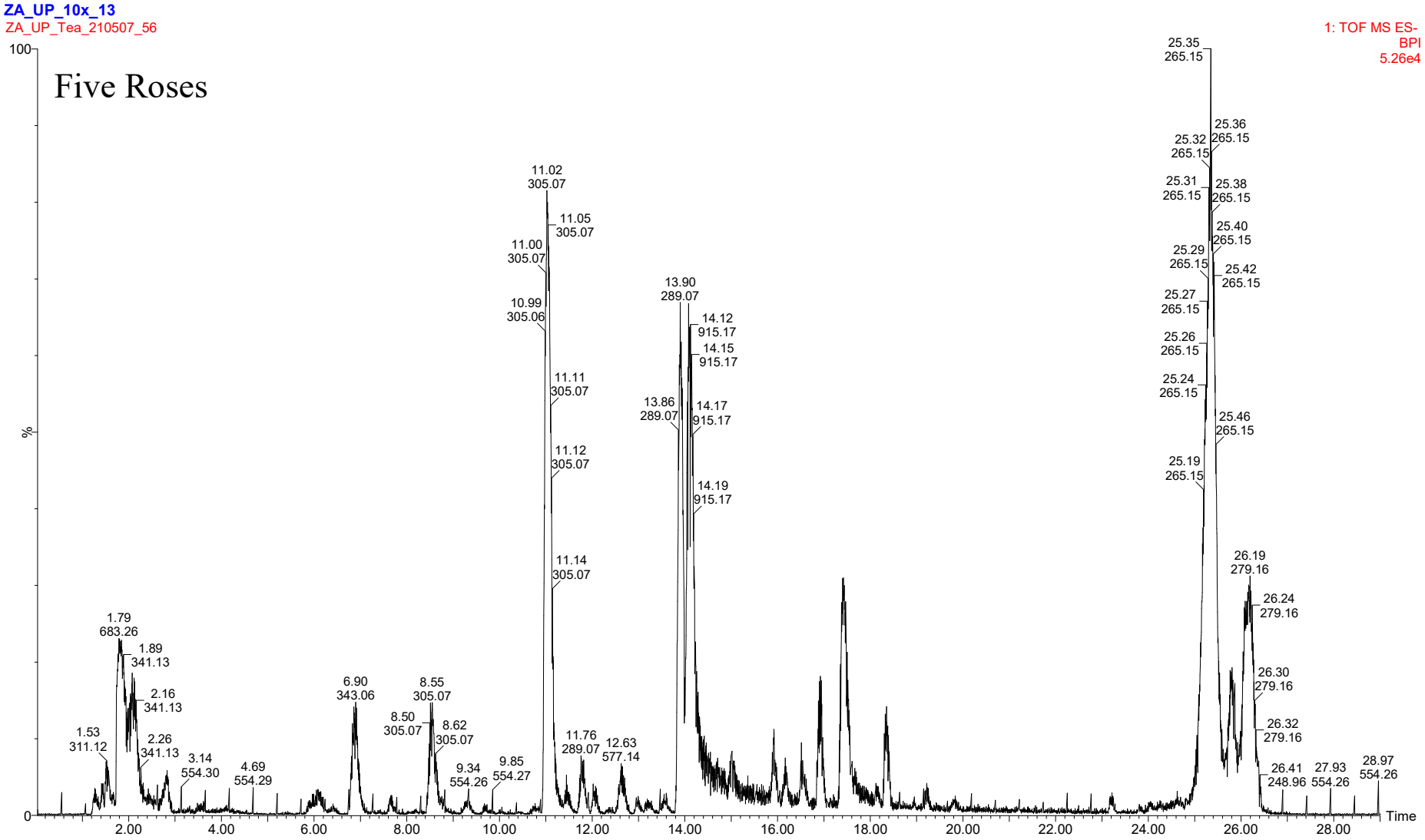
ZA_UP_10x_13
ZA_UP_Tea_210507_56
1: TOF MS ES-
BPI
5.26e4
Five Roses
100
%
0
Time
2.00
4.00
6.00
8.00
10.00
12.00
14.00
16.00
18.00
20.00
22.00
24.00
26.00
28.00
1.53
311.12
1.79
683.26
1.89
341.13
2.16
341.13
2.26
341.13
3.14
554.30
4.69
554.29
6.90
343.06
8.50
305.07
8.55
305.07
8.62
305.07
9.34
554.26
9.85
554.27
10.99
305.06
11.00
305.07
11.02
305.07
11.05
305.07
11.11
305.07
11.12
305.07
11.14
305.07
11.76
289.07
12.63
577.14
13.86
289.07
13.90
289.07
14.12
915.17
14.15
915.17
14.17
915.17
14.19
915.17
25.19
265.15
25.24
265.15
25.26
265.15
25.27
265.15
25.29
265.15
25.31
265.15
25.32
265.15
25.35
265.15
25.36
265.15
25.38
265.15
25.40
265.15
25.42
265.15
25.46
265.15
26.19
279.16
26.24
279.16
26.30
279.16
26.32
279.16
26.41
248.96
27.93
554.26
28.97
554.26

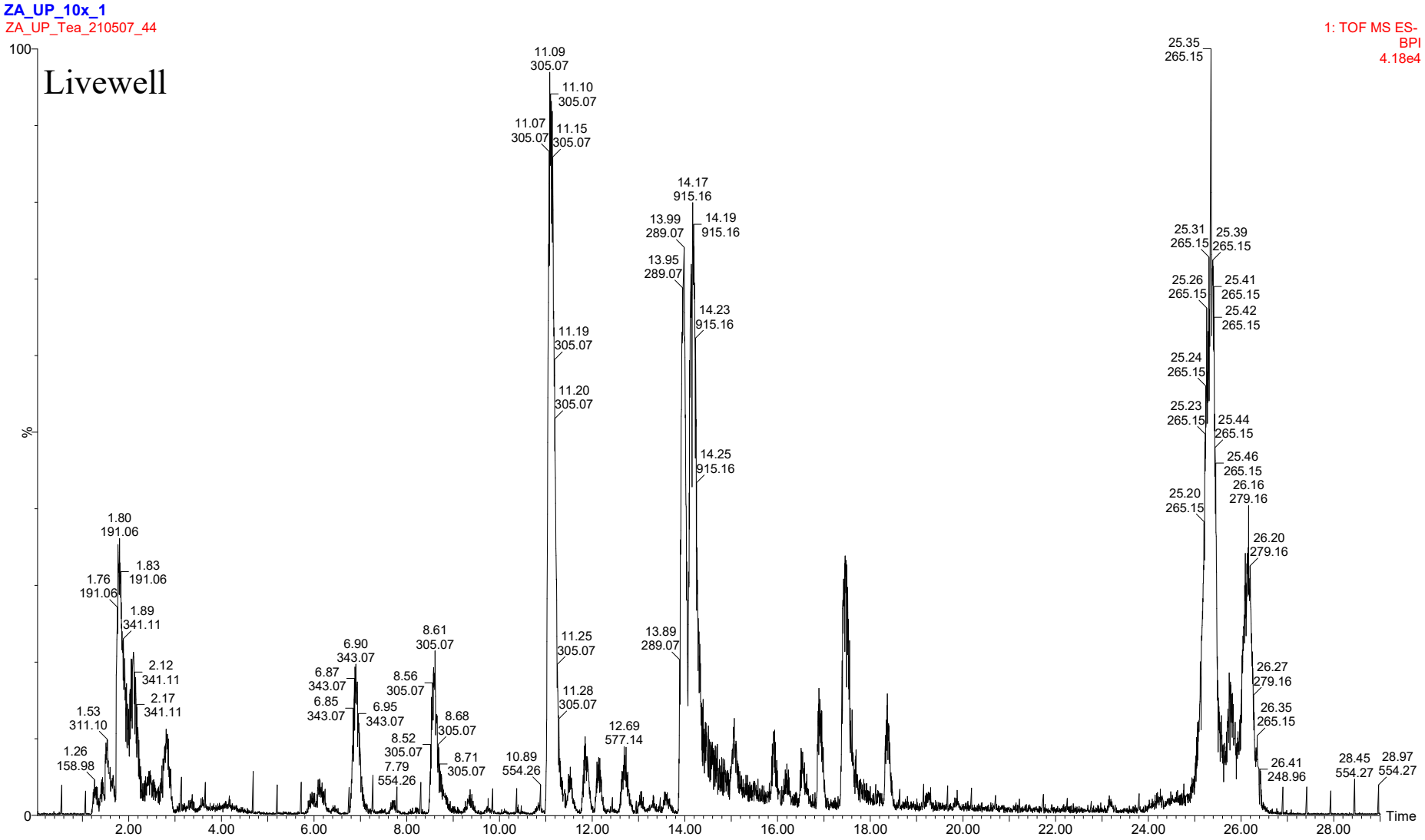
ZA_UP_10x_1
ZA_UP_Tea_210507_44
1: TOF MS ES-
BPI
4.18e4
Livewell
100
%
0
Time
2.00
4.00
6.00
8.00
10.00
12.00
14.00
16.00
18.00
20.00
22.00
24.00
26.00
28.00
1.26 158.98
1.53 311.10
1.76 191.06
1.80 191.06
1.83 191.06
1.89 341.11
2.12 341.11
2.17 341.11
6.85 343.07
6.87 343.07
6.90 343.07
6.95 343.07
7.79 554.26
8.52 305.07
8.56 305.07
8.61 305.07
8.68 305.07
8.71 305.07
10.89 554.26
11.07 305.07
11.09 305.07
11.10 305.07
11.15 305.07
11.19 305.07
11.20 305.07
11.25 305.07
11.28 305.07
12.69 577.14
13.89 289.07
13.95 289.07
13.99 289.07
14.17 915.16
14.19 915.16
14.23 915.16
14.25 915.16
25.20 265.15
25.23 265.15
25.24 265.15
25.26 265.15
25.31 265.15
25.35 265.15
25.39 265.15
25.41 265.15
25.42 265.15
25.44 265.15
25.46 265.15
26.16 279.16
26.20 279.16
26.27 279.16
26.35 265.15
26.41 248.96
28.45 554.27
28.97 554.27

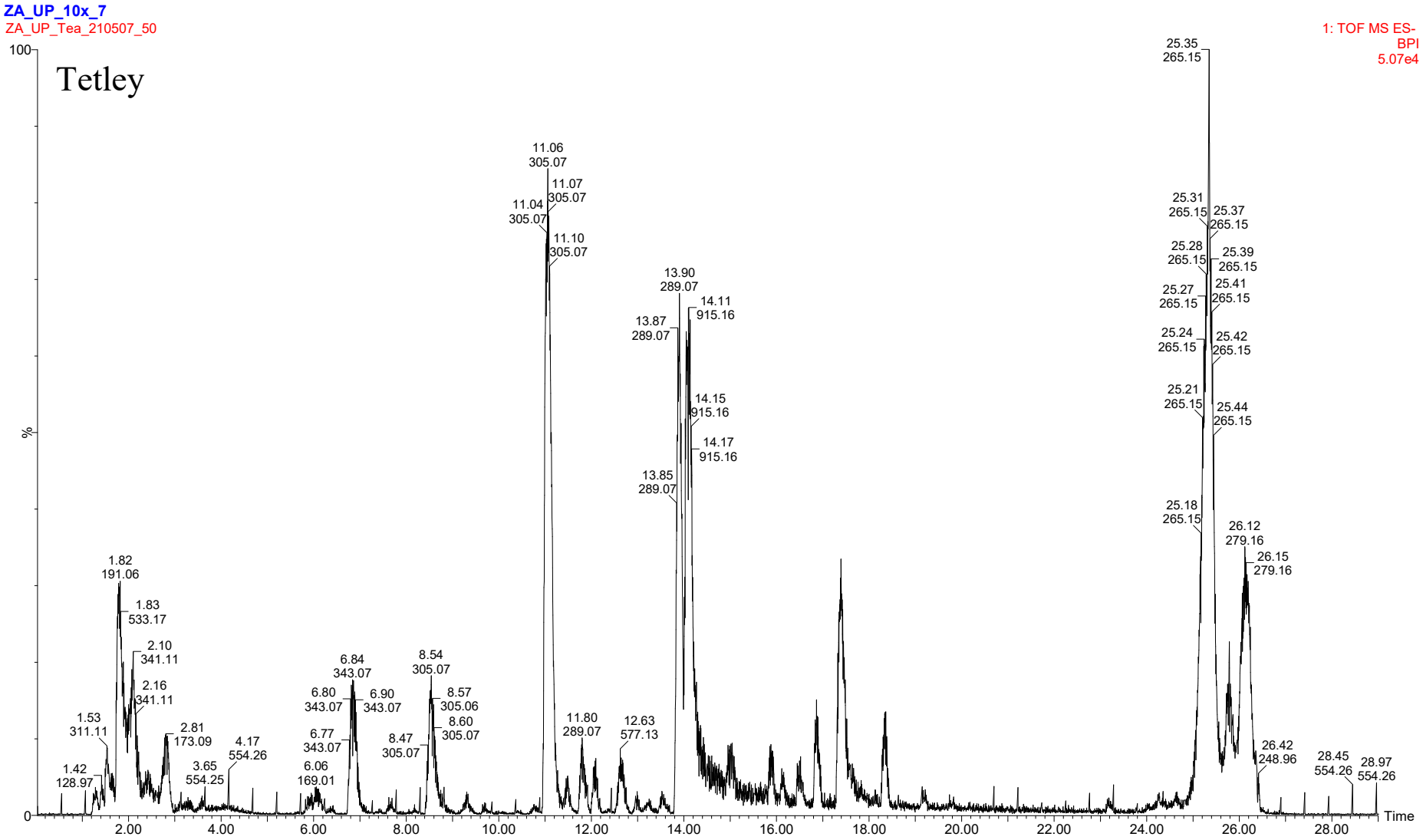

Supplementary Figure 3: The BPI chromatogram of green tea brands

Supplementary Table 6: The compounds putatively annotated in the five green tea brands

RT (min)	m/z	mDa	Formula	Name	Level of confidence
1.84	191.0575	+1.9	$C_7H_{11}O_6$	Quinic acid	Level 1
8.57	305.0668	+0.7	$C_{15}H_{13}O_7$	Gallocatechin	Level 2
11.06	305.0664	+0.3	$C_{15}H_{13}O_7$	Epigallocatechin	Level 1
11.78	289.0717	+0.5	$C_{15}H_{13}O_6$	Catechin	Level 1
12.23	353.0878	+0.5	$C_{16}H_{17}O_9$	Chlorogenic acid	Level 1
12.67	577.1346	-1.3	$C_{30}H_{25}O_{12}$	Procyanidin B5	Level 2
12.97	179.0350	+0.6	$C_9H_7O_4$	Caffeic acid	Level 1
13.90	289.0718	+0.6	$C_{15}H_{13}O_6$	Epicatechin	Level 1
14.07	457.0781	+1.0	$C_{22}H_{17}O_{11}$	Epigallocatechin gallate	Level 1
14.13	915.1612	-0.8	$C_{44}H_{35}O_{22}$	Assamicain A	Level 2
15.75	163.0401	+0.6	$C_9H_7O_3$	*p*-Coumaric acid	Level 1
17.40	441.0820	-0.2	$C_{22}H_{17}O_{10}$	Epicatechin-3-O-gallate	Level 1
17.66	609.1460	+0.4	$C_{27}H_{29}O_{16}$	Rutin	Level 1
20.70	359.0778	+1.1	$C_{18}H_{15}O_8$	Rosmarinic acid	Level 1
24.20	301.0348	+1.1	$C_{15}H_9O_7$	Quercetin	Level 1

The retention time (RT) of the putatively identified compounds and the m/z and error as mDa
The level of confidence was determined using the classification system described by Schymanski *et al.* (2014)

Annexure A: Reagents

Reagent	Catalogue number	Brand
2NBDG	N13195	Thermo Fisher Scientific
3,5-dinitrosalicylic acid	D0550	Sigma Aldrich (Merck)
4-Nitrophenyl (*p*NP)	241326	Sigma Aldrich (Merck)
4-Nitrophenyl α-D-glucopyranoside (*p*NPG)	N1377	Sigma Aldrich (Merck)
Acarbose	A8980	Sigma Aldrich (Merck)
α-Amylase from porcine pancreas	A3176	Sigma Aldrich (Merck)
α-Glucosidase from Saccharomyces cerevisiae	G5003	Sigma Aldrich (Merck)
Caffeic acid	C0625	Sigma Aldrich (Merck)
D-(+)-Maltose monohydrate	M5885	Sigma Aldrich (Merck)
Dimethyl sulfoxide (DMSO)	472301	Sigma Aldrich (Merck)
Dulbecco′s Modified Eagle′s Medium (DMEM)	P040-3500	Pan Biotech
Ethyl gallate	48640	Fluka
Glucose free DMEM	D5030	Sigma Aldrich (Merck)
Insulin	I0310000	Sigma Aldrich (Merck)
Metformin	317240	EMD Millipore Corp
Oxalic acid	75688	Sigma Aldrich (Merck)
***p*-Coumaric acid**	28200	Fluka
Rutin trihydrate	84082	Sigma Aldrich (Merck)
Sodium chloride (NaCl)	S9625	Sigma Aldrich (Merck)
Sodium hydroxide (NaOH)	221465	Sigma Aldrich (Merck)
Sodium phosphate dibasic (Na_2HPO_4)	795410	Sigma Aldrich (Merck)
Sodium phosphate monobasic (NaH_2PO_4)	S0751	Sigma Aldrich (Merck)
Sodium potassium tartrate tetrahydrate	S2377	Sigma Aldrich (Merck)
Starch from potato	S2004	Sigma Aldrich (Merck)
Vanillin	6469000	UniLab

Annexure B: Pancreatic alpha-amylase assay method

1. Stock solutions

1.1. 2 M NaOH: 4 g NaOH dissolved in 50 mL dH_2O.

1.2. 96 mM 3,5-dinitrosalicylic acid solution: 0.44 g 3,5-dinitrosalicylic acid in 20 mL dH_2O.

1.3. DNSA colour reagent: 12 g sodium potassium tartrate tetrahydrate + 8.0 ml 2 M NaOH + 20 mL 96 mM 3,5-dinitrosalicylic acid solution dissolved by heating.

1.4. 20 mM sodium phosphate buffer (pH 6.9): 1.2 g NaH_2PO_4 + 1.4 g Na_2HPO_4 + 0.4 g NaCl dissolved in 1 L dH_2O.

1.5. 0.2% (w/v) maltose: 0.02 g maltose dissolved in 10 mL buffer.

1.6. 4 U/mL pancreatic alpha-amylase solution: 12 mg pancreatic alpha-amylase dissolved in 30 mL buffer.

1.7. 2% starch: 1 g starch in 50 mL buffer dissolved by heating

1.8. 50 mM inhibitor solution:

Inhibitor	Mass (mg) inhibitor dissolved in 2 mL DMSO
Acarbose	65
Caffeic acid	18
Ethyl gallate	20
Oxalic acid	13
***p*-Coumaric acid**	16
Rutin	66
Vanillin	15

2. Standard curve

2.1. 96 well plate setup of standard curve:

Well	0.2% maltose (µmol -- µL)	Buffer (µmol -- µL)	DNSA reagent (µmol -- µL)
1	0.556 -- 100	2.0 -- 100	9.6 -- 100
2	0.444 -- 80	2.4 -- 120	9.6 -- 100
3	0.333 -- 60	2.8 -- 140	9.6 -- 100
4	0.222 -- 40	3.2 -- 160	9.6 -- 100
5	0.111 --20	3.6 -- 180	9.6 -- 100
6	0 -- 0	4.0 -- 200	9.6 -- 100

2.2. The 96 well plate was placed in an oven at 80°C for 25 min.

2.3. Fifty microliters from each well were transferred to another 96 well plate and diluted with 200 µL dH_2O, in triplicate.

2.4. The absorbance was measured at 540 nm.

2.5. A standard curve was produced by plotting the absorbance values against the maltose concentration.

2.6. The gradient of that line represents Abs/[maltose].

3. IC_{50} assay

3.1. Preparation of 2 mL inhibitor concentrations:

Number	Volume inhibitor (µL)	Volume buffer (µL)	[Inhibitor] (mM)
I1	800 (of 50 mM)	1200	20.0
I2	100 (of 20 mM)	1900	1.0
I3	200 (of 1.0 mM)	1800	0.1

3.2. 96 well plate setup of IC_{50} assay:

Well	Inhibitor (µmol -- µL)	Buffer (µmol -- µL)	Amylase (U -- µL)	Incubate for 10 min at RT	2% Starch (mg -- µL)	Total reaction volume of 200 µL	Final [inhibitor] (µM)	Incubate for 10 min at RT	DNSA reagent (µmol -- µL)
1	1000 -- 50 (of I1)	0 -- 0	0.2 -- 50		2 -- 100		5000		9.6 -- 100
2	500 -- 25 (of I1)	500 -- 25	0.2 -- 50		2 -- 100		2500		9.6 -- 100
3	200 -- 10 (of I1)	800 -- 40	0.2 -- 50		2 -- 100		1000		9.6 -- 100
4	50 -- 50 (of I2)	0 -- 0	0.2 -- 50		2 -- 100		250		9.6 -- 100
5	25 -- 25 (of I2)	500 -- 25	0.2 -- 50		2 -- 100		125		9.6 -- 100
6	10 -- 10 (of I2)	800 -- 40	0.2 -- 50		2 -- 100		50		9.6 -- 100
7	5 -- 50 (of I3)	0 -- 0	0.2 -- 50		2 -- 100		25		9.6 -- 100
8	3 -- 25 (of I3)	500 -- 25	0.2 -- 50		2 -- 100		13		9.6 -- 100
9	1 -- 10 (of I3)	800 -- 40	0.2 -- 50		2 -- 100		5		9.6 -- 100
10	0 -- 0	1000 -- 50	0.2 -- 50		2 -- 100		0		9.6 -- 100

3.3. The blank received 50 µL buffer instead of 50 µL amylase for all inhibitor concentrations.

3.4. The 96 well plate was placed in an oven at 80°C for 25 min.

3.5. Fifty microliters from each well were transferred to another 96 well plate and diluted with 200 µL dH_2O, in triplicate.

3.6. The absorbance was measured at 540 nm.

3.7. The Abs for each inhibitor concentration was the absorbance of the blank subtracted from the average absorbance of each triplicate.

3.8. An IC_{50} graph was produced by plotting the %inhibition ((Abs without inhibitor – Abs with inhibitor)/Abs without inhibitor) against the final inhibitor concentration.

4. Pancreatic alpha-amylase assay

4.1. Two millilitres of each inhibitor concentration were prepared:

Inhibitor	Volume inhibitor (µL)	Volume buffer (µL)	Initial [inhibitor] (µM)	Final [inhibitor] in 200 µL reaction (µM)	Nanomoles inhibitor in 50 µL
***p*-Coumaric acid**	160 (of 50 mM)	1840	4000	1000	50.0
	120 (of 50 mM)	1880	3000	750	37.5
	80 (of 50 mM)	1920	2000	500	25.0
	40 (of 50 mM)	1960	1000	250	12.5
Oxalic acid, and rutin	160 (of 20 mM)	1840	1600	400	20.0
	80 (of 20 mM)	1920	800	200	10.0
	40 (of 20 mM)	1960	400	100	5.0
	20 (of 20 mM)	1980	200	50	2.5
Acarbose, caffeic acid, ethyl gallate, and vanillin	320 (of 1.0 mM)	1680	160	40	2.0
	160 (of 1.0 mM)	1840	80	20	1.0
	80 (of 1.0 mM)	1920	40	10	0.5
	40 (of 1.0 mM)	1960	20	5	0.3

4.2. Ten millilitres of each starch concentration (mg/mL) were prepared:

Number	Volume 2% starch (mL)	Volume buffer (mL)	Initial [starch] (mg/mL)	Final [starch] in 200 µL reaction (mg/mL)
S1	10.0	0	20.0	10.0
S2	5.0	5.0	10.0	5.0
S3	3.3	6.7	6.6	3.3
S4	2.5	7.5	5.0	2.5
S5	2.0	8.0	4.0	2.0
S6	1.7	8.3	3.4	1.7
S7	1.4	8.6	2.8	1.4
S8	0	10.0	0	0

4.3. 96 well plate setup of pancreatic alpha-amylase assay:

Well	Volume of inhibitor (µL)	Amylase (U -- µL)	Incubate for 10 min at RT	Starch (mg -- µL)	Total reaction volume of 200 µL	Incubate for 10 min at RT	DNSA reagent (µmol -- µL)
1	50	0.2 -- 50		2.00 -- 100 (of S1)			9.6 -- 100
2	50	0.2 -- 50		1.00 -- 100 (of S2)			9.6 -- 100
3	50	0.2 -- 50		0.66 -- 100 (of S3)			9.6 -- 100
4	50	0.2 -- 50		0.50 -- 100 (of S4)			9.6 -- 100
5	50	0.2 -- 50		0.40 -- 100 (of S5)			9.6 -- 100
6	50	0.2 -- 50		0.34 -- 100 (of S6)			9.6 -- 100
7	50	0.2 -- 50		0.28 -- 100 (of S7)			9.6 -- 100
8	50	0.2 -- 50		0 -- 100 (of S8)			9.6 -- 100

4.4. The blank received 50 µL buffer instead of 50 µL amylase for all starch concentrations.

4.5. The 96 well plate was placed in an oven at 80°C for 25 min.

4.6. Fifty microliters from each well were transferred to another 96 well plate and diluted with 200 µL dH_2O, in triplicate.

4.7. The absorbance was measured at 540 nm.

4.8. The Abs for each starch concentration was the absorbance of the blank subtracted from the average absorbance of each triplicate.

4.9. The velocity (µmol/min) was calculated as follows:

$$\frac{Abs}{Gradient\ of\ the\ standard\ curve\ (in\ mM^{-1})} \times 0.2\ mL\ \div 10\ min$$

4.10. A Lineweaver-Burk plot was produced by plotting the velocity against the final starch concentration.

Annexure C: Alpha-glucosidase assay method

1. Stock solutions

1.1. 0.8 M NaOH: 3.2 g NaOH dissolved in 100 mL dH_2O.

1.2. 100 mM sodium phosphate buffer (pH 6.8): 7.1 g NaH_2PO_4 + 7.8 g Na_2HPO_4 dissolved in 1 L dH_2O.

1.3. 1 mM *p*NP: 0.014 g *p*NP dissolved in 100 mL buffer.

1.4. 0.2 U/mL alpha-glucosidase solution: 100 µL of 100 U/2 mL stock solution added to 25 mL buffer.

1.5. 2 mM *p*NPG: 0.06 g *p*NPG dissolved in 100 mL buffer.

1.6. 50 mM inhibitor solution:

Inhibitor	Mass (mg) inhibitor in 2 mL DMSO
Acarbose	65
Caffeic acid	18
Ethyl gallate	20
Oxalic acid	13
***p*-Coumaric acid**	16
Rutin	66
Vanillin	15

2. Standard curve

2.1. 96 well plate setup of standard curve:

Well	1 mM *p*NP (µmol -- µL)	Buffer (µmol -- µL)	0.8 M NaOH (µmol -- µL)
1	100 -- 100	10000 -- 100	40000 -- 50
2	80 -- 80	12000 -- 120	40000 -- 50
3	60 -- 60	14000 -- 140	40000 -- 50
4	40 -- 40	16000 -- 160	40000 -- 50
5	20 --20	18000 -- 180	40000 -- 50
6	0 -- 0	20000 -- 200	40000 -- 50

2.2. Each reaction was performed in triplicate.

2.3. The absorbance was measured at 405 nm.

2.4. A standard curve was produced by plotting the absorbance values against the *p*NP concentration.

2.5. The gradient of that line represents Abs/[*p*NP].

3. IC_{50} assay

3.1. Preparation of 2 mL inhibitor concentrations:

Number	Volume inhibitor (µL)	Volume buffer (µL)	[Inhibitor] (mM)
I1	2000 (of 50 mM)	0	50.0
I2	200 (of 50 mM)	1800	5.0
I3	400 (of 5.0 mM)	1600	1.0

3.2. 96 well plate setup of IC_{50} assay:

Well	Inhibitor (µmol -- µL)	Buffer (µmol -- µL)	Glucosidase (U -- µL)	Incubate for 10 min at RT	2 mM *p*NPG (µmol -- µL)	Total reaction volume of 200 µL	Final [inhibitor] (µM)	Incubate for 30 min at 37°C	0.8 M NAOH (µmol -- µL)
1	2500 -- 50 (of I1)	0 -- 0	0.01 – 50		200 -- 100		12500		40000 -- 50
2	1250 -- 25 (of I1)	2500 -- 25	0.01 – 50		200 -- 100		6250		40000 -- 50
3	500 -- 10 (of I1)	4000 -- 40	0.01 – 50		200 -- 100		2500		40000 -- 50
4	250 -- 50 (of I2)	0 -- 0	0.01 – 50		200 -- 100		1250		40000 -- 50
5	125 -- 25 (of I2)	2500 -- 25	0.01 – 50		200 -- 100		625		40000 -- 50
6	50 -- 10 (of I2)	4000 -- 40	0.01 – 50		200 -- 100		250		40000 -- 50
7	50 -- 50 (of I3)	0 -- 0	0.01 – 50		200 -- 100		250		40000 -- 50
8	25 -- 25 (of I3)	2500 -- 25	0.01 – 50		200 -- 100		125		40000 -- 50
9	10 -- 10 (of I3)	4000 -- 40	0.01 – 50		200 -- 100		50		40000 -- 50
10	0 -- 0	5000 -- 50	0.01 – 50		200 -- 100		0		40000 -- 50

3.3. The blank received 50 µL buffer instead of 50 µL glucosidase for all inhibitor concentrations.

3.4. Fifty microliters from each well were transferred to another 96 well plate and diluted with 200 µL dH_2O, in triplicate.

3.5. The absorbance was measured at 405 nm.

3.6. The Abs for each inhibitor concentration was the absorbance of the blank subtracted from the average absorbance of each triplicate.

3.7. An IC_{50} graph was produced by plotting the %inhibition ((Abs without inhibitor – Abs with inhibitor)/Abs without inhibitor) against the final inhibitor concentration.

4. Alpha-glucosidase assay

4.1. Two millilitres of each inhibitor concentration were prepared:

Inhibitor	Volume inhibitor (µL)	Volume buffer (µL)	Initial [inhibitor] (µM)	Final [inhibitor] in 200 µL reaction (µM)	Nanomoles inhibitor in 50 µL
For all inhibitors	160 (of 50 mM)	1840	4000	1000	50.0
	120 (of 50 mM)	1880	3000	750	37.5
	80 (of 50 mM)	1920	2000	500	25.0
	40 (of 50 mM)	1960	1000	250	12.5

4.2. Ten millilitres of each *p*NPG concentration (mM) were prepared:

Number	Volume 2 mM *p*NPG (mL)	Volume buffer (mL)	Initial [*p*NPG] (mM)	Final [*p*NPG] in 200 µL reaction (mM)
S1	10.0	0	2.00	1.00
S2	5.0	5.0	1.00	0.50
S3	3.3	6.7	0.66	0.33
S4	2.5	7.5	0.50	0.25
S5	2.0	8.0	0.40	0.20
S6	1.7	8.3	0.34	0.17
S7	1.4	8.6	0.28	0.14
S8	0	10.0	0	0

4.3. 96 well plate setup of pancreatic alpha-amylase assay:

Well	Volume of inhibitor (µL)	Glucosidase (U -- µL)	Incubate for 10 min at RT	*p*NPG (µmol -- µL)	Total reaction volume of 200 µL	Incubate for 30 min at 37°C	0.8 M NAOH (µmol -- µL)
1	50	0.01 – 50		200 -- 100 (of S1)			40000 -- 50
2	50	0.01 – 50		100 -- 100 (of S2)			40000 -- 50
3	50	0.01 – 50		66 -- 100 (of S3)			40000 -- 50
4	50	0.01 – 50		50 -- 100 (of S4)			40000 -- 50
5	50	0.01 – 50		40 -- 100 (of S5)			40000 -- 50
6	50	0.01 – 50		34 -- 100 (of S6)			40000 -- 50
7	50	0.01 – 50		28 -- 100 (of S7)			40000 -- 50
8	50	0.01 – 50		0 -- 100 (of S8)			40000 -- 50

4.4. The blank received 50 µL buffer instead of 50 µL glucosidase for all starch concentrations.

4.5. Fifty microliters from each well were transferred to another 96 well plate and diluted with 200 µL dH_2O, in triplicate.

4.6. The absorbance was measured at 405 nm.

4.7. The Abs for each starch concentration was the absorbance of the blank subtracted from the average absorbance of each triplicate.

4.8. The velocity (µmol/min) was calculated as follows:

$$\frac{Abs}{Gradient\ of\ the\ standard\ curve\ (in\ mM^{-1})} \times 0.2\ mL\ \div 30\ min$$

4.9. A Lineweaver-Burk plot was produced by plotting the velocity against the final *p*NPG concentration.

5. Difference in fits (DFFITS) method to identify influential data points

5.1. Lineweaver-Burk lines were plotted for each inhibitor concentration.

5.2. The gradient of the Lineweaver-burk line was taken as m.

5.3. The first x-value was removed, and the new gradient was taken as m_1.

5.4. The first x-value was returned, and the second x-value was removed, and the gradient was taken as m_2.

5.5. The standard deviation between all the different gradient values was taken as SD.

5.6. DFFITS = $(m - m_n)$/SD.

5.7. If the DFFITS was greater than 2 or less than -2, that x-value was removed.

Annexure D: Cytotoxicity assay method

1. Stock solutions

1.1. Growth media: DMEM supplemented with 1% nonessential amino acids, 1% L-glutamine, penicillin (100 U/mL), streptomycin (100 U/mL), 25 mM dextrose, and 10% (v/v) heat-inactivated foetal calf serum.

1.2. Phosphate buffered saline (PBS): 9.23 g FTA hemagglutination buffer dissolved in 1 L dH_2O and adjusted to pH 7.2.

1.3. 0.1% (w/v) Trypan Blue: 50 mg trypan blue dissolved in 50 mL PBS.

1.4. 50% (w/v) trichloroacetic acid (TCA): 50 g TCA dissolved in 100 mL dH_2O.

1.5. 1% (v/v) acetic acid: 10 mL acetic acid added to 1 L dH_2O.

1.6. 0.057% (w/v) sulforhodamine B: 57 mg SRB dissolved in 100 mL 1% acetic acid.

1.7. 10 mM tris buffer: 120 mg tris buffer dissolved in dH_2O and adjusted to pH 10.5.

1.8. 20 mM inhibitor solution:

Inhibitor	Mass (mg) inhibitor dissolved in 2 mL DMSO
Acarbose	25.8
Caffeic acid	7.2
Ethyl gallate	7.9
Oxalic acid	5.0
***p*-Coumaric acid**	6.8
Rutin	2.7
Vanillin	6.9

2. Preparation of cell concentration of $1x10^5$ cells/well

2.1. The selected cell lines were grown in T75 culture flasks at 37°C in a humidified incubator with 5% CO_2 until 70-80% confluency was reached.

2.2. Trypsin was added for 30 to 60 min to detach the cells from the flask.

2.3. The cell suspension was centrifuged at 200 *g* for 5 min.

2.4. The supernatant was discarded, and the pellet of cells was resuspended in 1 mL supplemented media.

2.5. Twenty microliters of the cell suspension were added to 180 µL 0.1% trypan blue.

2.6. The cell-trypan blue solution was viewed on a hematocytometer under a microscope.

2.7. The number of cells was counted in 3 or 4 blocks of the hematocytometer.

2.8. The number of cells in the field was calculated by dividing the total number of cells counted by the number of blocks counted.

2.9. The $1x10^5$ cell concentration = (The number of cells in the field ×10 times dilution in Trypan Blue $\times 10^4$/(The cell concentration needed for the plate which was 10^5).

2.10. Ten millilitres of $1x10^5$ cell suspension for the plate was prepared from the original cell suspension: 10 mL/the above equation to obtain the volume of original cell suspension added to 10 mL supplemented media.

2.11. One hundred microlitres of the $1x10^5$ cell suspension was added to each well of a 96 well plate and incubated for 24 h at 37°C.

3. Cells treated with selected compounds

3.1. Compound preparation:

Number	Volume compound (µL)	Volume DMEM (µL)	Initial concentration (µM)	Final concentration (nmol -- µM)
C1	200 (of 20 mM)	1800	2000	100 -- 1000
C2	200 (of C1)	1800	200	10 -- 100
C3	200 (of C2)	1800	20	1 -- 10
C4	200 (of C3)	1800	2	0.1 -- 1
C5	200 (of C4)	1800	0.2	0.01 -- 0.1
C6	200 (of C5)	1800	0.02	0.001 -- 0.01
C7	200 (of C6)	1800	0.002	0.0001 -- 0.001

3.2. 96 well plate layout:

	1	2	3	4	5	6	7	8	9	10	11	12
A	DMEM media (no cells)						Cells (100 µL DMEM)					
B	1000 µM			1000 µM			1000 µM			1000 µM		
C	100			100			100			100		
D	10		**Compound 1**	100		**Compound 2**	100		**Compound 3**	100		**Compound 4**
E	1			10			10			10		
F	0.1			1			1			1		
G	0.01			0.1			0.1			0.1		
H	0.001			0.01			0.01			0.01		

3.3. One hundred microliters of each compound concentration were added to the 100 µL cells.

3.4. The cells were incubated with the compounds for 72 h at 37°C.

3.5. Fifty microliters 50% TCA was added to the cells and incubated for 24 h at 4°C.

3.6. The cells were washed with tap water four times and allowed to dry for 24 h in the oven (70°C).

3.7. One hundred microliters 0.057% SRB was added for 30 min at room temperature.

3.8. The cells were washed with 150 µL 1% acetic acid 4 times and dried in the oven for 24 h.

3.9. Two hundred microliters 10 mM tris buffer was added to the cells and was allowed to shake for 1 h at 550 rpm.

3.10. The absorbance was read at 540 nm.

3.11. The percentage survival was calculated by dividing the Abs with compound by the Abs without the compound and multiplying by 100%.

3.12. A cell survival plot was generated by plotting the percentage survival against the log concentration of the compound.

Annexure E: Glucose-uptake assay method

1. Stock solutions

1.1. Glucose-free DMEM: Glucose-free DMEM powder was added to 1 L dH_2O and 3.7 g $NaHCO_3$

1.2. 2.5% FCS supplemented media: 1.250 mL foetal calf serum was added to 50 mL glucose-free DMEM.

1.3. 1000 µM insulin solution: 1.375 mL glucose-free DMEM was added to the 8 mg insulin bottle.

1.4. 20 mM metformin solution: 5 mg metformin was dissolved in 2 mL dH_2O.

1.5. 200 µM 2NBDG solution: 2 mL glucose-free DMEM was added to the 5 mg 2NBDG bottle. (7.3 mM) and 550 µL of the 7.3 mM 2NBDG was added to 20 mL glucose-free DMEM.

1.6. Phosphate buffered saline (PBS): 9.23 g FTA hemagglutination buffer dissolved in 1 L dH_2O and adjusted to pH 7.2.

1.7. Insulin concentrations:

Number	Volume insulin (µL)	Volume glucose-free DMEM (µL)	Initial Concentration (nM)	Final concentration (pmol -- nM)
In1	10 (of 1000 µM)	990	10000	-
In2	100 (of In1)	900	1000	-
In3	100 (of In2)	900	100	-
In4	163 (of In2)	900	163	8 -- 100
In5	810 (of In3)	190	81	4 -- 50
In6	405 (of In3)	595	41	2 -- 25
In7	160 (of In3)	840	16.3	0.8 -- 10
In8	100 (of In4)	900	1.63	0.08 -- 1
In9	100 (of In8)	900	0.163	0.008 -- 0.1

1.8. Compound concentrations:

Number	Volume concentration (µL)	Volume glucose-free DMEM (µL)	Initial Concentration (µM)	Final concentration (nmol -- µM)
C1	100 (of 20 mM)	900	1000	
C2	100 (of C1)	900	163	8 --100
C3	100 (of C2)	900	16.3	0.8 -- 10
C4	100 (of C3)	900	0.163	0.08 -- 1

2. 2NBDG uptake assay in C2C12 cells

2.1. 96 well plates were seeded with 80 µL of the $1x10^5$ cell suspension as prepared in the cytotoxicity assay and incubated for 24 h at 37°C.

2.2. The media was replaced with 80 µL 2.5% FCS supplemented media and incubated for 24 h at 37°C.

2.3. That media was then removed (without disturbing the cells) and 80 µL of the compounds was added and incubated for 24 h at 37°C.

2.4. 96 well plate layout:

	1	2	3	4	5	6	7	8	9	10	11	12
A	Cells (only 2NBDG and 50 nM insulin for insulin resistant cells)						Cells (no 2NBDG)					
B	100 µM			100 µM			100 µM			100 µM		
C	10 **Caffeic acid**			10 **p-Coumaric acid**			10 **Ethyl gallate**			10 **Metformin**		
D	1			1			1			1		
E	100 µM			100 µM			100 µM			100 nM		
F	10 **Rutin**			10 **Vanillin**			10 **Oxalic acid**			10 **Insulin**		
G	1			1			1			1		
H										0.1		

2.5. Fifty microliters 200 µM (3.85 nmol) 2NBDG was added to the 80 µL compound-cell solution (final concentration of 77 µM 2NBDG) for 1 h at room temperature (except for the cells in A1-A6).

2.6. The 2NBDG solution was removed from the cells.

2.7. The cells were washed twice with cold PBS.

2.8. The fluorescence was measured at an excitation wavelength of 485/40 nm and emission wavelength of 590/35 nm in 100 µL PBS.

2.9. The results can be represented as a bar graph with the fluorescence on the y-axis and the different compound concentrations on the x-axis.

3. <u>2NBDG uptake assay in HepG2 cells</u>

3.1. 96 well plates were seeded with 80 µL of the $1x10^5$ cell suspension as prepared in the cytotoxicity assay and incubated for 24 h at 37°C

3.2. The media was replaced with 80 µL 2.5% FCS supplemented media or 100 nM insulin DMEM to induce insulin resistance and incubated for 24 h at 37°C

3.3. That media was then removed (without disturbing the cells) and 80 µL of the compounds (with 50 nM insulin for insulin resistant cells) was added and incubated for 45 min at 37°C

3.4. 96 well plate layout:

	1	2	3	4	5	6	7	8	9	10	11	12
A	Cells (only 2NBDG and 50 nM insulin for insulin resistant cells)						Cells (no 2NBDG)					
B	100 µM			100 µM			100 µM			100 µM		
C	10 **Caffeic acid**			10 **p-Coumaric acid**			10 **Ethyl gallate**			10 **Metformin**		
D	1			1			1			1		
E	100 µM			100 µM			100 µM			100 nM		
F	10 **Rutin**			10 **Vanillin**			10 **Oxalic acid**			10 **Insulin**		
G	1			1			1			1		
H										0.1		

3.5. Fifty microliters 200 µM (3.85 nmol) 2NBDG was added to the 80 µL compound-cell solution (final concentration of 77 µM 2NBDG) for 1 h at room temperature (except for the cells in A1-A6).

3.6. The 2NBDG solution was removed from the cells.

3.7. The cells were washed twice with glucose-free DMEM.

3.8. The fluorescence was measured at an excitation wavelength of 485/40 nm and emission wavelength of 590/35 nm in 100 µL PBS.

3.9. The results can be represented as a bar graph with the fluorescence on the y-axis and the different compound concentrations on the x-axis.

Annexure F: Green tea IC_{50} method

1. Green tea preparation

1.1. Twenty-five millilitres of boiling dH_2O was added to two green tea bags of each brand (2 tea bags = 2.5 g, therefore two tea bags in 25 mL water were 5.0 g/ 25 mL or 20% dry weight).

1.2. The green tea bags were left to stand in the 25 mL water for 10 min with occasional stirring.

1.3. The tea bags were removed by squeezing the water out of the tea bags with a spoon.

1.4. The green tea solution was transferred into Eppendorf tubes and centrifuged at 10 000*g* for 10 min.

1.5. The supernatant (20% dry weight green tea stock solution) was used to make the green tea dilutions for the pancreatic alpha-amylase and alpha-glucosidase assays.

1.6. Green tea dilutions for pancreatic alpha-amylase IC_{50}:

Number	Volume (µL)	Volume dH_2O (µL)	Initial concentration (% dry weight)	Final concentration (% dry weight)
T1	1000 (20% stock)	0	20	5.0
T2	900 (of T1)	100	18	4.5
T3	890 (of T2)	110	16	4.0
T4	875 (of T3)	125	14	3.5
T5	855 (of T4)	145	12	3.0
T6	830 (of T5)	170	10	2.5
T7	800 (of T6)	200	8	2.0
T8	750 (of T7)	250	6	1.5
T9	665 (of T8)	335	4	1.0
T10	500 (of T9)	500	2	0.5
T11	500 (of T10)	500	1	0.25
T12	0	1000	0	0

1.7. Green tea dilutions for alpha-glucosidase:

Number	Volume (µL)	Volume dH_2O (µL)	Initial concentration (% dry weight)	Final concentration (% dry weight)
T1	1000 (of 0.04% tea solution)	0	0.040	0.010
T2	900 (of T1)	100	0.036	0.009
T3	890 (of T2)	110	0.032	0.008
T4	875 (of T3)	125	0.028	0.007
T5	855 (of T4)	145	0.024	0.006
T6	830 (of T5)	170	0.020	0.005
T7	800 (of T6)	200	0.016	0.004
T8	750 (of T7)	250	0.012	0.003
T9	665 (of T8)	335	0.008	0.002
T10	500 (of T9)	500	0.004	0.001
T11	500 (of T10)	500	0.002	0.0005
T12	0	1000	0	0

2. Green tea IC_{50} for pancreatic alpha-amylase

2.1. The same method and reagents were used as described in **Annexure B.**

3. Green tea IC_{50} for alpha-glucosidase

3.1. The same method and reagents were used as described in **Annexure C.**

Annexure G: LC/MS method

1. Dry green tea sample preparation

1.1. The green tea powder from two tea bags was ground using an electric coffee grinder for 20 s.

1.2. The ground powder was sieved using a steel sieve with the smallest aperture opening of 355 µm.

1.3. The finest green tea powder was transferred into Eppendorf tubes and used for the extraction process.

2. Stock solution preparation

2.1. Extraction solvent: 50% (v/v) methanol with 1% (v/v) formic acid in HPLC grade water.

2.2. Standard solvent: 70% (v/v) acetonitrile with HPLC grade water.

2.3. Solvent A: 0.1% (v/v) formic acid in HPLC grade water.

2.4. Solvent B: 0.1% (v/v) formic acid in acetonitrile.

3. Green tea extraction

3.1. 1.6 mL extraction solvent was added to 250 mg of the fine green tea powder sample in a 2 mL centrifuge tube.

3.2. The solution was vortexed for 1 min and placed in an ultrasonic bath for 1 h.

3.3. The solution was then centrifuged at 14 000 rpm for 5 min.

3.4. The supernatant was diluted 10x by transferring 100 µL of the supernatant into a 1.5 mL glass vial with 900 µL extraction solvent which was injected into the column.

4. Standards cocktail preparation

4.1. One milligram of each standard was dissolved in one millilitre of the standard solvent.

4.2. These standards were: epigallocatechin gallate, epicatechin, epigallocatechin, epicatechin-3-o-gallate, catechin, chlorogenic acid, rutin, caffeic acid, *p*-coumaric acid, quercetin, quinic acid, rosmarinic acid.

4.3. Ten microliters of each 1 mg/mL standard were mixed to create the standard cocktail (120 µL with all 12 standards).

4.4. Dilution of standards cocktail:

Number	Volume of standards cocktail (µL)	Volume of 50% methanol (µL)	Final concentration (mg/L or ppm)
Std1	200	0	83.33
Std2	120	80	50.00
Std3	80	120	33.33
Std4	40	160	16.67
Std5	20	180	8.33
Blank	0	200	0

5. Waters Acquity UPLC

5.1. Injection volume: 5 µL.

5.2. Column: Waters HSS T3, 2.1 x 100 mm, 1.7 µm column.

5.3. Mobile phase: 100% solvent A for 1 min and changed to 28% solvent B over 22 min with a linear gradient.

5.4. Wash step: 28% to 40% solvent B in 50 s then to 100% solvent B in 1.5 min.

5.5. Re-equilibration: to initial conditions for 4 min.

5.6. Flow rate: 0.3 mL/min.

5.7. Column temperature: 55°C.

6. Negative ion mode electrospray

6.1. Cone voltage: 15 V.

6.2. Desolvation temperature: 275°C.

6.3. Desolvation gas: 650 L/h.

7. Waters Synapt G2 QTOF-MS

7.1. Column eluate was passed through a PDA detector.

7.2. Scan range: 150 to 1500 m/z.

7.3. MSE mode: low collision energy of 4 V and a collision ramp between 40 and 100 V.

7.4. Leucine enkephalin: used as the reference mass.

7.5. Sodium formate: used to calibrate the instrument.

8. MSDIAL and MSFINDER annotation

8.1. Freeware downloaded from CompMS (http://prime.psc.riken.jp/compms/index.html).

8.2. Waters MassLynx .raw file was converted into analysis base file (ABF).

8.3. ABF was imported into MSDIAL (SWATH-MS All-ions method).

8.4. Minimum peak height: 300 amplitude.
8.5. Retention time tolerance: 0.15 min.
8.6. The peak height intensity file was exported from MSDIAL alignment results.
8.7. The formula and structure of all peaks was searched on MSDIAL.
8.8. The "All peaks" file was exported from MSDIAL and imported into MSFINDER.
8.9. The compounds were putatively annotated.
8.10. Databases: FooDB, PlantCyc, ChEBI, STOFF, NPA, NANPDB, COCONUT, KNApSAcK, PubChem, UNPD.
8.11. The batch results were exported.
8.12. The structure file and the height file were combined in Excel.
8.13. Putatively annotated compounds that had peak heights less than 40 (the blank) were removed.

9. Standard curve generation

9.1. The standard curve of the peak height for each standard against the amount (ng) of standard.
9.2. The amount (ng) of each standard present in the tea samples was calculated using the equation of the line of the standard curve and the peak height of that standard (set intercept).
9.3. The percentage dry weight was calculated by dividing the amount of standard (ng) by the amount of green tea (ng) multiplied by 100%.
9.4. The amount of green tea (ng) = 250 mg green tea / 1.6 mL methanol x 0.005 mL injection volume x 10 dilution factor = 7.8125 mg or 7812.5 ng.

10. MetaboAnalyst

10.1. Statistical Analysis [one factor] was selected.
10.2. The csv file containing peak intensity values of putatively annotated compounds was submitted.
10.3. The data was processed using the default settings (no missing values were detected).
10.4. The data was filtered using the interquartile range.
10.5. No sample normalization or data transformation was selected.
10.6. Auto data scaling was performed.
10.7. p-Value obtain as adjusted p-value (FDR).